2008

Increasing the sensitivity of a surface plasmon resonance biosensor

Fatemeh Parayandeh
San Jose State University

INCREASING THE SENSITIVITY OF A SURFACE PLASMON RESONANCE BIOSENSOR

A Thesis

Presented to

The Faculty of the Department of Chemical Engineering and Materials Engineering

San Jose State University

In Partial Fulfillment

of the Requirements for the Degree

Master of Science

by

Fatemeh Parayandeh

December 2008

INFORMATION TO USERS

The quality of this reproduction is dependent upon the quality of the copy submitted. Broken or indistinct print, colored or poor quality illustrations and photographs, print bleed-through, substandard margins, and improper alignment can adversely affect reproduction.

In the unlikely event that the author did not send a complete manuscript and there are missing pages, these will be noted. Also, if unauthorized copyright material had to be removed, a note will indicate the deletion.

ProQuest LLC
789 E. Eisenhower Parkway
PO Box 1346
Ann Arbor, MI 48106-1346

APPROVED FOR THE DEPARTMENET OF
CHEMICAL AND MATERIALS ENGINEERING

Melanie McNeil 11-04-08

Dr. Melanie McNeil

Dr. Roger Terrill

Dr. Joseph Sly, IBM Almaden Research Center

Dr. Robert Miller, IBM Almaden Reseach Center

APPROVED FOR THE UNIVERSITY

1/7/09

ABSTRACT
INCREASING THE SENSITIVITY OF A SURFACE PLASMON RESONANCE BIOSENSOR

by Fatemeh Parayandeh

Sensing methods that can detect and characterize specific interactions that occur between biomolecules without affecting their native structure are of great interest. An example of such sensors is a surface plasmon resonance (SPR). SPR-based biosensors are real-time analytical devices capable of highly sensitive detection of biomolecules without the need for labeling or tagging the analyte of interest. In this work, a highly sensitive SPR biosensor was designed with complementary LabView data acquisition programs to facilitate measurements and data analysis. The functionality of the SPR machine was tested with confirmational experiments.

The SPR biosensor sensitivity was further increased by incorporating size-selective components, nanoporous organosilicate films, onto an SPR sensor surface to provide a novel combination of both chemical and physical molecular recognition. This novel combination aims to enhance sensitivity and selectivity when screening complex biological mixtures.

ACKNOWLEDGMENTS

I would first like to thank my research advisor, Dr. Melanie McNeil, for her guidance and support throughout the period of my study at San Jose State University. Her patience and enthusiasm have greatly enhanced the quality of my graduate research and allowed me to experience so much as a Masters student at SJSU. My sincere thanks are also given to Dr. Robert Miller for allowing me the opportunity to work in the IBM Almaden Reseach Center and be part of his team. I would like to thank him for his guidance, time, and effort in making this experience unique; his wisdom and passion for science have inspired me. My sincere appreciation goes to Dr. Joseph Sly, without whom my experience at IBM would have not been the same. I would like to thank him for his brilliant and distinct ideas, invaluable guidance, and support. He has unselfishly given his time, council, and expertise on all professional matters. He has truly been an excellent mentor.

My special thanks go to Dr. Michael Jefferson without whom the instrumentation design of this work would have not been accomplished. I am grateful for his immense help, advice, time, and effort in making the design a master piece. I would like to thank Dr. William Risk whose tremendous help allowed me to better understand some of the fundamentals of optics and providing invaluable feedback on my work. I would like to thank Victor Lee for his help and for providing a comfortable environment in his lab. Thanks also to Dr. Roger Terrill for his valuable feedback during my research.

I appreciate the comments on my thesis provided by my advisor Dr. Melanie McNeil, Dr. William Risk, Dr. Joseph Sly, and my friend Natali Krajnovich.

My sincere thanks to all of the staff of the Chemical Engineering Department and all of the staff at IBM Almaden Reseach Center and especially all my group members at IBM and my friends, who have made my stay in San Jose a unique and unforgettable experience.

Finally a very special thank you to my family, my parents for their unconditional love and support; and Amir, Nazanin, and Najmeh who all always bring so much joy to my life.

I dedicate this thesis to my loving parents Nasrin and Abbas, without their sacrifice and enormous love and support I could have not experienced any of these great opportunities.

TABLE OF CONTENTS

LISTS OF FIGURES

LISTS OF TABLES

CHAPTER ONE
INTRODUCTION

During the last two decades, the use of optical sensors for chemical and biological studies has been an exciting area of focus. The improvements in the sensitivity and analysis capabilities of optical sensors have been a major focus of many researchers, resulting in advances in many areas of studies such as drug discovery, environmental studies, and food analysis. Such sensors are able to reveal the behavior of molecules adsorbed on a surface, providing valuable information about the adsorbed molecules. Over the years many different types of biosensors have been designed to monitor chemical and biological interactions [1]. Surface Plasmon Resonance (SPR) is a popular type that has been used as an analytical method in measuring chemical and biological bindings. In 1990, a commercially available SPR biosensor was introduced by BIAcore [1], which provides a convenient platform for doing SPR experiments, and made it possible for researchers doing different experiments to use the same apparatus [1]. The SPR detector offers an advantage over other detectors as it is capable of real time binding analysis in its design, where other binding assays (e.g., ELISA assay) often are not, and this is a significant improvement in capability. Additionally, the SPR detector has the ability to monitor low concentration levels without the need for fluorescent or radioactive labels. It also provides an extra advantage in sensitive measurements as it can measure a large range of interactions from small molecules through the analysis of complex systems such as multilayer organic films. With the most recent developments and advancements in SPR, this technique has become widely used in food sciences, protein interactions,

bioprocessing, drug discovery, cell biology, and environmental studies [2]. For instance, in the analysis of drug delivery, it is important to ensure that the desired molecules bind to the surface. An SPR sensor is able to examine these bindings.

A 2001 survey of commercial applications of biosensors found 3000 articles in the area of biosensors were published over the past twelve years, signifying heavy use of the SPR technique for different applications that may determine more sensitive binding measurements [2].

The phenomenon of SPR was first described by Wood in 1902 based on his study of light intensity diffracted from metal grating. The practical methods to generate and study surface plasmons in thin metal films, however, were not developed until 1968. The application of SPR was first studied in 1980 [1].

Surface plasmon resonance is an optical technique that is sensitive to the refractive index changes that occur near the detector. SPR is a charge-density wave phenomenon that can occur at the boundary between a metal and a dielectric which corresponds to the detector surface and a sample in SPR biosensors. A commercial SPR consists of a noble metal layer, a dielectric, and a glass prism, as shown in Figure 1, in order to generate SPR phenomenon [3].

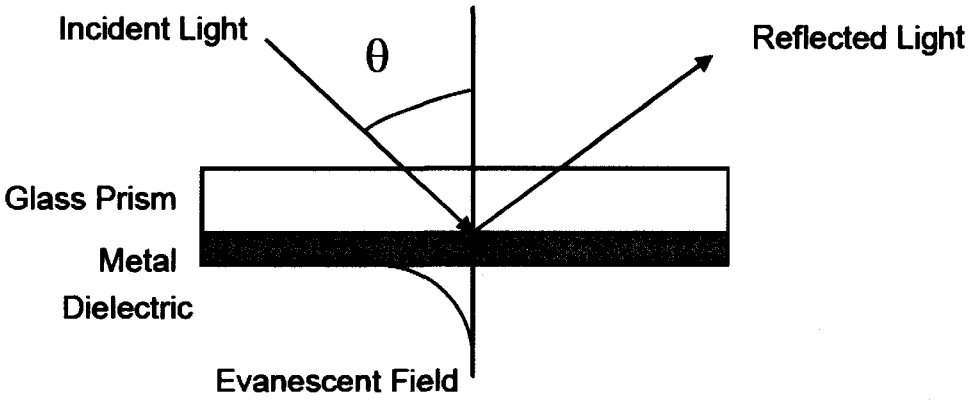

Figure 1. Typical SPR schematic with a noble metal film, prism, and dielectric. θ_c in the critical angle for TIR to occur.

A dielectric is a nonconducting substance, i.e., an insulator. Many SPR papers show a dielectric as a liquid, solvent, air, or gas sample. In order to excite SPR with an external light source (e.g., laser beam), momentum matching requires that the external light source be incident upon the metal-dielectric interface through a medium having a higher refractive index, such as glass, than the dielectric. In practice, typically a prism is used to provide a medium that has a higher refractive index than the dielectric (sample solution). The angle of incidence (measured from the plane of the interface) is typically greater than the critical angle for total internal reflection [3]. It is necessary to understand TIR theory before understanding the concept of SPR.

1.1 Background

1.1.1 Total Internal Reflection

The SPR biosensor is an optical detector that uses the phenomenon of total internal reflection (TIR). In order to describe SPR, it is necessary to understand TIR theory first. When a beam of light from a material with a high refractive index (such as

glass) passes through another material with a low refractive index (such as air), some of the light is reflected from the interface in a process called internal reflection. If the incident light hits the interface at an angle greater than the critical angle, the light is completely reflected and Total Internal Reflection (TIR) takes place, as shown in Figure 1(I) [3, 4].

The critical angle is determined based on Snell's law, as shown in Equation 1, where n_d is the refractive index of the low index material and n_p is the high refractive index material [4].

$$\sin \theta_c = \frac{n_d}{n_p} \qquad \text{Equation 1}$$

1.1.2 Principle of Surface Plasmon Resonance

As shown in Figure 1, as light travels through the prism towards the plane of interface (prism/ dielectric) at the angle greater than θ_c, all the optical power is reflected and TIR takes place, as shown by the dotted line in Figure 2 (I).

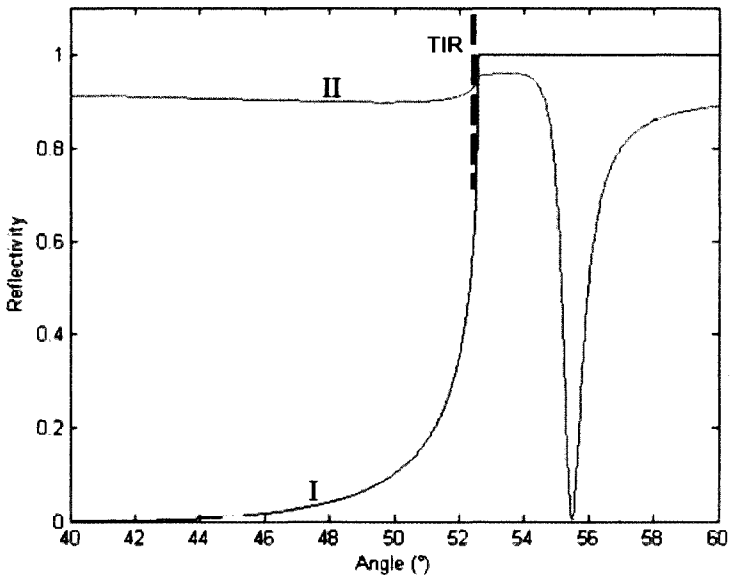

Figure 2. TIR phenomenon (I) and Surface Plasmon Resonance (II) (reprinted with permission from B. Risk).

However, if a thin film of a noble metal is interposed between the prism and the dielectric and the plane-polarized light (polarization occurring parallel to the plane of incidence) hits the interface at a specific angle greater than the critical angle, the free electrons on the surface of the metal film are excited and move along the surface (the concept of polarized light will be explained later in section 1.3). As a result, instead of being reflected, the energy couples to electrons. The moving electrons are called surface plasmons. The oscillation of mobile electrons generates a surface plasmon wave, propagating at the interface between the metal film and dielectric [5].

The surface plasmon wave is an electromagnetic mode (e.g., a solution of Maxwell's equations) bound to the metal-dielectric interface. This mode is characterized by a propagation constant β given by [1]:

$$\beta = k_0 \sqrt{\frac{\varepsilon_m n_d^2}{\varepsilon_m + n_d^2}} \qquad \text{Equation 2}$$

where $k_0 = \frac{2\pi}{\lambda}$ is the wavevector of light having a wavelength λ in a vacuum, ε_m is the (complex) dielectric constant of the metal, and n_d is the refractive index of the dielectric. It can be shown that for a fixed frequency, $\beta > k_d$, where k_d is the wavevector of a freely propagating beam in the dielectric. Hence, a surface plasmon cannot be excited simply by shining light on the metal-dielectric interface. Instead, light having a propagation constant larger than β must be produced. This is most conveniently done by using a prism with a refractive index, $n_p > n_d$. Then, as shown in Figure 3, an angle θ can be chosen such that $k_p \cos\theta = \beta$.

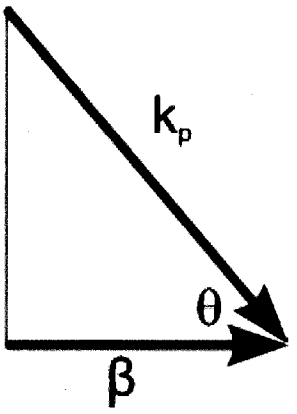

Figure 3. The surface plasma wave is an electromagnetic mode characterized by a propagation constant β.

Under this condition (which can also be thought of as momentum matching), energy is efficiently transferred from the incident light beam into the surface plasmon, and the reflected power is diminished. Hence, as the angle θ is scanned, a dip occurs in

reflected intensity, as shown in Figure 2 (II). The reflectivity and intensity are two terms that are interchangeably used in the SPR concept. The angle at which this dip is most pronounced is called the "minimum angle" or the "surface plasmon resonance angle" and is where the energy is transferred to the surface plasmons instead of being reflected. The drop in intensity can be measured as either a function of the angle of incidence or the wavelength.

The electric field associated with the surface plasmon resonance decays quickly with distance away from the metal-dielectric interface (decay length typically ~$\lambda/5$) above and below the interface; hence, the characteristics of the resonance are affected by the environment within a few hundred nanometers of the interface, which is why SPR provides a very sensitive way to monitor interactions occurring at the boundary that locally change the refractive index [5].

It is important to be able to calculate the variation of reflectivity versus an angle, as shown in Figure 2, in order to predict the location of the minimum angle and in order to permit fitting to experimental data. For a three-layer system, the Fresnel reflectivity can be calculated from the following set of equations [5]. The three layers include the prism, the metal layer, and the dielectric.

$$R = |r_{pms}|^2$$

Equation 1

with

$$r_{pms} = \frac{r_{pm} + r_{ms}\exp(2ik_{mz}d)}{1 + r_{pm}r_{ms}\exp(2ik_{mz}d)}$$

Equation 2

$$r_{pm} = \frac{k_{pz}\varepsilon_m - k_{mz}\varepsilon_p}{k_{pz}\varepsilon_m + k_{mz}\varepsilon_p}$$

Equation 3

$$r_{ms} = \frac{k_{mz}\varepsilon_s - k_{sz}\varepsilon_m}{k_{mz}\varepsilon_s + k_{sz}\varepsilon_m}$$

Equation 4

and

$$k_{jz} = \left(\varepsilon_j \frac{\omega^2}{c^2} - k_x^2\right)^{1/2} \quad \text{for } j = \mathrm{p, m, s}$$

Equation 5

$$k_x = \sqrt{\varepsilon_p}\frac{\omega}{c}\sin\theta$$

Equation 6

$$\omega = \frac{2\pi c}{\lambda}$$

Equation 7

Equations one through seven combined can predict the shift in SPR angle if the index of refraction is known. Based on the theoretical calculations, experimental results can be analyzed to determine the actual shifts due to the binding interactions.

There is a different setup available for SPR, either a commercial type (BIAcore) or one based on optical components. Regardless of the type, the following conditions have to be satisfied in order to observe a surface plasmon resonance phenomenon:

1. Not every metal will support a surface plasmon mode. Two common types that have been widely used are gold and silver [7]. Gold is sufficiently reactive and will allow other materials to bind to the surface, and, most importantly, it has a conduction band electron that is capable of resonating upon excitation by light at a proper wavelength.

Silver results in a narrower minimum resonance angle so can generate a deeper angle. However, silver is less resistant to oxidation compared to gold.

2. The thickness of the metal layer must be carefully chosen to give a deep dip. A vast number of studies have shown that a 50 nm gold or silver sensing layer provides an optimum behavior for the SPR curve [2].

3. Only a plane-polarized light that is, either a p-polarized or transverse magnetic (TM)-polarized incident light (polarization occurs parallel to the plane of incidence) can excite surface plasmons.

4. It is essential that the energy of the incident light matches with the surface plasmon energy so that an instance of resonance can be achieved [1].

To facilitate the coupling of light with the surface plasmons, different configurations of SPR have been investigated. The most widely used SPR detector is the prism-based SPR system known as the Kretchsmann configuration. Other types of SPR detectors include the optical waveguide and grating-coupling system. These two configurations will be addressed later in this chapter. The prism-based SPR can be arranged in different configurations and makes each SPR setup a unique design. The SPR detector in this project is set up based on the Kretchsmann configuration.

1.2 Kretchsmann Configuration

The Kretchsmann configuration (prism-based) is a common type of SPR setup. There is another configuration using a prism called the Otto configuration; this uses a small air gap between the prism and metal, which is not as common as the Kretchsmann configuration. The Kretchsmann type includes a light source, a prism, a flow cell, a

noble metal film, and a photodetector, as shown in Figure 1 [3]. The base of the prism is coated with approximately 50 nm of noble metal film. The advantage of this configuration is the ability to measure different analytes while obtaining high resolution measurements.

Figure 4 shows the flow cell and detector components of a typical Kretchsmann configuration. As the light source hits the prism with an angle greater than the critical angle for TIR, all of the light is expected to be reflected. However, due to a placement of the noble metal layer at the interface of the prism, the incident light passes through the prism toward the noble metal film. The light reflects off the metal film and travels back to the photodetector [8]. The sensogram, as shown in Figure 4, was used to study the antibody-antigen binding interaction as an example of biological bindings. As the antibody binds to the metal surface, the condition in a medium in contact with the evanescent field changes (changes in refractive index) which affects the velocity of the plasmons and changes the momentum matching. As a result a, shift in incident angle (θ_1) occurs. When the antigen is injected in the flow system, a new angle (θ_2) is detected as a result of the binding interaction of antigen to antibody because of the same phenomenon explained for θ_1. Therefore, a shift in resonance angle indicates the binding interaction of antibody-antigen compounds [2]. The resonance angle shifts also provide valuable information in analyzing the binding interactions in terms of the amount of the bound molecules and the kinetics performance since the stronger the binding the greater resultant shift [5].

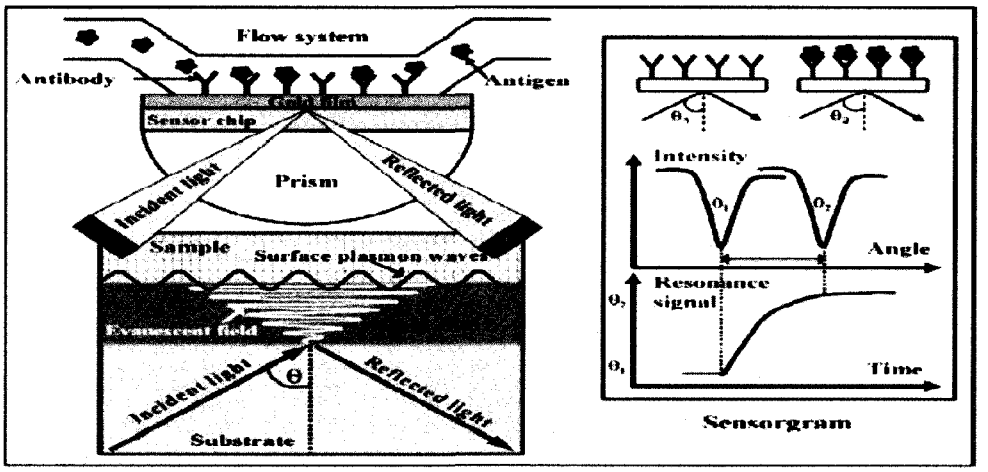

Figure 4. SPR setup-a prism based SPR which includes flow cell, prism, light source and, detector [2] (reprinted with permission from Elsevier Limited).

Both concentrations of analyte and the kinetic performance can be evaluated in more depth, by analyzing the association and dissociation kinetics between the binding compounds. The typical sensogram for studying these parameters is shown in Figure 5, with the important characteristics of the resulting sensogram labeled. Basically, sensogram raw data are presented as a real-time graph of response units (RU) versus time. During the injection of analytes, changes in signals result from two processes: association to and dissociation from the surface. When molecules in the solution bind to target molecules on the surface, the amount of analyte increases resulting in an association phase. When they dissociate from the sensor surface the amount of the analyte decreases [9].

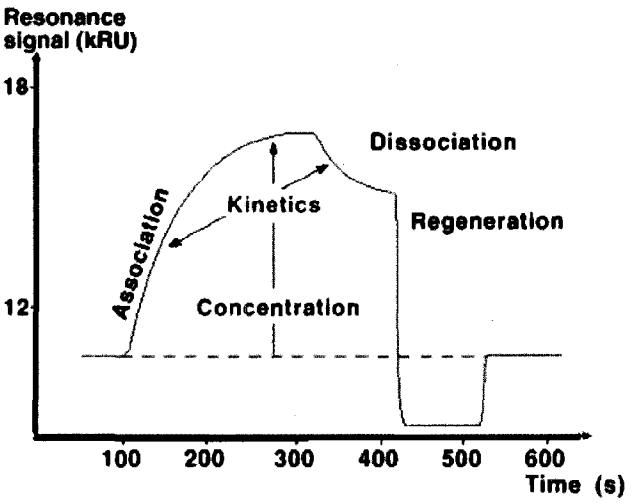

Figure 5. Kinetics analysis of binding compounds in terms of association and dissociation rate constant.

In general, there are two main detection approaches in SPR sensing: an angular and a wavelength modulation [10]. The angular interrogation is the common type used in SPR sensors. At a fixed wavelength, the intensity of the reflected light (SPR angle) is measured relative to the resonance angle. The range of angles is scanned, and the intensity of the reflected light is monitored to precisely detect the reflectivity minimum. Typically, a single wavelength (often HeNe, 632 nm) excitation source is used for the angular modulation. Near IR, diode lasers, and emitting diodes have also been used for this SPR mode [11]. For the wavelength mode, a fixed angle and a collimated beam of white light are employed. At the fixed angle, the reflected light spectrum contains a SPR dip. The SPR dip shifts when material binds to the interface. The 600 to 800 nm wavelength is usually used in this mode. This so called multi-wavelength SPR could be an advantage for studies that require a wider range of spectrum based on the samples to be analyzed [10].

1.3 Optical Configurations of SPR Sensors

The propagation length of the surface plasmon wave (SPW) is limited, so the sensing action requires that binding occurs in the area where the SPW is occurring [11]. There are three common optical configurations that allow such binding to occur: prism couplers, grating couplers, and optical waveguides as shown in Figure 6.

1.3.1 Prism Couplers

In the prism couplers configuration a light wave is completely reflected at the interface of the metal layer and the prism coupler and an excited SPW that evanescently penetrates into the thin metal layer. Particularly, the Kretchmann configuration has been known as the most common type of SPR sensing techniques. The main detection approaches: measurement of the SPR angle, measurement of the resonant wavelength, and measurement of the intensity of the reflected light can be achieved with this geometry [12].

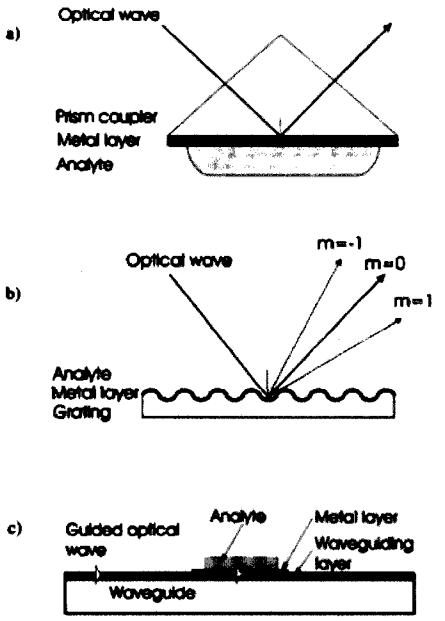

Figure 6. Optical configurations of SPR sensors, a) prism coupler-based, b) grating coupler-based, and c) optical waveguide [11] (reprinted with permission from Elsevier Limited).

1.3.2 Grating Couplers

The grating coupler is usually advantageous when an external light reflection is being used. If the interface between the metal and dielectric layer is distorted, the optical wave is diffracted forming a beam at a variety of angles. The modeling of this system and analysis of the sensor data is more complex [11]. It is convenient that the thickness of the gold or silver layer is not critical for grating coupling as it is for the attenuated total reflection (ATR) prism based. A gold-based SPR sensor has been used to monitor the bimolecular interactions in an aqueous environment [1]. The disadvantage of this system is that the analyte and the flow cell need to be transparent unlike prism-based systems, as the incident light is transparent through the sample solution [12].

1.3.3 Optical Waveguide

The principle of exciting a surface plasmon waveguide based SPR is similar to the Kretchsmann attenuated coupler. This configuration has been used for the benefits of small size, ruggedness, and the ability to suppress the stray light. A light is guided by the waveguide and enters the region with a thin metal overlayer and evanescently penetrates through the metal layer. This method provides the highest level of miniaturization of all SPR devices [12].

1.4 Quantitative Measurement of SPR Data

In principle, the capability of SPR sensors to operate in real time mode provides the possibility of analyzing the mechanism of chemical and biological events using kinetics, mass transport, and thermodynamics features. These quantitative data analyses provide valuable information about the bindings of the molecules, equilibrium constants of surface reactions, and the overall structure of the analyte of interest. The two general methods are the kinetics and thermodynamic analyses [13].

1.4.1 Kinetics Analysis

Kinetics analysis is by far the leading tool in obtaining information in chemical and physical binding events, specifically in analyzing protein-protein interactions. This analysis has been used in many different research studies to understand the fundamental properties of molecules.

Kinetic analysis approaches that have been used in many studies, however, have fundamental flaws in their equations and assumptions. Also, a number of experimental

factors can cause even more complications in understanding the kinetics data. These factors are mass transport, nonspecific binding, and matrix effects associated with heterogeneity [11, 14]. A study by Geordiagis et al. proposed to directly create a self-assembled monolayer film on the SPR gold sensor surface [14]. With this, the signal levels are significantly decreased as there are fewer molecules in the interfacial region. The *in situ* SPR measurements can also result in a more viable technique to monitor the kinetics analysis and more importantly to reproducibly obtain the accurate results without changing any conditions or the environment where sample is analyzed [14].

1.5 Optical Components of SPR

In the Kretchsmann configuration, light travels from the source to the detector. Therefore optical components are required to transfer light along the optical path. The selection of the optical components has a significant effect on the performance of the SPR and consequently the accuracy and sensitivity of the measurements. The major optical components used in the SPR design include a light source, a mirror, a polarizer, and a lens.

A diode laser or a white light can be the choice of the light source based on the angle variation or the wavelength variation and the requirements of the experiment. A broad range of wavelengths can be obtained using commercially available lasers. A common laser (helium-neon) has a wavelength of 632.8 nm. The white light offers the multiple wavelengths at a fixed angle [10].

Mirrors are one of the most commonly used optical components of any optical arrangement. In any optical path, regardless of the existence of other components, there

is often a need to fold or bend the optical path. This is achieved by placing mirrors in the path to transfer light from one point to another [6, 15].

An important concept in optical systems is the polarization of light. Light is an electromagnetic wave made up of mutually perpendicular, fluctuating, electric (E) and magnetic fields (B), as shown in Figure 7 (a). Figure 7(b) shows the electric field in plane xy, the magnetic field in plane xz, and the propagation of the wave in direction x. The directions of the vibrating electric and magnetic vectors are perpendicular to the direction of propagation instead of being parallel, as shown in Figure 7.

Since the electric and magnetic fields are forced by Maxwell's equations to have a specific relationship to each other, it is sufficient in most cases to consider only one or the other [3, 4]. A wave with a behavior described above is called plane polarized, and the light contains waves that only fluctuates in one specific plane. The phenomenon of polarization is achieved by using a polarizer in the optical systems. The reason to use such a device is that ordinary light is unpolarized meaning that the light waves have different planes of polarization. Therefore, a polarizer is required to direct light in one polarization plane [15]. It worth mentioning that laser light is typically already polarized because of how the laser is designed by the manufacturer.

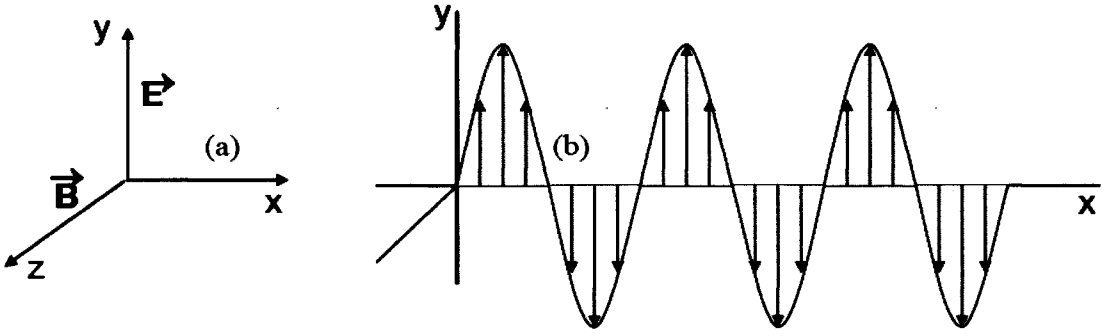

Figure 7. Plane-Polarized wave showing the vectors E and B along a particular array.

When light strikes a surface such as a beam splitter at a non-perpendicular angle, the reflection and transmission of light depend on the polarization type. The system is usually defined by a plane containing the input and reflected beam. The two types are known as s and p polarization. In p-polarization, the electric field vector lies in the plane defined by the incident and reflected beams; in s-polarization, the electric field vector is perpendicular to this plane. These two phenomena are shown in Figure 8.

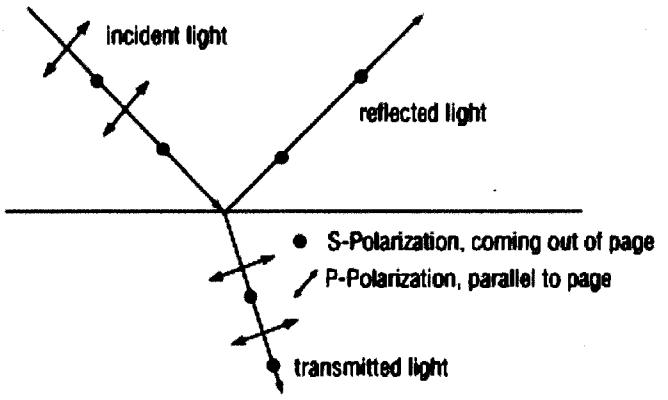

Figure 8. The two types of polarization: s-polarization and p-polarization.

Another important concept related to polarization is called Brewster's angle. It is defined as an "angle of incidence at which light with a particular polarization is perfectly transmitted through a surface, with no reflection" [3]. When light travels between two transparent media with different refractive indices, generally some of the light is reflected at a boundary and some is transmitted through it. At one particular angle, however, light with one specific polarization is no longer reflected, and this angle is defined as Brewster's angle, θ_B. The polarization that is not reflected at this angle is the polarization when the electric field lies in the same plane of incidence and is known as p-

polarized since it is parallel to the plane. At Brewster's angle, p-polarized light is completely transmitted through the interface. When unpolarized light strikes the surface, the reflected light is always s-polarized and perpendicular to the plane of incidence.

Beside the polarization effect in the optical path, the other main component in transformation of light in the optical path is the lens. A lens is typically made of glass or other transparent materials. There are different types of lenses based on the curvature of the two optical surfaces. The different types are shown in Figure 9 below. If both surfaces are convex, the lens is called biconvex, or if one surface is flat, then the lens is plano-convex [16].

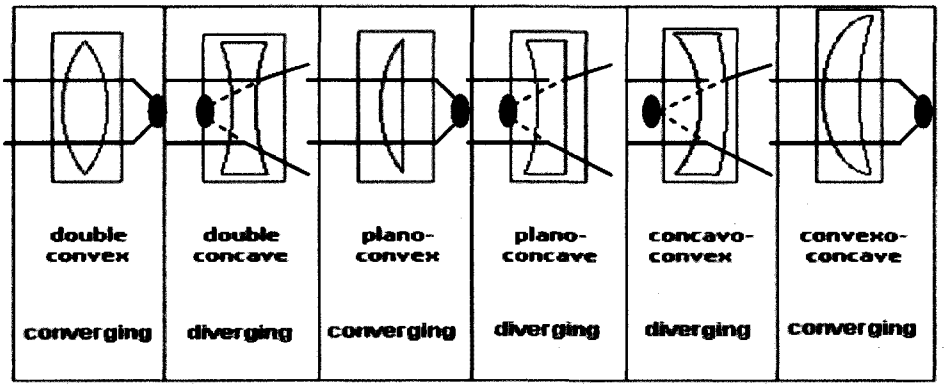

Figure 9. Different types of lenses are categorized to convex and concave shapes.

Light that transfers through a convex lens converges to a spot on the axis known as the focal point, as shown in Figure 10. If the lens is concave, light passing through it diverges. In SPR design, convex lenses are used to converge light in the optical path.

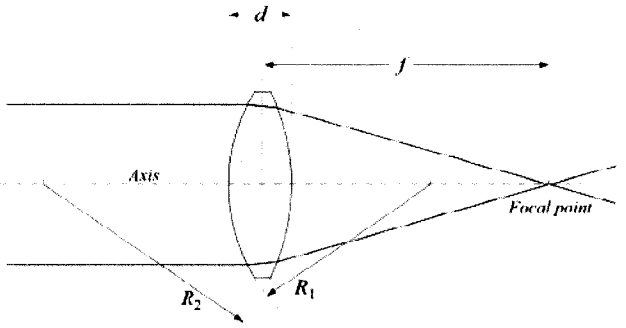

Figure 10. The performance of light through the convex lens. Light converges to a single point on the axis.

The two common types of lens used in this study are spherical and cylindrical lenses with plano-convex curvature. A spherical lens has two surfaces with the same axis on each surface of spheres. Each of the surfaces can be convex, concave or planar. The center of spheres is joined by the line known as the axis of the lens and that completes the lens surface. With this type of lens, the focused light passes onto a point. The cylindrical lens is another common type, where the focused light passes through a line instead of a point [15]. The curved faces are parts of a cylinder and focus the light onto a light which is parallel to the intersection of the lens surface and a plane tangent to it. The two types of lenses are shown in Figure 11.

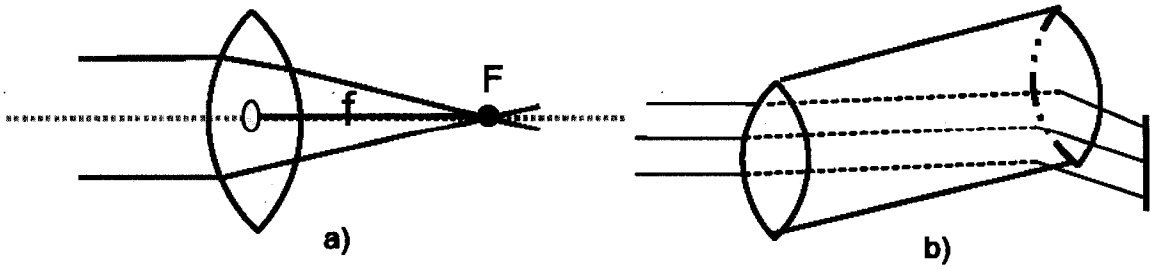

Figure 11. a) spherical lens and b) cylindrical lens.

To better understand the behavior of different lenses, the concept of focal length and focal point has to be defined first. The focal length measures the strength of a lens and how strongly a lens can possibly converge or diverge light. An optical system with a shorter focal length has a greater optical power than the system with a longer focal length [15]. The spot where rays pass or originate is known as a focal point, F. The focal length, f and focal point, F are shown in Figure 10.

1.6 Factors Affecting Biological Measurements

Several factors can highly affect the biological responses in biosensor applications. In this section, the following factors will be presented and discussed, detection formats, biorecognition elements, immobilization techniques, and the non-specific adsorption on a sensor surface.

1.6.1 Detection Formats

Various detection formats have been used in SPR sensors in measuring chemical or biological interactions. The detection format is chosen based on the size and type of the analyte of interest, range of concentrations of the analyte to be measured, the binding characteristics of biomolecular recognition elements, and any other surface chemistry [17]. The three most frequently used detection formats are direct, sandwich, and inhibition format.

The direct detection method is a direct way of measuring the binding interactions. The biomolecular recognition element is immobilized on the sensor surface and the analyte in the solution binds to this element of the surface, producing a

refractive index change measured by SPR. This technique, however, is only applicable when the direct binding produces a sufficient response [17]. The limit of detection and specificity can be improved by employing a sandwich assay, in which the surface is incubated with a secondary biorecognition element that captures the analyte.

In cases where smaller analytes, with a molecular weight of 5000, are the target molecules, they often do not generate a measurable change in a refractive index; therefore the use of either an inhibition or competitive format is required. Figure 12 shows the behavior of the three detection formats. In inhibition format, a fixed concentration of antibody with affinity to analyte is mixed with a sample containing an unknown concentration of analyte. The mixture is then injected in the flow cell that passes over the sensor surface to which analyte is then immobilized [18]. The antibodies are measured as they bind to the analyte molecule immobilized on the sensor surface. The binding response is inversely proportional to the concentration of analyte [17].

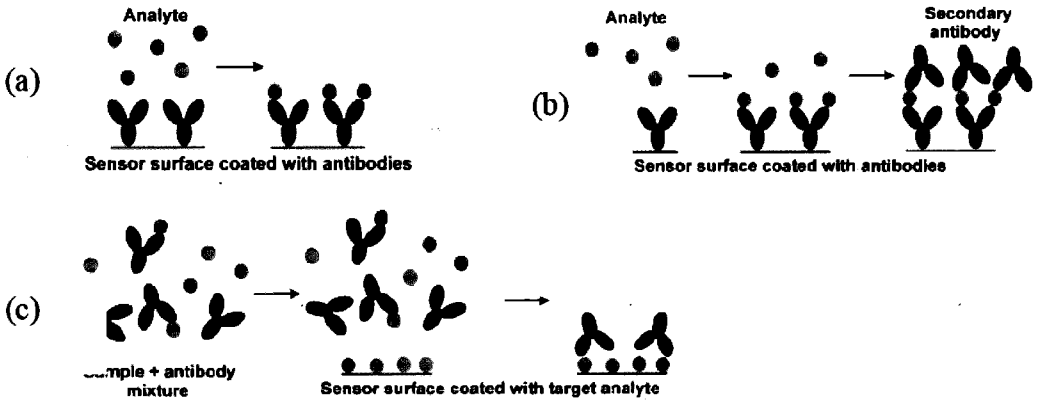

Figure 12. Different detection formats: a) direct detection, b) sandwich format, and c) inhibition format [17] (reprinted with permission from Elsevier Limited).

1.6.2 Biomolecular Recognition Elements and Immobilization Techniques

Another important factor in biosensing is the biorecognition element. Selecting a relevant biorecognition element ensures that the binding interactions take place. In principle, one of the biorecognition elements or target molecules is immobilized on the sensor surface and the other molecule is contained in the sample. The choice of the molecule to be immobilized depends on the detection format, characteristics of the study and performance of the sensor surface. The choice of an appropriate biorecognition element can vastly affect the performance characteristics of the sensor surface such as sensitivity, specificity, and limit of detection [19]. In this section, biorecognition elements, immobilization techniques, and the property of the sensor surface especially the non-specific adsorption on the surface, will be discussed.

1.6.2.1 Biorecognition Elements

Various kinds of biorecognition elements have been employed in SPR biosensors. Antibodies are one of the most common types, as they offer high specificity and affinity against different target analytes. Also, antibodies against different target molecules are commercially available [20, 21]. Another type of biomolecular recognition element is peptides. Compared to antibodies, peptides are generally more stable, less expensive, and easier to use [22, 23]. Also, DNA and RNA apatmers, single-stranded oligonucleotides can be manipulated to bind to different molecular targets, tissue, and organisms [18].

1.6.2.2 Immobilization Techniques

In order to prepare a surface for biosensing, one of the interacting molecules is immobilized on the sensor surface. The surface chemistry has to be designed in a way that provides immobilization of a sufficient number of biomolecular recognition elements on the surface while minimizing nonspecific adsorption (which will be discussed in the next section). The immobilization can directly take place on the surface which is known as a more straightforward method compared to using a three dimensional matrix. The number of accessible biorecognition elements is, however, limited by the capacity of the sensor surface. Immobilization on a three-dimensional matrix, such as using carboxymethylated dextran, provides more binding sites on the sensor surface [24]. For two-dimensional immobilization surfaces, self-assembled monolayers (SAM) of alkanothiolates or disulfides on the gold surface have been widely used [3].

The key parameter in selecting the appropriate immobilization techniques is based on physical adsorptions, electrostatic interactions, hydrophobic interactions, and covalent bindings [18].

1.6.3 Non-specific Adsorption on the Sensor Surface

The last factor of interest is the property of the sensor surface, specifically; non-specific adsorption. The adsorption of the protein has been a major concern for biological applications. Non-fouling surfaces are one of the primary challenges for affinity biosensors, especially SPR sensors [25]. This is a more complex problem when complicated mixtures such as blood are required for investigations. It is especially

important to create non-fouling surfaces which also provide abundant binding sites so that a complex mixture with specificity and sensitivity can be applied. One of the options to create nonspecific adsorption is to use hydrophobic polymers such poly-ethylene glycol (PEG). These types can be used to design a protein-resistant coating on the surface for SPR detectors. The key parameters that qualify PEG molecules are steric-entropy barrier characteristics and a high degree of hydration [26].

1.7 Applications of SPR

1.7.1 Biological Measurements

The absorption of proteins on material surfaces has been a focus of many studies for several decades because of the importance of these types of protein applications in drug delivery, biomaterials, and diagnostics. Such applications continue to receive a large amount of attention [27]. Therefore, techniques that are able to monitor binding interactions and performance are the focus of most researchers. Many of the techniques such as detection of fluorescence and radioactive assays are based on labeled molecules. SPR is one of the practical methods that can directly measure the protein interaction without any labeling materials, a great advantage since the addition of labeling materials may change the interaction under study. The applications of SPR detectors range from food and safety analysis to medical diagnostics and environmental studies, which will be discussed. Although, drug delivery and medical diagnosis gained increasing potentials for SPR studies, the major emphasis will be on the medical diagnostic, especially the protein binding interactions as relevance to the focus of this thesis[17]. In that regard, there are also an extended number of studies that have been

focused on cancer makers, antibodies, drug delivery, DNA-hybridization, and enzyme-substrate interaction [28].

1.7.2 Self-Assembly of Thin Film Monolayers

As the SPR sensor characteristic exploits real-time analysis, it can be used in many applications [5]. One of the major applications is in thin film studies. The SPR sensor for the detection of the self-assembly of the thin film monolayer was first initiated by measuring the refractive index of the thin cadmium arachiadate monolayer on silver films

[29]. In most of the cases, the thickness of the film is known, so the optical constants can be determined. It can also be advantageous in forming organo-layer and multi-layer films on metal surfaces. The SPR sensor is becoming one of the most essential tools in characterization techniques. The SPR detector is receiving much interest in layer-by-layer self-assembly of complementary polymers. The self-assembly process of polyelectrolyte self-assembled film of PAA (poly acrylic acid) and PSS (poly styrenesulfonate) linear polymers and immobilized urease was studied with a SPR biosensor [30]. The formation of the self-assembly process of functionalized star polymers and valuable data about the thickness and uniformity of the layers havebeen determined by a SPR detector [31].

The improvements in sensitivity and selectivity of SPR biosensors to increase the ability to analyze multiple components for biomolecular interactions still remain as one of the major challenges in SPR studies. This project also focuses on increasing the sensitivity and selectivity of the SPR technique by incorporating the size-selective

component to complement the chemical ligation. This novel combination of physical and chemical molecular recognition for sensor development greatly enhances the sensitivity of the biosensor when screening complex biological mixtures. The ultra thin and nanoporous films were made and were characterized by an AFM tool. The two methodologies were evaluated further with a SPR tool. The chemical functionalization of the nanostructured surface was pursued by gamma-aminopropyltiemethoxysilane. The binding capacity of physically nanostructured sensor surface with chemical functionality was tested with sequential coupling chemistry and surface modification.

1.8 Significance

As part of the ongoing development in detection methods, surface plasmon resonance biosensors have been selected in this study as an analytical method, as they provides an instantaneous analysis and the ability to monitor low concentration levels without the need for fluorescent tagging. These unique characteristics allow for measuring different types of chemical or biological binding as they provide vital information in drug discovery and treatments. It is of utmost importance to familiarize students with such analytical techniques, to expand their knowledge and to gain practical skills for ongoing research in biosensing areas. The SPR machine designed in this project provides such means. Also, improvements such as increasing the sensitivity and selectivity of SPR are required in order to use SPR for analyzing complex biological mixtures. The possibility of incorporating a size-selective component onto an SPR sensor surface to provide a novel combination of chemical and physical molecular recognition was investigated. Research projects such as protein bindings can

be designed as a simple standard model to employ SPR to learn about the different limitations and constraints of certain types of proteins. Clearly, for many applications such a model seems a perfect construct for students to gain hands-on interaction with the science of biotechnology.

CHAPTER TWO
LITERATURE REVIEW

Surface Plasmon Resonance (SPR) is a widely used optical sensor for various applications and, more importantly, for biological studies. The developments of SPR as a detector, along with a literature review of the evolution of SPR including strengths and weaknesses will be explained in this chapter. The review of the commercial optical biosensor literature of the year of 2004 and 2005 collected by Rich and Myszka [32, 33] will be included in this review. This will provide a better understanding of the critical parameters in SPR experiments in order to obtain more relevant data. In addition, the applications of SPR in biological studies, specifically the protein binding will be explained.

2.1 Early Development of the SPR Biosensor

In 1975, the first optical chemical sensor was used for measurements of CO_2 and O_2 concentrations [1]. Since then, several other chemical sensors were discovered for chemical and biological studies such as ellipsometry, spectroscopy (Raman, phosphorescence, fluorescence), interferometry, spectroscopy in optical wavelength structures (grating coupler, resonant mirror), and SPR. In all of these detectors, the measurements were determined based on the natural phenomenon that occurs between the sensor and absorbed materials and reported as intrinsic values of absorbance, fluorescence, and refractive index [27].

Surface Plasmon Resonance (SPR) as one of the optical sensors, has been receiving considerable attention from researchers. This method has the advantage of

real-time binding, label-free and sensitive measurements which can reproducibly generate the results. The concept of SPR was first introduced in the early twentieth century by Wood when he first described the phenomenon of surface plasmon resonance due to the excitation of surface plasmon waves [35]. In the late sixties, Kretschmann and Ott demonstrated the excitation of surface plasmon resonance by total reflection [29, 36]. The prism-based SPR known as the Kretschmann configuration was listed as the first commercial and practical SPR detector.

In 1978, Pockars et al. suggested the use of SPR to study properties of thin films [29]. They investigated the effect of coating a thin layer of cadmium arachidate at different thicknesses on silver films. There was a significant change observed in the surface plasmon resonance with thickness variation. This study initiated the future applications of making thin monolayers. Three years later, they extended the usage of SPR for monitoring processes at the metal interface [36]. The main application of SPR was claimed by Liedberg in 1982 [37]. In their study, the Kretschmann configuration was implemented as a sensing tool for gas absorption studies. In order to test the quality and characteristics of these materials, a thin layer of these materials is formed on a noble metal layer, and even a small change in the refractive index upon gas absorption can be detected by SPR. Since then, SPR has been intensely studied and has received growing attention from the scientific community. In 1983, the initial study of SPR as a biosensor based on the Kretschmann configuration for immunosensing purposes was published by Liedberg et al. [5].

The prism-based SPR known as the Kretschmann configuration (prism-based) has been listed as the first commercial SPR detector. This configuration provides more flexibility for analyzing different studies arranged by researchers.

2.2 Commercialization of SPR Detectors

Because of all these initial observations in the process of SPR development, a Swedish company became interested in using the SPR detector as a commercial sensor to measure bimolecular interactions. It was in 1984 that Pharmacia of Sweden initialized the idea of the commercial biosensor, and two years later the Pharmacia Biosensor was developed [38]. In 1990, the BIAcore commercial biosensor and in 1994, another biosensor known as the BIAlite were developed [5]. Since then, the BIAcore sensor has been improved upon for higher accuracy, sensitivity, speed, and throughput. The current models are BIAcore 3000, BIAcore 2000, BIAcore1000, and BIAcore Quant [9, 34]. Because of the substantial interest in optical biosensors, another type of biosensor was developed by Texas Instruments, employing the same theory of BIAcore with the addition of incorporating temperature sensors to control temperature variations [39]. The only wave guide-based SPR as opposed to prism-based was commercialized by EBI, bought by BIAcore a few years later and has since become commercialized as one of the BIAcore biosensors [5].

The next step in the developments of the SPR sensor led to the miniaturization of the sensor. In some cases, the conventional SPR biosensor, like BIAcore could be cost-intensive and require large instrumentation. Therefore, the miniaturization of SPR was considered to optimize instrument sensitivity and reduce cost. After reviewing a major

amount of studies, the most practical model found was introduced by Texas Instruments and is known as Spreeta™ [40].

The Spreeta sensor-chip, as shown in Figure 13, has all the necessary components of the SPR configuration at a cost $50.

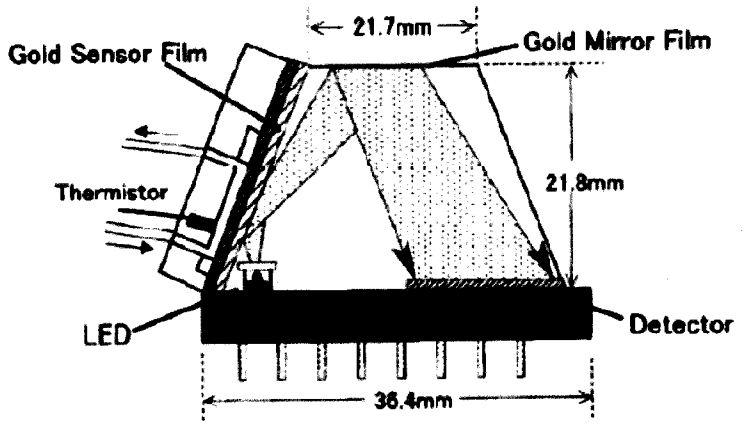

Figure 13. Structure of miniature SPR sensor Speeta [40] (reprinted with permission from Elsevier Limited).

The light source, polarizer, and photodetector are placed on a miniature platform and then "encapsulated in the optical material using a cast mold process." The size of this sensor measures only 2.2 cm height x 3.0 cm length.

2.3 Materials

Another important step in the development of the SPR was the use of noble metal films at the surface. The requirement for the SPR technique is the excitation of the free electrons on the metal surface. This is accommodated by the use of a noble metal film that exhibits free electron behaviors while restricting the type of metal surfaces employed

for this purpose. Metals like gold, silver, copper, and aluminum are good candidates for the electron excitation. The average thickness of a metal film used in SPR studies is 50 nm. Among these metals, silver and gold are the most well- known types that have been used for many experimental works. The characteristics of the metal are introduced by the "free-electron model", where characteristics are related to the propagation constant [3]. Table 1 shows the comparison of two metals (gold and silver) relevant to the propagation constant. Either a gold or a silver metal film can be applied to a surface according to measurement parameters of the experiment.

Table 1. Properties of gold and silver [1].

Metal layer supporting SPW	Silver		Gold	
Wavelength	$\lambda = 630$ nm	$\lambda = 850$ nm	$\lambda = 630$ nm	$\lambda = 850$ nm
Propagation length (μm)	19	57	3	24
Penetration depth into metal (nm)	24	23	29	25
Penetration depth into dielectric (nm)	210	443	162	400
Concentration of field in dielectric (%)	90	95	85	94

Figure 14 shows the metal thickness for gold, silver, and aluminum. The metal thickness of the gold is about 50 nm while silver is 56 nm. The use of silver leads to a more sensitive SPR sensing due to its sharp resonance peak ability of that metal. Silver, however, easily corrodes compared to gold. The metal type should be chosen in order to avoid any corrosion during the experiment.

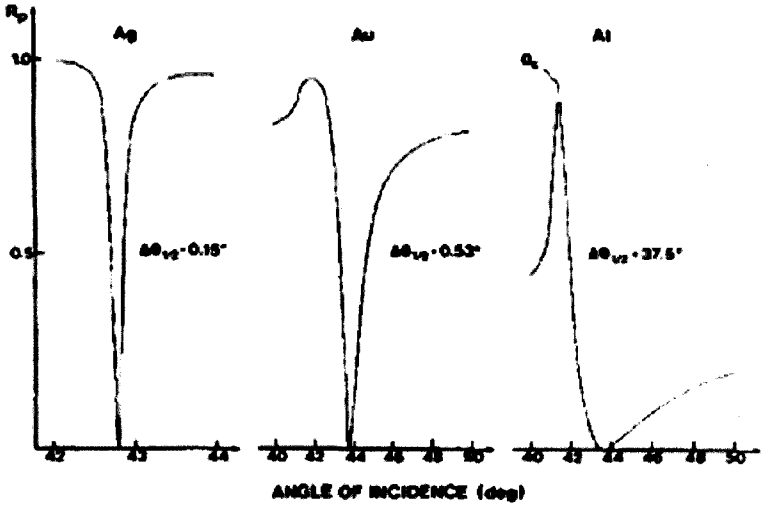

Figure 14. Calculated reflectance curves for three metals in air with metal thickness 56 nm (Ag), 48.5 nm (Au), and 8.5 nm (Al) [29] (reprinted with permission from Elsevier Limited).

All of the detectors discussed here are prism-based detectors. The most commonly used material is an optical glass. Relatively, the material of optical glass is chosen based on the analytic refractive index range covered by the detector. Therefore, the sensitivity and accuracy of the sensor are highly affected by these refractive type parameters. The two widely used, are BK7 with refractive index of 1.51 and SF11 with refractive index of 1.63 [29].

The types of materials used in the SPR instrument are required to be compatible with the experimental samples to be measured and the different measuring parameters. In addition, the quality of the biosensor data must be improved in order to characterize the binding mechanism and rate constants properly. From Myszka reviews, a number of artifacts that affect the accuracy of data will be addressed [34]. Rich and Myszka's reviews are the valuable resources for any SPR user to learn the current experimental errors and issues associated with the use of these biosensors [37, 38].

2.4 Experimental Techniques

According to Rich and Myszka, many of the artifacts associated with binding properties can be avoided by designing the correct experimental procedure. Although the commercial biosensors, such as BIAcore are simple to operate, the correct interpretation of the results is not that simple. Based on their reviews of 2006, 70% of SPR research groups took advantage of biosensors to measure the binding constants; the other 30% only presented their data in a qualitative manner [42].

Data presentation plays an important role in biosensor analysis. In principle, figures of binding responses help to better understand and interpret the quality of the experiment and validity of the data. However, only 70% of the studies included at least one figure and only 20% showed overlaid responses of different analytes together in one graph.

In this section, several important parameters that seem to be essential in achieving appropriate biosensing data will be discussed. In the survey of 2004, 2005, and 2006, Rich and Myszka presented so called biosensor myths that would help the user to prevent any existing experimental errors and flaws in the technology itself. Many of the errors are associated with improper conditions in the experimental procedure rather than flaws in the technology itself. There are several experimental parameters that can also complicate the biosensor analysis including "surface-imposed heterogeneity, mass transport, aggregation, avidity, crowding, and non-specific bindings" [34]. All of these parameters will be discussed in this section to show more clearly how to set up, analyze and interpret the results. It should be a primary goal of each user to improve the

experimental design to prevent the occurrence of the previously mentioned factors. The quality of the materials is one of the critical parameters in any experimental design which can directly affect the correctness of the generated data.

2.4.1 Interpretation of Biosensor Signals

With the new technology that was specifically provided by the BIAcore instrument, it is possible to easily obtain biological data. However, the main concern is the ability to correctly analyze the biological responses. Signal outputs from experimental artifacts such as, instrument shift, TIR shift, and non-specific adsorption can often be attributed to binding events. One needs to be more precise on how to investigate the proper binding signals.

2.4.2 Mass Transport Effect and Kinetics Data

For years, experts have been using modeling tools to extract the binding information for kinetics analysis from the mass transport responses. Perhaps users do not notice the mass transfer effects in their data and try to fit the responses to a simple 1:1 interaction model. The most apparent effect of the mass transport model occurs in the first part of the association phase in which the curve becomes more linear and the dissociation phase appears slower than expected based [33].

The next three sections are to present a better guideline of what type of sensograms to expect how to design an experiment, and how to process or analyze the signal responses.

2.4.3 What the SPR Sensogram Should Look Like

In order to investigate any study that presents a sensogram, one needs to ask first if the data presented are reasonable, second if the graphs are exponential, and third if the response intensity is reasonable. Myzka and Rich studied many papers based on these criteria. They first investigated the papers based on whether or not any graph was presented. With no figures, the quality of the experiment and the reliability of the obtained results can not be evaluated. Unfortunately, 70% of studies only showed one sensogram. Also, some of the papers did not include the data along with the sensogram. It is essential that papers present a sensogram with the data and rate constant together [32].

One common pitfall in the majority of the papers is how the sensogram is presented in the final format. In a large number of instances, the spikes at the beginning and the end of the injection phase are shown rather than zooming in on relevant portions of the sensogram. Figure 15 (a) and Figure 16 (b) show the differences of appropriate figure presentations. In Figure 15 (a), the graph completely focuses on the binding events, whereas, Figure 15 (b) presents data exactly obtained from the experiment without any appropriate adjustments.

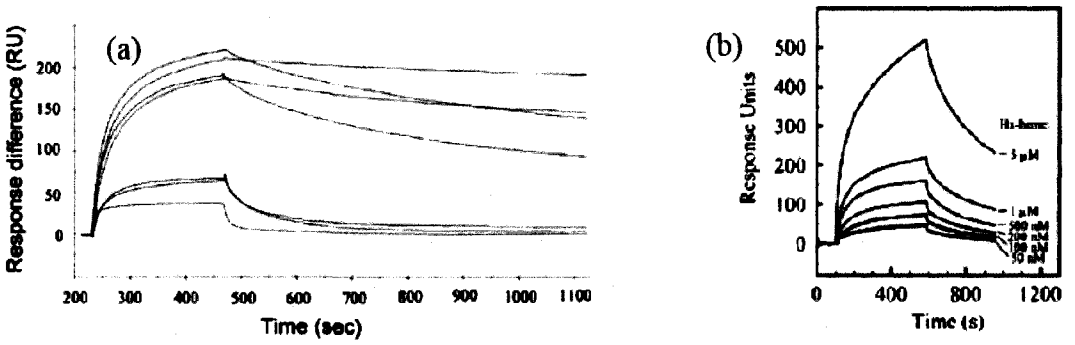

Figure 15. Responses related to emphasis on the proper part of the sensor and mostly on the sensorgram [32] (reprinted with permission from Wiley-Blackwell).

The second step is to check the shape and size of the sensogram. A simple molecular binding should provide an exponential graph, in which the responses are stable before analyte injection and the response increases as the ligand surface binds to the analyte in the association phase and decreases as the analyte dissociates from the ligand surface and washes away. This behavior is shown in Figure 16 [32].

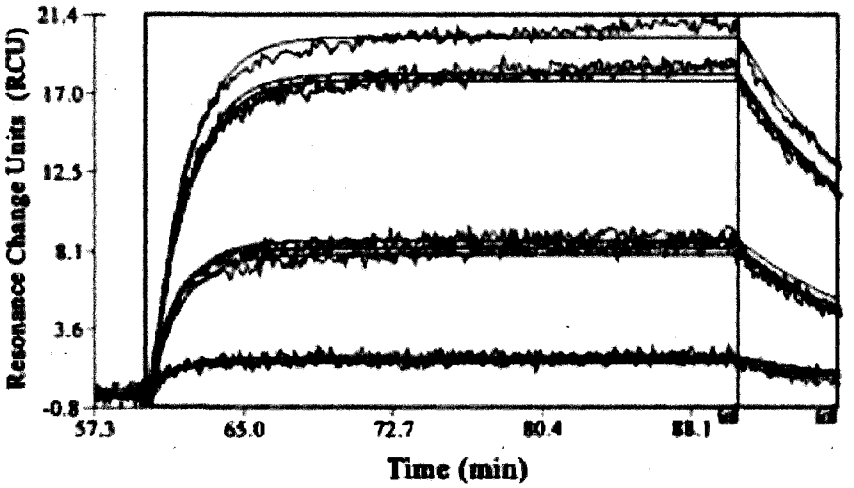

Figure 16. Behavior of binding events in association and dissociation phase [32] (reprinted with permission from Wiley-Blackwell).

The responses have to be proportional to the mass of the analyte and the density of immobilized ligand. Therefore, it is easier to evaluate the intensity of binding interactions [42].

2.4.4 How the Experiment is Designed

The biosensor is mainly used to determine kinetics and affinity constants. The performance of experimental design of any experiments can be evaluated based on the following: if the association phase includes any curvature, if there is a decay in the dissociation phase, or if the analyte concentration covers a wide range. The reason to check if the analyte concentration spans a wide range is that the analyte injection should be long enough to produce curvature in the association phase and also to observe a decay in the dissociation phase.

Since users are familiar now with the type of graph and experimental techniques, it would then be necessary to learn how to process or analyze the data, which will be explained in the next section.

2.4.5 How to Analyze or Process the Data

In data analysis, the equilibrium and kinetics data are the major focus for biosensors. Two main questions associated with the analysis are first if the data in the equilibrium analysis includes a plateau in the association phase, and second, if the kinetics data overlays with the model fit. The correct interpretation of the equilibrium analysis is one of the most common pitfalls.

The primary issue of many of the articles is the fact that many of the researchers have forgotten about the theoretical behavior of the measurements. For instance, one should understand what data to expect from a given detector for a given bimolecular interaction. The equilibrium analysis is based on how to process or analyze the data. First would be to confirm that the responses are accurately referenced. Second would be to ensure that the responses follow a plateau in the equilibrium analysis and the kinetic data fit the model. The last criterion would be to explain how a bulk-shift correction is applied appropriately. It was suggested by Persson et al. to double reference the response with small signals before fitting them to the model [32, 33].

In the equilibrium analysis, each singular response has to reach a plateau. As shown in Figure 17 (a), (b), the behavior completely follows the plateau. However, as shown in Figure 17 (c), the response has not reached the plateau and it is surprising how some of the users publish such data.

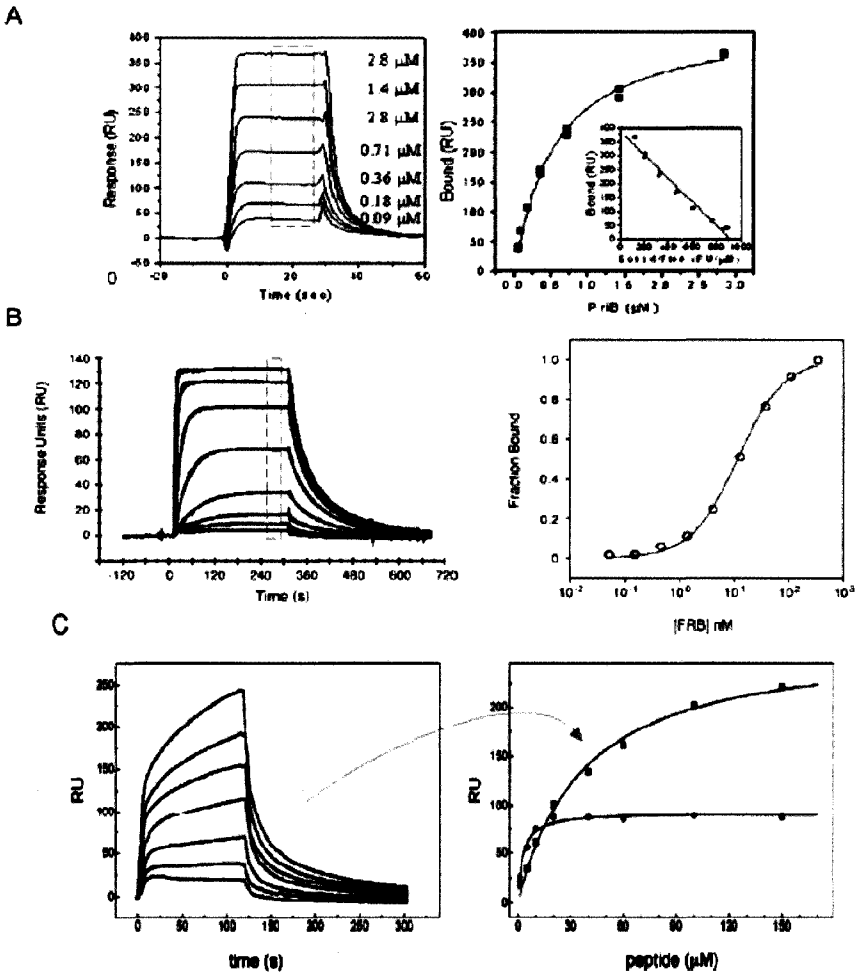

Figure 17. Fitting equilibrium responses [32] (reprinted with permission from Wiley-Blackwell).

2.4.6 Critical Parameters to Obtain Accurate SPR Results

The cleanliness of the instrument can also affect the quality of the measured data. The proper cleaning of the apparatus can reduce the chances of contamination of different materials in the flow system.

One main parameter that should be noted by any SPR user is the conformity of the occurrence of the baseline before injecting any samples. The baseline can be

generated with the choice of any compatible solvent with the testing samples. It is also important to ensure the baseline responses do not change over the course of the experiment. The baseline shift could be the consequence of temperature changes in the beginning of the experiment as the instrument begins to equilibrate [33].

The temperature effect is one of the primary concerns in the experimental procedure. The refractive index is dependent on temperature variations and any changes can affect the occurrence of the SPR angle. Therefore, the SPR is sensitive to changes in a temperature and should be properly controlled. The solution is to control the temperature with a sensor to ensure the optimum performance regardless of any changes due to temperature increase. One commercially available, regulated, and portable SPR that incorporates a temperature control is the Texas Instruments ©SPR module, Spreeta™ [39]. However, not many of the studies have illustrated the temperature effects as part of their investigation in SPR technique. There is still a need to study the effect of temperature and design appropriate protocols to control it.

Bubble formation can drastically affect the accuracy and sensitivity of the measured values, as well. This could be prevented by eliminating a bubble in a sample stream, or by drying out the flow cell. In this way, an air bubble would not go through the sample line.

2.5 Organic Thin Film Monolayers

The SPR sensor for the detection of the self-assembly of the thin film monolayer was first initiated by Pocket el al. to measure the refractive index of the thin cadmium arachiadate monolayer on silver films [29]. The formation of a thin film led to the next

concept of the self-assembly of thin film monolayers. In 1998, Beketov et al. studied self-assembly of poly acrylic acid and polystyrenesulfonate polymers [30]. The formation of the layer was investigated using a SPR and a shift in SPR angle due to the subsequential layer formation of polymer was determined as the thickness of the polymer layer. In addition, the morphology of the surface was determined, as shown in Figure 18 . In comparison to the gold substrate, an SPR curve for the layers has a broader plasmon, meaning that the surface is significantly rougher than the gold itself.

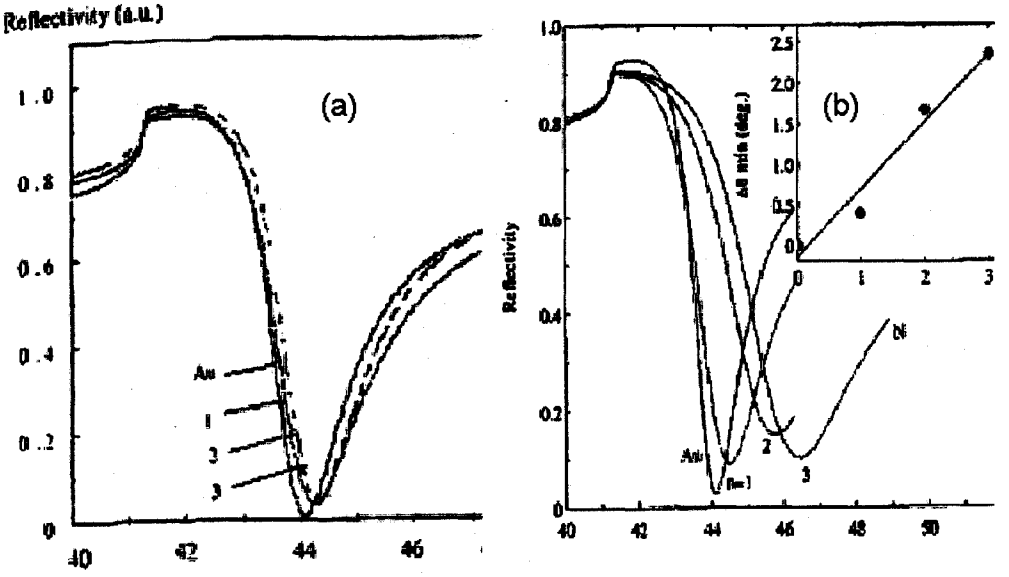

Figure 18. a) SPR curve of gold with three layers of LBL self-assembly process and b) SPR curves of the same experiment with different layers as immobilization layer [30].

Also, some researchers are investigating the use of micropatterning the sensor surface in order to create multi-channel capabilities. Ho-Choel et al. introduced a method to produce hydrophilicity-contrasted patterns on porous films [43]. The porous thin films were generated by the removal of the organic polymer, known as porogen, from

nanohybrid of poly (methylsilsequioxane) (PMMSQ). The patterns of contrasted hydrophilicity were achieved by UV/ozone treatment. The nanoporous structure provides more reaction site, this was tested with the intensity of a fluorescent dye attached on patterns [43].

2.6 Drug Research and Development Using SPR

The development of the SPR biosensor to analyze biological interaction for medical and commercial use has generated extensive interest for both science and industry. The applications of SPR in drug delivery and biological studies are of primary interest to researchers. Among all the biosensors, SPR has shown to be the best potential instrument to use for direct measurements in the evaluation of biological interactions. With a SPR sensor there is a real time binding, which allows immediate detection and evaluation of the properties and materials, without the constraints of labeling that is common for many other techniques.

Different types of biomolecular interactions have been studied using the SPR detector such as antibody-antigen, receptor-ligand, and hormone-receptor binding. In this section, the protein binding interaction of streptavidin-biotin and immunosensing will be reviewed.

The use of an antibody as a detection element, known as immunosensing is one the main interests of this project. The initial study of immunosensing was carried in 1983 by Leidberg et al. [5]. The silver deposited on the microscope slide was used as a sensing surface. The antigen (immunoglobin in this case) was adsorbed on the silver surface. The subsequent binding of an antibody, a-IgG was detected with SPR, as shown in Figure

1[1]. This experiment was a driving force for the later development of a practical immunosensor. As mentioned in Section 2.2 the most developed type of commercial bio-detector known as BIAcore has been used to investigate the biomolecular interactions [44].

2.6.1 Biosensor Surfaces

It was found that the metal surface for SPR is not compatible with biological systems and the immobilization of bimolecular interactions directly on the metal surface is not appropriate because it causes lower sensitivity and detection. Therefore, various types of surface chemistries have been developed for this purpose [45]. The majority of studies employed standard dextran surface as their immobilization technique; however, direct immobilization was used the majority of the time. In general, 90% of users preferred to immobilize the ligand through amine coupling, although a few groups used thiol coupling. Later in 1988, Daniel et al. applied avidin-biotin and fetoprotein antibody-antigen as a model system to increase the surface detection [45].

Morgan et al. proposed one approach for stable and defined binding to use a streptavidin monolayer immobilized onto a gold film on biotin [46]. Another is to form a self-assembled monolayer (SAM) of thiol molecules [45, 46]. Haussling and coworkers first suggested the use of biotin functionalized self-assembled monolayer. The monolayer of thiols on gold is a good example of the SAM process [47]. Although the interaction of biotin-streptavidin has been known for a while, the biological meaning has not been understood completely. In Figure 19, the binding interaction of this compound is illustrated. Curve II demonstrates the adsorption of an incomplete monolayer of thiol

and curve III exhibits the subsequent adsorption of a layer of streptavidin. The shift is observed as the streptavidin binds to the biotin based on SAM.

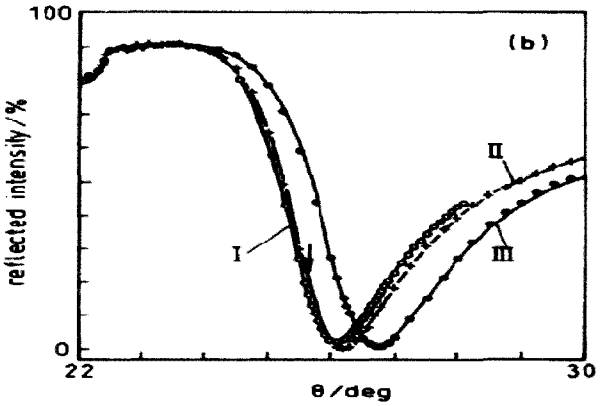

Figure 19. Behavior of streptavidin–biotin bindings [46] (reprinted with permission from Elsevier Limited).

In more general terms, the real-time bimolecular interaction analysis (BIA) of antibody (ligand) on a sensor chip with the antigen (analyte) flowing continuously was studied by Lofas and Johnsson [47]. Figure 20 illustrates the simple binding of antibody and antigen. After the sample is injected, the association of the analyte to the ligand is observed, and the response is increased in response unit (RU). After this, the dissociation phase confirms the decrease in the response of the analyte to the ligand. This graph is acceptable compared to the conditions introduced in Section 2.4.3. The shape of the sensogram is exponential and the responses increase in the association phase and decrease in dissociation phase. Even though each singular response has to reach a plateau, this curve could have been stopped by users before showing the complete

plateau. Nevertheless, the trend shows that the curve is progressing towards a complete plateau.

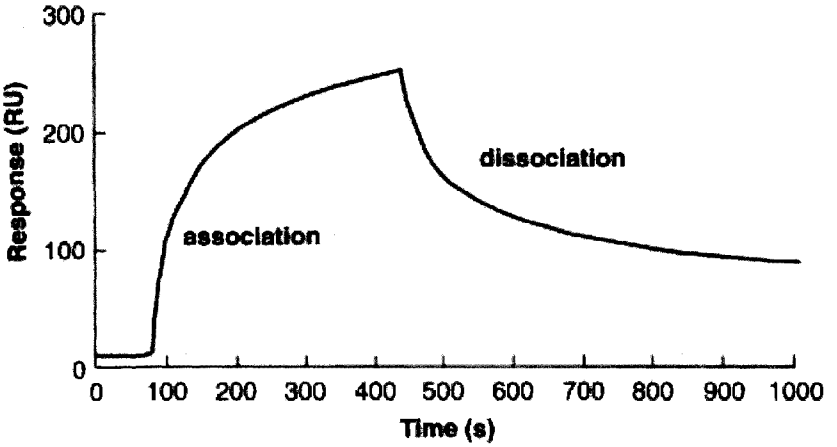

Figure 20. In this figure, the simple sensogram illustrated the binding of antibody-antigen [46] (reprinted with permission from Elsevier Limited).

The data collected from the two phases can be used to calculate the rate constant of the binding interaction. The kinetic theory of the antigen-antibody interaction was first analyzed by Karlsson et al. [46]. In his analysis, the adsorption of analyte to the ligand follows the first order reaction kinetic. In some cases, there may be deviations from the kinetic model. These include the mass transport limitation, the rebinding of the released antigen during the dissociation phase, and the heterogeneity of the immobilized ligand.

CHAPTER THREE
OBJECTIVES

The main objective of this project was to design and set up a viable, robust, and accurate SPR instrument that could be used as a teaching tool for engineering students. The capabilities of the SPR design components to detect surface changes by varying the angle of incidence at the fixed wavelength of 635 nm were assessed by 1) measuring the TIR, 2) obtaining the air plasmon, and 3) studying the effect of different solvents on the SPR output.

The possibility of increasing the sensitivity of the SPR sensor surface was investigated by incorporating a size-selectivity component onto the SPR sensor surface. The purpose of this study was to provide a novel combination of both chemical and physical molecular recognition in order to monitor complex biological mixtures.

The surface modification and coupling chemistry were performed on the surface to evaluate the binding capacity of the nanostructured sensor surface.

CHAPTER FOUR
MATERIALS AND METHODS

The proposed experimental design and setup of the SPR apparatus is based on the Kretchsmann configuration, as described in this chapter. Additionally, the major components that have been selected, in particular the significant elements to facilitate this experimental design, are discussed in detail in order of importance. The criteria used for the selection of major components along with the factors employed in designing the SPR detector, will be further addressed in the Results and Discussions chapter. The crucial ingredients of the SPR design optics, flow cell, and data acquisition were studied. Finally, the nanostructuring of the SPR substrate and binding interaction based on the created nanosurfaces were studied by implementing SPR design to demonstrate its applicability and accuracy in coupling chemistry.

The process of creating a nanoporous SPR substrate is discussed here. Characterization tools such as SPR and AFM were used to determine the behavior of the sensor surfaces and morphology of the surface. The surface modification and coupling chemistry were further done on the surface to investigate the binding capacity of the films with series of typical chemistry coupling. The Processing conditions of how to build successful layers for increasing the sensitivity and selectivity of an SPR substrate are explained here. Table 2 includes the experiments run to understand the behavior of the newly designed SPR and to check the functionality and accuracy of the setup. These sets of experiments had to be considered before employing the SPR machine for any biological applications. Table 3 is an experimental matrix showing the framework of the

main experiments to achieve the targeted objectives. First, the experiments were designed to achieve a desired film thickness by changing the concentration of methyl silsesquioxane (MSSQ). An ellipsometry technique was used to measure the thickness. Second, the process of producing different porous films was verified by SPR measurements and an AFM tool. Third, the created porous films were used to study further non-specific adsorption and biological bindings. The results provided information on increased detection of protein bindings using nanoporous film compared to usual SPR substrates introduced in other studies.

Table 2. Experiments to investigate the behavior of the SPR machine.

Experiments	Surface Layers	Exp.	No. of runs	Output/Analysis
To check the TIR	SF11 wafer/ SF11 Prism	1	3	• To achieve an accurate TIR that matches the theoretical value
	SF11 full radius prism*	2	3	• To monitor the effect changes in TIR curve and Brewters's angle with no gap between the wafer and prism
Air Plasmon	BK7 wafer with stack of Cr/Au/SiO_2 (SPR Substrate)	3	3	• To ensure the functionality of the optical system and obtain air plasmon with SPR substrate
	SF11 wafer with stack of Cr/Au/SiO_2 (SPR Susbtrate)	4	3	• To ensure the functionality of the optical system and obtain air plasmon with SPR substrate

* A Full radius has the radius of 0.365 which equals the radius of a normal prism, wafer and index matching fluid combined.

Table 3. Main experimental matrix to study the effect of nanoporous films and biological bindings

Experiments	Surface Layers	Exp.	No. of runs	Output/Analysis
Control the thickness of nanoporous film on substrate stack	MSSQ/PM Acetate on SPR substrate*	5	3	• To find an optimum concentration of MSSQ to produce a thin film
Nanostructured Porous films	SPR substrate/ Porous films (Porogen)	6	2	• To monitor the effect of different porosities and shift in SPR angle
Stability study of porous films	SPR substrate/ Porous films (Porogen)	7	2	• To ensure the Stability of created porous films before testing with biological compounds
Surface modifications and coupling chemistry	SPR substrate/Porous films/	8	3	• To test the performance and binding capacity of the sensor surface

* SPR substrate ($Cr/Au/SiO_2$)

4.1 Materials

The materials that will be discussed in this chapter are divided into two categories: 1) SPR design and set up and 2) nanoporous SPR substrate. They are presented in order of importance for designing a SPR machine.

4.1.1 SPR Design and Set up

This section will focus on the three main parts of the SPR sensor known as optics, flow cell design, and relevant mechanical components to rotate the flow cell.

4.1.1.1 Optics

Establishing the main components of any SPR detector begins with the selection of the optics. The SPR was designed based on the Kretchsmann configuration. The major optics that were selected included a laser, mirrors, lenses, and a calcite polarizer. The optic components such as the laser and mirrors were purchased from THORLABS. The laser chosen for this setup was a 635 nm diode, 1 mW collimated. The four mirrors were 1.0 inch Broadband. These are the four essential optics for this design, chosen to transfer light from the source to the detector. A complete overview of the optical path selected for this design will be explained briefly and a detailed explanation will be provided in Results and Discussion chapter. The overview of the optical path is shown here in Figure 21.

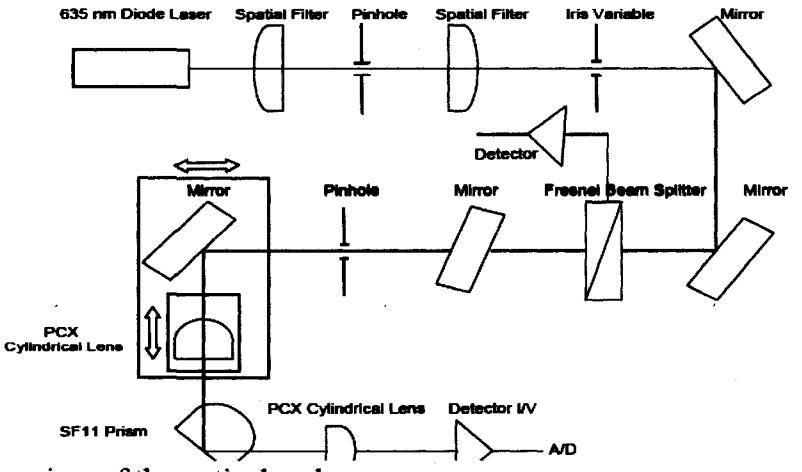

Figure 21. Overview of the optical path.

It can be seen that the path starts from a laser source, passes through plano-convex spherical lenses, a pinhole, a variable iris, and then hits the first mirror. The light reflected from the mirror strikes the second mirror, goes through the polarizer and hits the beam splitter. The out beam of the beam splitter is divided into two separate beams. One is collected by the detector to measure the noise of the system. The other beam continues through the pinhole and hits the fourth mirror and traveled through the first plano-convex cylindrical lens and strikes the center of the SF11 hemicylindrical prism. Then, the light goes through a second cylindrical lens and is collected by the photodetector which is placed right after the lens at the same height chosen. The fourth mirror and the first plano-convex cylindrical lens are placed on a moving rail to facilitate the alignment technique. Also, the second cylindrical lens is placed on a moving rail to obtain a good collimation on a prism. Each optical component with the detailed selection criteria is provided in the next chapter.

The SPR sensor was designed based on the Kretchsmann configuration (Prism-based type). This would lead to a design of the flow cell that will be explained in the next section.

4.1.1.2 Flow Cell

In order to perform any testing or experimental procedure in SPR detectors, in order to facilitate any testing or experimental procedure an essential component known as a flow cell is required. In general, either a custom-designed flow cell or a readily available type known as BIAcore will be part of a SPR set-up. Many SPR users use a BIAcore flow cell due to the convenience of purchasing the complete format which can

be found in different varieties depending on the nature of the molecule that needs to be coupled to the surface [9]. There are some disadvantages, however, associated with this type. They come with a limited lifetime and expiration dates. Also, if the sensor is damaged after the experiment sets, it has to be replaced. As this project has been considered as a teaching tool to be used to study different binding structures, it would be wiser to implement a self-designed flow cell rather than the ready made BIAcore chip.

The flow cell used in this project is an in-house design by Dr. Michael Jefferson at IBM Almaden in San Jose. The flow cell was designed to ensure accuracy and compatibility with an overall setup and is easy for any user to employ. The flow cell is implemented in the SPR apparatus to facilitate the measurements of the samples. It has a rotational configuration which complements the optical configurations in order to obtain an accurate light transformation to observe the surface plasmon phenomenon.

The three main components associated with the design of the flow cell are 1) a step motor system (DAEDEL), 2) spindle, gears, bearer, and 3) encoder shown in Figure 22.

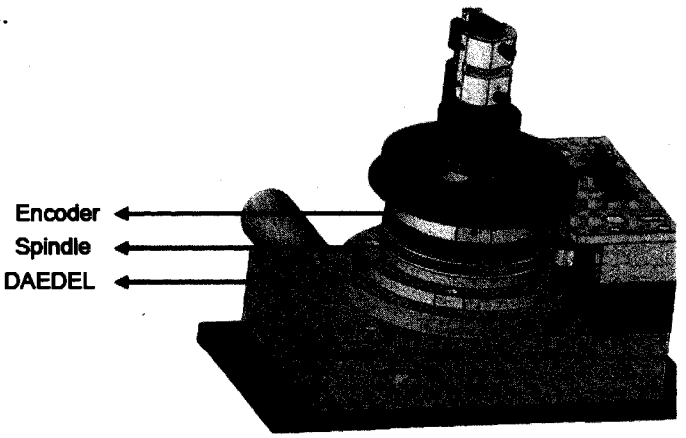

Figure 22. The schematic of flow cell design step motor, spindle, and encoder (reprinted with permission from C.M. Jefferson).

The DAEDEL motion controller, with the flow cell mounted on top, moves the complete stacks of all the different parts. The stepper motor controller is connected to the computer through an interface called motion control. The rotator moves 12,500 steps per one degree, which provides the flexibility of moving the prism in order to find the exact SPR angle.

The spindle was incorporated as the center piece and connected to the cell on one side and the motion controller on the other side. The gear on the spindle connects to the gear on the bearer. The detector that collects the generated signals is placed on the bearer and rotates freely with a constant value of 2x of the rotation of spindle through the placement of gears on the bearer. Essentially, the rotation from the step motor transfers to the spindle, through the sets of gears included on both the spindle and bearer that moves the flow cell. The precise movement of the spindle plays an important role in the overall accuracy of flow cell rotation which is conducted by including an encoder from Renishaw which has an optical home position with an arc to second positioning, allows for the accuracy of the spindle measurement.

The key factor to remember in any flow cell design is the concept of light transformation on the prism of the cell. The light has to hit the surface exactly at the center. The center of the rotation or the cell could be placed in a way to meet this requirement. The main focus of the new design was to apply an extreme mechanically fabricated and precise methodology so the spindle would stay on the center. The overall configuration of the design is shown in Figure 23.

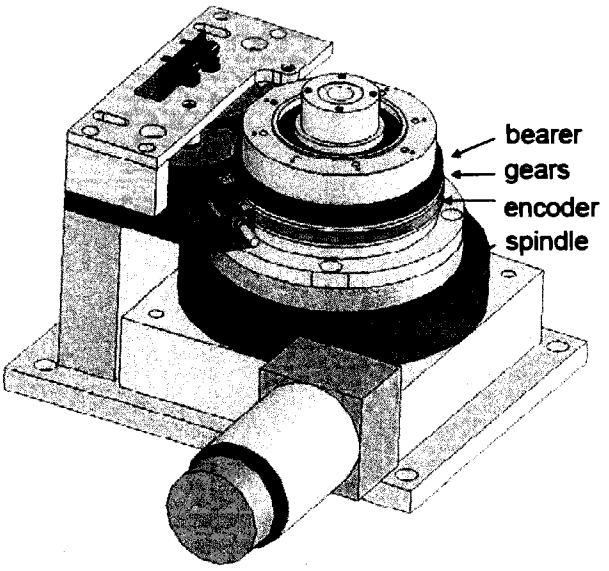

Figure 23. The overall configuration of mechanical components (reprinted with permission from C.M. Jefferson).

As a result, the center of the rotation from the bottom parts had to be transferred up to the center of the cell holes concentric to the location of the sample without introducing any tilt. All of the parts related to the design of this section is shown in Figure 24 below.

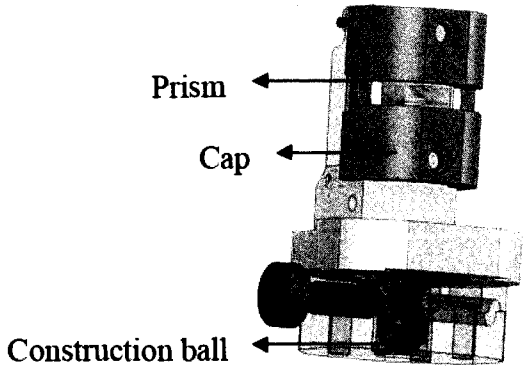

Figure 24. The main components of the flow cell design (reprinted with permission from C.M. Jefferson).

To achieve this, a construction ball shown in red which has a precision fixture was adopted in the setup with a diameter well fixed and concentric with the center of the rotation. The axis of the ball goes through the center of the prism. Another orthogonal constraint was a cap (in orange) placed on the prism. The cap was constructed by a precise mode of wire EDM (electrode discharge machining) which offers a process accuracy of less than 5 microns, but keeps the whole component from moving around.

In the new design a true kinematics positioning, meaning any constraint has to be unique, was considered. As a result, the entire system is precisely located in a space which will be easily reproducible to make. The light transformation on the center of the prism can easily be achieved by initially aligning the system so that the light appears on one plane. This will be explained further in optical alignment in chapter five.

In addition, the flow cell was designed with elliptical dimensions, allowing a smooth fluid movement to prevent bubble formation. The other advantages of the new design are that the flow cell can be easily removed; it is more convenient to place the substrate and any essential elements. It should be noted when placing a substrate on the flow cell, the system has to be under vacuum to hold the substrate in place. This would avoid any extra movement of the prism which can result in mispositioning the liquid index matching fluid and not forming a smooth layer on the substrate. The index-matching fluid is also required to match the refractive index of the solutions depending on the usage of SF11 or BK7 substrate. As already mentioned, bubble formation can drastically affect the measurements; therefore, extra cautions should be taken when placing a prism on the substrate.

As the light reflects out of the prism, a photodetector implemented in the system will collect the reflected light as an output signal. The output signals will be observed as the data point and curve through the data acquisition called LabView. The signal generated is known as an analog signal which needs to be changed into digital signals to be compatible with data processing on the computer. For this matter, a digital/analog interface (A/D controller) purchased from National Instrument was used in the apparatus. The interface was connected to the computer and also to the photodetector that was used to collect the generated signals. The data acquisition program, so called LabView, was used to program all the features for the analog to digital converter as well as the rotation of the flow cell. A brief explanation of the software is included in the Materials and Methods chapter.

4.1.2 Nanostructuring SPR Substrate

Two common types of substrates used in the SPR apparatus are BK7 and SF11. The type of prism is dependent on the refractive index of the prism in the apparatus. Two types of wafers were purchased in the beginning for the experiments: Schott SF11 wafers and BK7 wafers. The optical system explained above was set according to the SF11 prism as the final configuration. Prior to changing to the SF11, however, the experiments were conducted based on BK7, which means using a BK7 wafer, and prism. BK7 is borosilicate optical glass with an index of refraction (n) 1.515 at 635 nm wavelength at 25 ^{0}C [48]. The BK7 wafers are 1.0 inch in diameter and 0.5 mm thick and were purchased from Esco products. When using BK7 for the initial experiments, it was observed that the SPR angle occurred at the limit of the SPR instrument and a full scan

could not be measured. As a result, the system was switched to an SF11 wafer with the necessary optical parts. The SF11 wafer was used in this project to correlate the SF11 prism and index matching fluid which was used to build a consistent layer throughout. SF11 is a dense silicate glass with less than 47% of lead oxide (PbO) and has an refraction index (n) of 1.778 at a wavelength of 635 nm at 25 ^{0}C [48]. The wafers are 1.0 inch diameter and 1mm thick with a surface roughness (root mean square, RMS) of less than 10 A^{0}. After the selection of the proper wafer, the standard micro fabrication technique, which is a standard in-house procedure at IBM, was applied to prepare the substrates. One side of the SF11 glass was coated with a 3 nm adhesion layer of chromium (Cr), followed by a 50 nm layer of gold (Au) using an in-house thermal evaporator, and then the samples were further sputtered with 4 nm of silicon dioxide (SiO_2) using an in-house AJA SiO_2 sputtering tool.

Methyl silsesquioxane (MSSQ) contained in LKD-2015 was purchased from JSR. Propylene glycol monomethyl ether acetate (PM Acetate) and propyl glycol n-propyl ether (Dowonal PnP) were purchased from Aldrich. Star polymer porogens were synthesized at IBM Almaden in San Jose by Victor Lee [49]. Porogen star polymers consist of a polystyrene (PS) core and a poly ethylene glycol (PEG) periphery. The PEG arm has M_w of 5 k, and PS core and arm has M_w of 600 k and 15 k, respectively.

One other set of materials was used in this thesis for the layer by layer (LBL) process to only test the functionality of the overall setup and kinetics mode of the software. The information provided here is based on the thesis work of a graduate student, Cecile Bonifacio [31]. The LBL process of building multilayer polymeric film

using functionalized star polymers was adopted. The LBL technique was achieved through electrostatic interaction of polystyrene amine (PS-NH_2), and polystyrene carboxylic acid (PS-COOH) star polymers as shown in Figure 25.

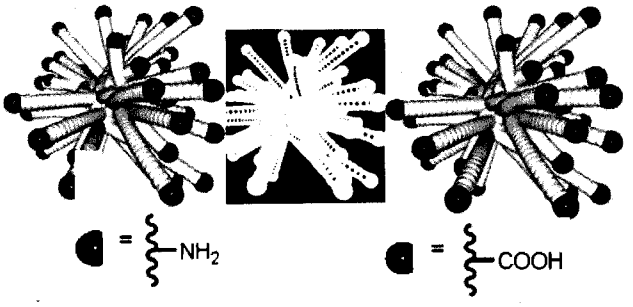

Figure 25. LBL technique using electrostatic interaction between PS-NH_2 and PS-COOH star polymers [31] (reprinted with permission from J. Sly).

4.2 Methods

4.2.1 Data Acquisition-LabView

For any analytical tools, it is essential to transfer real world signals to more meaningful information in order to study the behavior of the process. For instance, in an SPR sensor, the reflected light that is transferred to measurable signals through the photodetector has to be generated in a format so that the user can study the desired parameters. For this purpose, the data acquisition called National Instrument LabView was used to create a flexible and scalable design and test applications. LabView is a graphical programming language that has a wide range of features. It can gather thousands of data in a short period of time and this can also be used for the most complex systems. The software was used to write and generate the necessary function that can perform the required tasks. The author implemented different codes for measuring different parameters required for this project. The primary usage of the program was to

convert the signals to the curves that will demonstrate the changes of intensity versus the angle of incidence. In this work, the partial alignment of the system was achieved with some key features of this program.

4.2.2 Substrate Preparation

The choice of substrate is determined by the type of interaction and analytical method. The substrate that was used for this study was SF11glass deposited with gold (Au) followed by silicon dioxide (SiO_2) as a top layer. Prior to metal deposition by thermal evaporation technique, the SF11 wafer had to be cleaned. According to the procedure in literature, a gentle manual cleaning with a combination of commercial grade polished SF11 glasses presents better surface uniformity than using the ultrasonic automation technique [50]. The SF11 glasses were coated with a 3 nm Cr adhesion layer and 50 nm Au layer, and then immediately sputtered with 4 nm of SiO_2. Both pieces of equipment were existing pieces in-house and the process was conducted under a vacuum to prevent contamination on the surfaces. Prior to using any of the prepared substrate, substrates were treated by UV/ ozone to remove organic debris and were rinsed with Millipore water, blown gently by nitrogen line, and rinsed further with pure ethanol to remove any water residue from the surface. The final samples were placed in a wafer holder and wrapped in aluminum paper for later usage.

4.2.3 Substrate Placement in the Flow Cell

The choice of the material for substrate and prism in the SPR instrument was SF11 to meet the required optical index matching. It can be seen in Figure 18 (a) the top

part of the flow cell is detachable to provide a convenient means for locating the substrate before the placement in the setup. The SF11 substrate shown in Figure 18 (b) was placed with the metal coated side down on the flow cell and approximately 5 μL of refractive index matching fluid was dropped on the top of the uncoated side of the substrate. The index matching fluid is purchased from Cargille with specific refractive index of 1.7650 which correlates with the optical index matching. The drop should be adequate to cover the surface, while the excessive amount should be prevented so that a smooth layer can be formed. A SF11 hemi-cylindrical prism was slowly placed on the SF11 substrate as shown in Figure 26 (c). This was done carefully to avoid any bubble formation in the index matching fluid between the prism and the substrate. The cap was tighten with two screws to ensure that there is no displacement of the prism nor the substrate. The substrate is held in place with the O-rings, as shown in Figure 26 and spring in the back to fasten the position. The O-rings seals are Perlast- high performance perfluoroelastomer O-rings, which are resistant to a wide range of chemicals. In the case of solvent injection, two fluid ports were incorporated, as shown in Figure 26 with the inlet and outlet lines to deliver the solvent of interest to the flow cell.

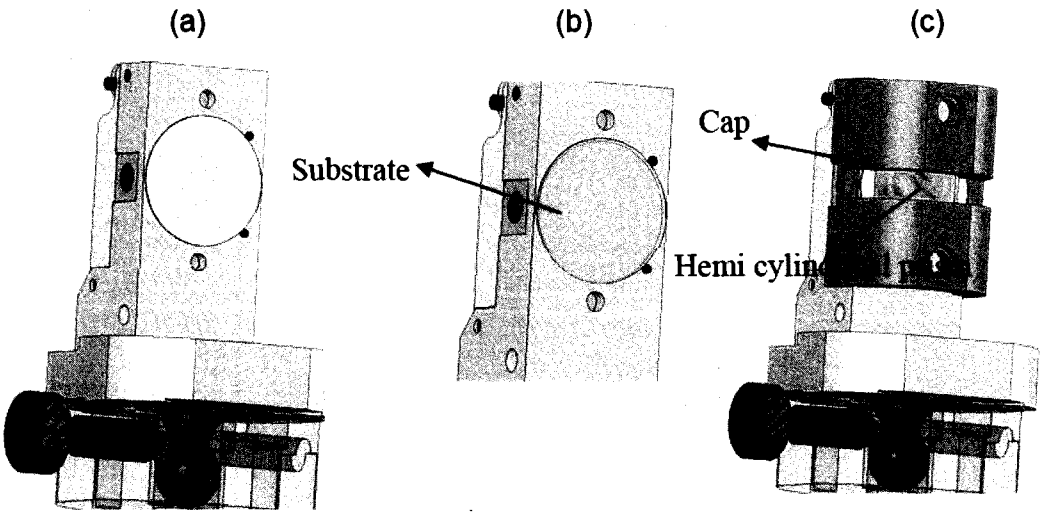

Figure 26. a) Top part of the flow cell is used to place the substrate, b) substrate placement, and c) the prism and cap are placed on the substrate and are fixed with two screws (reprinted with permission from C.M. Jefferson).

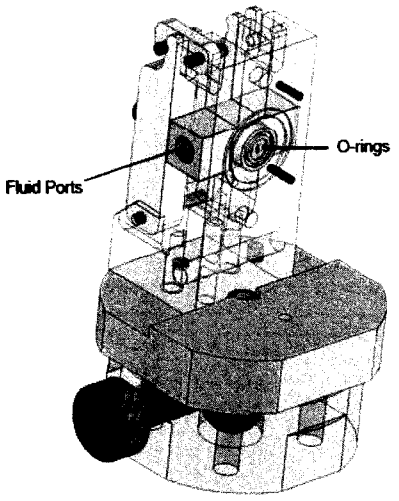

Figure 27. O-rings and fluid ports (reprinted with permission from C.M. Jefferson).

4.2.4 Ultra Thin Film Preparation

A solution of MSSQ and Dowonal PnP was first mixed based on a desired thickness of thin films and was gently mixed with a wrist action shaker. The optimum concentration of MSSQ- LKD 2015 for this study was found to be 2.5 wt %. Samples

were then filtered using 2 μm Teflon filters. The solution was spin coated on substrates using a Headway Research thin film spin coater at a rate of 3000 RPM for 30 sec. The samples were then thermally cured using a VWR programmable hotplate which formed organosilicate. The hotplate temperature started at 50 ^{0}C, was raised 5 ^{0}C per minute, reaching 450 ^{0}C after 1 hour and 20 minutes and held at 450 ^{0}C for 1 hr. During thermal curing, samples were place under nitrogen to prevent any contamination. The dense thick film was also prepared in the same manner using 21.5 wt % concentration to obtain a refractive index of the thick film.

4.2.5 Porous Film Preparation

A porous film was prepared using star polymer porogen and LKD 2015 and PM Acetate solvent. Based on a final thickness of the thin films the concentration of LKD had to be determined. According to the final decision of using a 2.5 wt % LKD 2015, PM Acetate was used to dilute MSSQ 21.5 wt % to 2.5 wt %. The dissolvability of star polymer in MSSQ is exceedingly sensitive to water. So, the MSSQ had to reach room temperature to avoid water moisture in the mixture. Porogens were dissolved in PM Acetate to make a 2.5 wt % porogen solution. Due to the presence of star polymer, the solution takes a longer time to dissolve, and it is important to ensure the polymers are completely dissolved. The wrist shaking technique can help dissolve particles, or if a stronger force was needed, then a heat gun and sonication could be applied as well. Based on different porosity of the thin films (once a porogen loading was determined), a new solution was prepared where the percent loading consists of 2.5 % porogen and

2.5 wt% LKD 2015. The final solution was spin coated and thermally cured which upon the curing, formed a random porous film.

4.2.6 Characterization Methods for Porous and Nonporous Films

A filmetrics thin film analyzer and Gartner ellipsometer were used in thick film and thin film analysis, respectively. The contact angle of the samples was measured by an Olympus light microscope with a 20X objective lens and an Olympus digital camera. Also an atomic force microscopy (AFM) was used to determine the roughness and morphology of the samples.

4.2.7 Chemical Functionalization with APTMS

Chemical functionalization of the sensor's surface was achieved with APTMS using vapor phase silylations. The vapor phase silylations involving vacuum distilled γ-aminopropyl trimethoxysilane (APTMS) were conducted on a YES Model 1224 chemical vapor deposition system. This system has an approximately 80 L oven chamber and allows for direct delivery of the reagent from the source bottle to the vaporization flask and then the oven chamber without exposure to moisture.

Sample specimens were placed on an electropolished stainless steel tray holding up to 25 specimens and placed into the oven chamber. To facilitate the removal of any surface moisture and water vapor, the heated chamber was then pumped down and refilled with preheated nitrogen. This cycle was repeated twice. Following the last dehydration purge, the system was pumped down to 1 torr and the silylation agent was pumped into the vaporization flask and delivered into the chamber. 60 pulses of APTMS

were delivered into the vaporization flask amounting to 5.0 gm of reagent and giving rise to a chamber vapor pressure of 9.05 torr at 150 ^{0}C. Vapor exposure time is variable, but in this case was fixed at 30 minutes. Following the vapor phase silylation step, a triple pump down/nitrogen filling cycle was employed to insure complete removal of any excess reagent vapor prior to opening the oven chamber.

4.2.8 Coupling Chemistry on the Surface

The surface chemistry on the SPR substrate was performed with amide reacted between primary amine and activated succinimidyle ester and carboxylic acid esters. The reagents used for the sets of reactions were *N*-Boc-protected succinimidyl ester of L-alanine (0.2 g), dichloromethane (CH_2Cl_2) (5 mL), Net_3 10% (5 mL), and TFA 10% (0.5 mL), prepared at room temperature (RT) for 18 hrs. The other reactions were carried with dye molecule, of 7-diethylaminocoumarin-3-carboxylic acid, succinimidyl ester (0.2 g) and CH_2Cl_2/Net_3 (5.5mL).

4.2.9 Layer by Layer Process *In situ*

The solutions of amino and carboxylic acid star polymers were prepared with a 1:1 weight per volume ratio of star polymers and solvent dichloromethane. The layer by layer process (LBL) deposition was achieved through a flow cell in the SPR *in situ* experimental setup with manual injection. The SPR substrate was placed in the flow cell with the extra layer of refractive index matching liquid (same as SF11:1.76) on top. The *in situ* process of LBL began with a surface preparation and solvent exchange of dichloromethane with a THF volume of 1.5 mL. The 1 mL volume of PS-NH2 star

polymers was dissolved in dichloromethane and then injected into the flow cell for two minutes. This was immediately followed by a wash cycle of 3 mL dichloromethane and 3 mL THF. The entire cycle generated layer 1 of the LBL process. Layer 2 was deposited using a PS-COOH followed by a standard sequence of dichloromethane surface preparation, injection of PS-COOH followed by wash cycles of dichloromethane and THF solvents. These steps can be repeated based on the desired number of layers to be formed. The kinetics mode of the LabView program was used to monitor the layer formation on the SPR substrate. The flow cell was first rinsed with 1 mL of THF until 1.5 mL of solvent was reached and then injected into the system. The angular scan mode of the SPR machine was used to collect a baseline for THF as a comparison to subsequent angular shift which occurred as layers were deposited.

CHAPTER FIVE
RESULTS AND DISCUSSION

5.1 Surface Plasmon Resonance

The following sections discuss and assess the functional parameters required in aspects of SPR biosensor design. These include, 1) the optical components, 2) LabView features, 3) SPR optical alignment and the use of LabView program to facilitate this mean, 4) review of SPR machine capabilities, and 5) flow cell functionality and the effects of different solvents. All of these mentioned parameters had to be assessed to ensure the functionality and accuracy of the designed SPR machine.

The optical components in Figure 28 are briefly introduced here along with the trace of the path light that follows through the system. For ease of explanation, the optical components are labeled alphabetically, and letters in the text will refer to it.

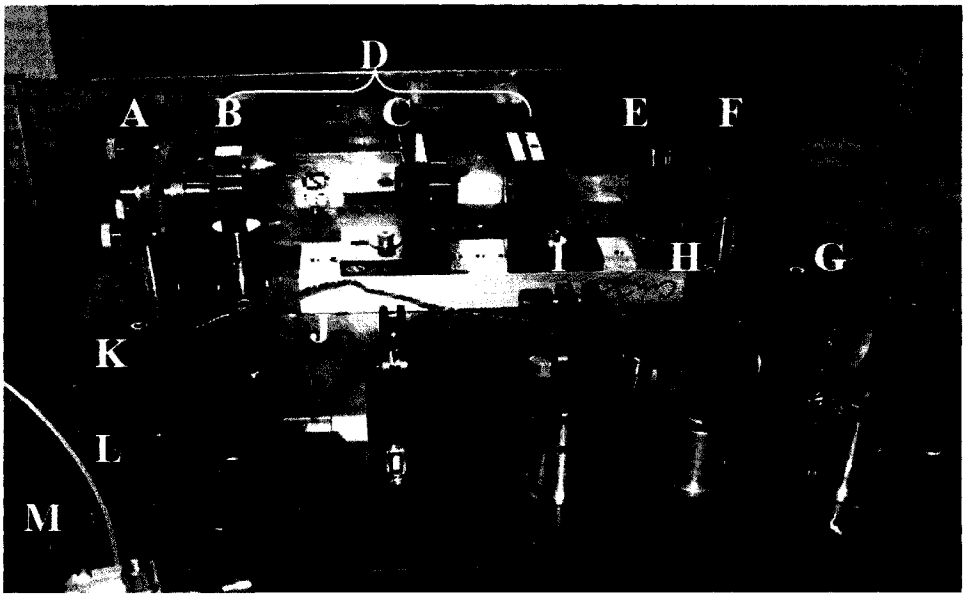

Figure 28. Optical components of the SPR machine.

A is the laser source, which in this apparatus is a 635 nm, single-mode diode laser. D is a spatial filter comprising a focusing lens B, that is placed one focal length in front of a pinhole C, and a collimating lens placed one focal length behind the pinhole. The purpose of the spatial filter is to improve the quality of the beam and to ensure that the beam is characterized by only a single wave vector along the optical axis of the system. A pair of irises E and J further define the optical path as it is bent through two 90^0 turns by mirrors F and G, and H is a polarizer that reduces any unwanted s-polarization present in the beam. I is the beam splitter in case the noise in the system is required to be measured with another detector. Mirror K produces another 90^0 bend in the beam, sending it through cylindrical lens L and finally to the SPR prism M.

5.1.1 Optical Components in SPR Biosensor Design

Detailed explanations of all the optical components used in the design of the SPR were provided in sections,1.8 and 4.1.1. In this section, the goal is to explain how some of these optical components were selected for this design. The optical system used three mirrors in order to transfer light from one point to another by changing the direction of the beam F, G, and K, as shown in Figure 28. Since the wavelength used in the optical system was 635 nm, stock mirrors of a round flat type having a highly reflective coating for 45° incidence over a range of 400-750 nm could be used. The overall goal of the optical selection was to generate high accuracy and sensitivity for the desired measurements since the light performance throughout the optical path can highly affect the sensitivity and accuracy of the results.

Because surface plasmons can be excited only with p-polarized light, a key component of (not all designs include polarizers) this optical design is the polarizer. A calcite polarizer was chosen to ensure that the light incident upon the SPR cell was highly p-polarized.

The chosen cylindrical lenses are BK7 which are the most common types. The cylindrical lenses were used to counteract the focusing effect of SF11 hemicylindrical prism. The cylindrical lens placed in the optical path before and after the prism, as shown in Figure 28 (schematic of the optical path), is a plano-convex type. Light passing through this positive convex lens converges to a spot before the prism. A second plano-convex lens placed after the prism collects the emerging and focuses it on the detector. Two pinholes (Iris Variable) are used in the optical path, to define the straight line in the optical path by blocking rays that are not traveling exactly along the straight line connecting the two pinholes.

5.1.2 LabView Features

One of the essential components of the SPR biosensor design was the incorporation of a programming tool. In the SPR sensor, the reflected light that is transferred to measurable signals through the photodetector has to be generated in such a format so that the users can study the desired parameters. This is achieved through LabView software. The program was primarily used to convert the signals to the curves that would demonstrate the changes of intensity versus the angle of incident. Also, the partial alignment of the system was achieved with some key features of this program. The author implemented different codes for measuring the different parameters required

in this project and also to facilitate the optical alignment. The three major codes associated with the program specifically written for this SPR were: 1) Scan Mode, 2) Kinetics Mode, and 3) Calibration Mode.

In order to facilitate any of the three codes, a set of programming codes had to first be implemented to initialize the motion controller (based on a specific type) and to connect the hardware. The hardware was connected to the computer through a National Instrument Interface to the software.

The main feature of the program is a Scan Mode which allows for the measurement of light intensity versus the angular response, so one can obtain the SPR angle. A feature of the scan mode is the ability to save the data file for every measurement taken in order to be able to analyze the data later.

Kinetics Mode is used to provide the measurements for change of intensity versus time. In most of the studies such as the layer by layer (LBL) process, the formation of layers can be tracked using the Kinetics Mode.

The Calibration Mode allowed one to easily calibrate the system after the complete alignment before any measurements taking. Calibration was not required for every measurement, but it was essential to do a random calibration after every couple of measurements or if any optical component was changed or readjusted in the system.

5.1.3 Alignment of the Optical Path

The SPR biosensor is designed with the inclusion of a set of optical components that are required to generate surface plasmon resonance phenomenon with proper transformation of light in the optical path. Therefore, the critical step investigated in the

design of this SPR biosensor was how to best place the optical parts such as lens, mirror, and pinholes in the optical path. The optical parts, as shown in Figure 28, are placed on a breadboard which provides a flexibility to move the parts to select the proper configuration and to achieve a careful alignment of the optical components throughout.

The process of aligning the optical components begins by checking whether the laser beam travels from laser source A, to the face of the prism M. A square white card was selected as a primary tool to visually track the light transformation in the path. The use of the white card in the path makes it possible to observe the red light beam. If the light is not apparent, the laser source has to be checked to ensure that the laser is on. The other highly important place to check for the laser light in the optical path is after the spatial filter (D). If there is no light or the power is not strong, the x,y coordinate on pinhole C has to be adjusted carefully until a round, complete, and strong beam appears on the white card placed in front of the spatial filter D. The other important check for the alignment is to ensure whether the light hits the center of the optical components pinholes, mirrors, and prism. A round small spot can be created in the center of the white card and can be placed in front of each part to check whether the light penetrates through the center. A quick check can be performed throughout the optical path. But in order to make it easier, it is required to check if the beam of light goes through the center of two irises E and J. This check basically defines the straight line for the optical path. It is strongly recommended not to move or change the physical position of the pinholes in the optical path since their placement is a key factor in defining the path in the system. If the light does not, however, penetrate through any of the pinholes, then the position of

pinholes should be adjusted to center the pinholes on the beam. Since the optical path is now defined based on the two irises E and J, the location of the laser beam can be checked on all the parts. The beam of light has to hit the surfaces of the mirrors and cylindrical lens L at the center. The light height and the location on the mirror can be adjusted with the knobs placed on the back of the mirrors. All of the conditions mentioned here are the primary factors that need to be considered in the optical alignment.

The second critical step, after these parameters involves the proper positioning of the light on the prism M. This step was a challenge in this work since the placement of the laser beam on the prism plays an important role in generating SPR phenomenon. As shown in Figure 28, a mirror K is placed on a translation stage that can move side to side. The cylindrical lens L is placed on a translation rail so that the distance can be adjusted. The use of the two configurations provides an optimum tool to overcome the challenge of the final alignment on the prism. The first step is to determine the rotation stage angle that produces the exact retro-reflection of the incident beam. This process calibrates the location of normal incidence, which is especially important for comparing measurement to theory. The second step is to position the beam so that it travels precisely along a radius of the prism. Turning mirror K and cylindrical lens L are both mounted on a translation stage that can be moved. Since the curve surface of the prism behaves as a convex mirror, the reflected beam will not travel back along the incident direction unless beam is precisely centered on the prim.

5.1.4 Primary Requirement for Excitation of Surface Plasmon Resonance Phenomenon

After the critical factor of the optical system was achieved, that is an accurate and complete alignment of the system, then the next step was to explore two main fundamentals of the SPR concept: 1) Total internal reflection (TIR) and 2) SPR resonant angle.

As explained earlier in chapter one, in order to excite surface plasmon the optical component has to meet the primary requirement to measure TIR as a check of the system since at the angle at which it occurs is a well-defined and simple function of indices of two materials. The TIR occurrence illuminates several major factors about the behavior of the optical components employed in the setup.

A medium having a higher refractive index than the dielectric is required for this phenomenon. Typically, a prism is used as it has a higher refractive index than the dielectric. The type of the prism depends on the type of wafer used, and since SF11 was selected as the optical type, an SF11 prism was used for the measurements. In a typical TIR measurement, an SF11 wafer (a dense alkaline silicate glass) is placed on the flow cell with the index matching fluid (1.765± 0.005 for SF11), and the SF11 prism is placed on top. For this study, a full radius prism with radius of 0.375'' was used instead of the combination of a truncated SF11 prism (radius 0.375'', thickness 0.335''), and wafer (thickness 0.040''). The "full radius prism" was substituted because there is no need to use index-matching fluid and the possibility of introducing a slight angle offset between prism and wafer is eliminated. After the full radius SF11 prism was placed in the flow cell, the scan mode of the LabView program was used to capture a full scan between the

angle ranges of 15-45^0 to explore for TIR. This range was selected based on the value predicated by theory which is explained later in this section. Figure 29 shows that the TIR occurred at an angle of 34^0. Because TIR characteristics are determined only by the refractive indices of the prism and air, both of which are known quite accurately, it provides a very good indication of whether the system is correctly aligned. The SPR response, as discussed below, is determined by several parameters (e.g., indices and thickness of Cr and Au layers) that are not known accurately. Hence, curve fitting must be used to try to see if agreement between theory and experiment is possible with parameters that are physically reasonable.

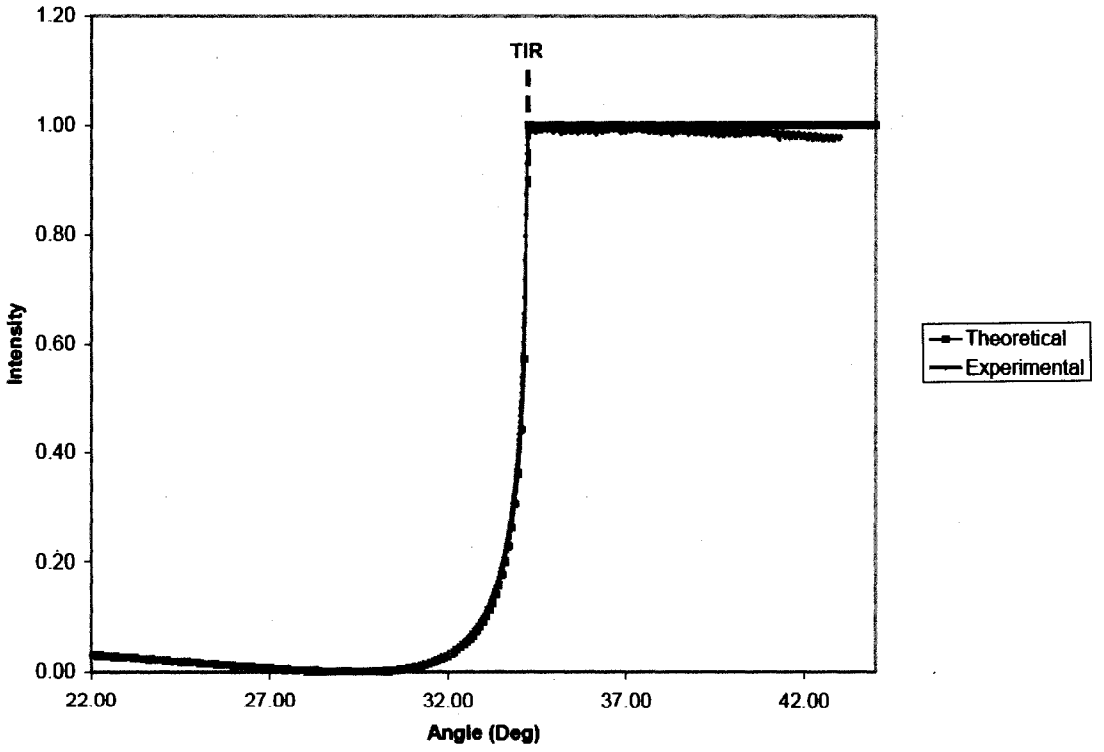

Figure 29. Comparison of experimental and theoretical SF11 TIR.

The experimental results were fitted to the model which was derived from the theoretical calculations carried out by Dr.William Risk at IBM Almaden in San Jose [51]. The good agreement between the experimental and theoretical calculation, as shown in Figure 29, confirms that the optical components were placed in the manner which resulted in an accurate alignment and as a result the precise occurrence of the TIR. If the TIR could not be observed, the effort would have to be initiated towards checking the alignment of the system to ensure the beam of light was directed in a way to account for all of the parameters mentioned in the alignment section. In Figure 24, a fairly sharp curve can be observed in the top corner of the graph. This implies that the cylindrical compensation optics were adjusted well and that a well-collimated beam was generated in the prism. Also, it was expected that the bottom part of the TIR graph would go to zero at Brewster's angle (30^0), which also can be seen. Thus, the experimental results also satisfied this criteria. The result proved that the SPR machine is capable of generating a correct and precise TIR which can be taken one step further to measure the SPR angle. The TIR measurement is one of the critical steps in checking the accuracy of the performance of the overall setup, and it is highly recommended that TIR be checked often.

5.1.5 Create an SPR Resonant Angle with SPR Substrate

The SPR detector was capable of showing TIR phenomena that correlated with what was expected from theory. After establishing this fact, the next step was to explore the observation of surface plasmon resonance. The SPR substrate consisted of SF11 glass, on which was deposited a gold sensing layer with a chromium adhesion layer

beneath and an overlaying cap of sputtered silicon dioxide placed in the flow cell. The substrate was treated with UV/ ozone and washed with Millipore water prior to use, as discussed in the Materials and Methods chapter. On the substrate, the refractive index matching fluid (1.765± 0.0005) was placed with the prism on top. A full scan was captured from 30-45 ^{0} to search for the surface plasmon angular response (SPR minimum angle). The SPR angle was observed at 36.22 ^{0}, as shown below in Figure 30. To determine the accuracy of the SPR angle measurement, the results were fitted to theoretical measurements carried out by Dr.William Risk which were derived based on the thickness of the gold layer and refractive indices of the layer [51].

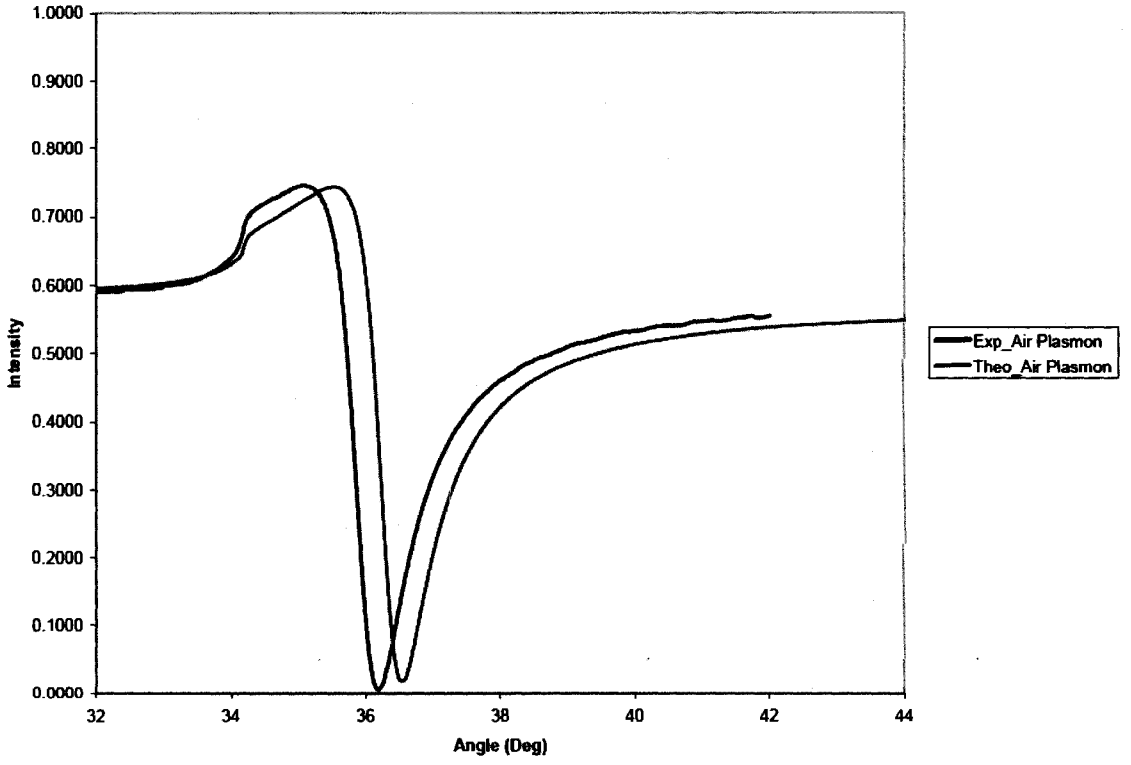

Figure 30. SF11 SPR substrate air plasmon.

The experimental graph shows that the SPR curve does not match the theoretical curve. The SPR angle from the theoretical model is 36.58^{0}. One initial guess for this could be that the theoretical model took into account 50 nm for the gold layer thickness, but the thermal evaporator which was used in this study for gold deposition may not have delivered exactly 50 nm of the gold layer on the substrate. This discrepancy associated with the thermal evaporator had to be considered when analyzing the data using the theoretical model. Therefore, further refinement of the fit to the theoretical model was pursued by Dr. Risk to investigate the difference in behavior of the SPR angle. The new fit revealed that the thickness of the gold layer was about 42 nm; usually ± 10% (47-53 nm) variance is expected. However, 42 nm could also be the result of any other factor that might have happened during the evaporation process. The prism is the only component that has a real index of refraction, but others can be complex which includes the imaginary part to the real part. Another factor that was corrected for the fitted model was the small changes to the complex refractive index, $n = n+ik$ substantiated, by Johnson and Christy, where 0.0451 had to be added to the real part and 0.037 to the imaginary part of the formula. The results of the new fit with the experimental data are presented in Figure 31.

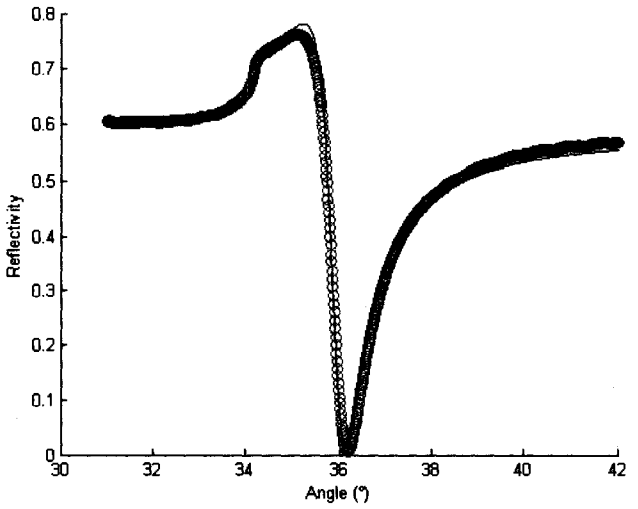

Figure 31. SF11 SPR substrate air plasmon based on the revised fit model.

The behavior of the experimental results confirms that the angular air plasmon resonance occurred at the accurate angle based on the theoretical measurements. The TIR of both graphs also lined up in the same spot. This highly indicates that the designed SPR machine can deliver accurate and precise measurements such as for air plasmon. The air plasmon measurement is an initial step in every SPR measurement regardless of the type of experiments or molecules used for measurements. The output of the theoretical model from the matlab program was normalized; therefore the experimental graph shown in Figure 31 was also normalized.

5.1.6 Studying the Effect of Solvents

After ensuring the accuracy of the designed SPR machine by determining the TIR and the SPR minimum angle, the functionality of the overall setup, flow cell with fluid injection, could be investigated. The functionality of the flow cell in terms of the ability to adsorb the fluid which was injected through the lines connected to the o-ring as part of

the flow cell and also the ability to push out the fluid and dry it out was a critical part. The flow was also required to pass through the flow cell with a smooth movement that would not create any bubble on the sensor surface. In order to test for these parameters, and also to investigate the behavior of the SPR machine with solvent in the system, several solvents were tested and were fitted to the theoretical model explained above. The only difference in the theoretical model for the solvent part was the model that was fitted based on the refractive index of any desired solvent than air. The three solvents that were used were Millipore water, isopropyl alcohol (IPA), and chloroform. After each of these solvents was injected manually through the lines connected to the flow cell, the scan mode feature was used to detect the SPR minimum angle. For each of these measurements the scan range was different. For example, the angular plasmon of Millipore water occurred at a resonant angle of about 56 ^{0}, which was completely different than the SPR angle of air at 37 ^{0}. Therefore, for every measurement the user should be familiar with the behavior of the experimental system and the range of angular scan that is required to be chosen. For example for the case of the solvent, the behavior of the system had to be understood in terms of the polarity of the solvent and how with a higher polarity a larger shift in SPR is detected. Also, knowing theoretical values can definitely assist in knowing approximately the range of the SPR angle that may occur. Each of the solvent's experimental measurements was fitted to the theoretical model designated to each specific solvent system to investigate whether the SPR angle occurred at the expected angle. Figure 32 below shows the experimental graphs for three solvents presented in colors and theoretical measurements shown with black curves. This

confirms the premise that the flow cell is capable of complete delivery of the fluid to the system with smooth and appropriate behavior.

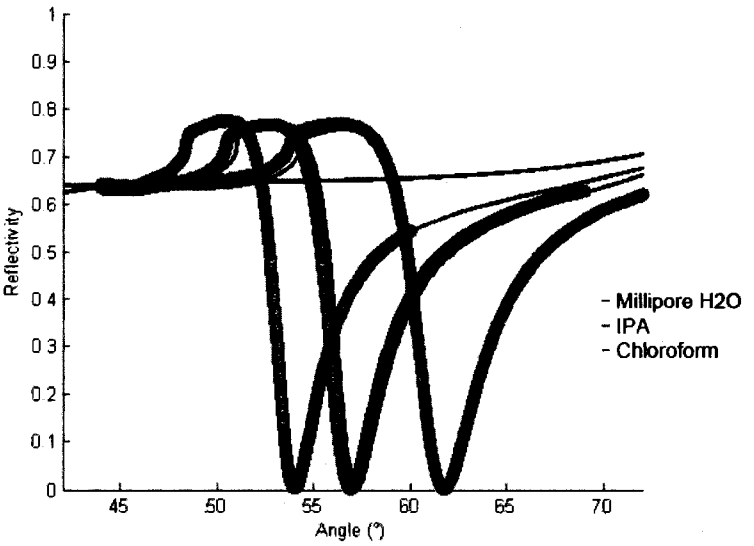

Figure 32. The effect of different solvents in the system.

5.1.7 Kinetics Mode of LabView Program: LBL Self-assembly Process

After ensuring the accurate performance of the SPR machine with measuring TIR and air plasmon and testing the functionality of the flow cell, the kinetics mode of the LabView program was verified with the LBL self-assembly of star polymers SPR substrate. As per the usual process used in this study, the substrates were cleaned with UV/ozone followed by a wash with Millipore water prior to use. The profiles were collected using kinetic mode (intensity vs. time) to provide information about the time required for layer formation which can be used to evaluate the stability of the layer formation. The scan mode was then chosen to determine the shift in resonance angle after the formation of a complete polymeric layer. The experiments were carried out using THF/CH_2Cl_2 solvent system for the deposition of 3K star polymers of PS-NH_2 and

PS-COOH *in situ*. First, the baseline with THF solvent was taken with an angular scan mode prior to dichloromethane injection. Dichloromethane is a vital addition to ensure the flow cell environment and the substrate is suitable for layer formation. Second, the kinetics profile of PS-NH_2 was collected with dichloromethane as a baseline. This was done because the rate of layer formation can be effectively observed if THF is used as a baseline of the kinetic mode. The process of creating PS-NH_2 (layer 1), and PS-COOH (layer 2) was explained earlier in section 4.2.6. After the injection of THF, the angular scan mode of the SPR machine was used to collect a baseline for THF as a comparison to subsequent angular shifts that occurred as layers were deposited.

In order to observe the layer formation, the mode had to be switched to the kinetics mode. The angle for the kinetics mode was selected at the point of inflection on the left side of the SPR graph. In the kinetics mode, reflectivity versus time was collected as shown in Figure 33.

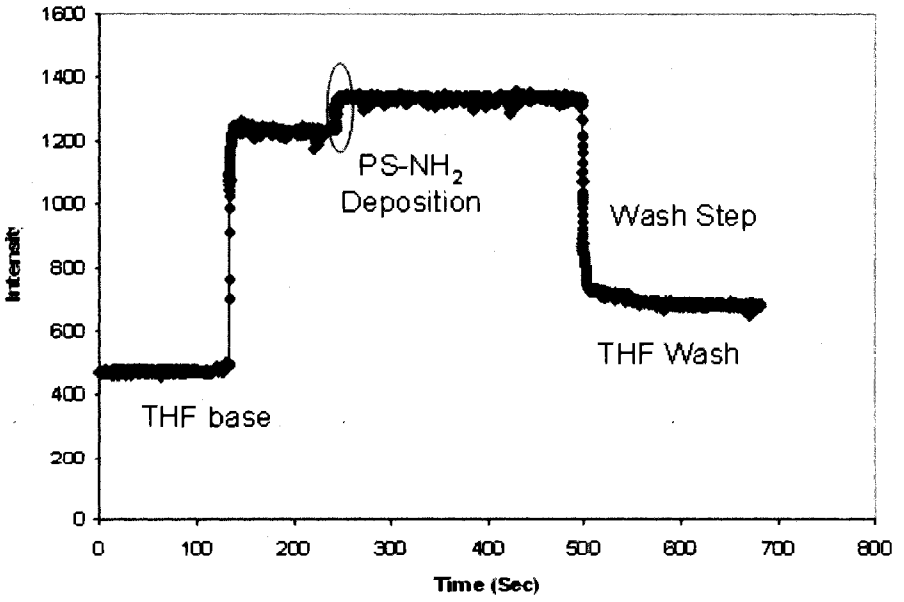

Figure 33. Kinetics mode plot for polymer (1st layer) deposition and wash step.

Initially, a reflectivity of 420 was recorded for THF injection, but immediately after the injection of dichloromethane, an increase in the intensity was observed. The PS-NH_2 formation was observed by monitoring the intensity versus time for 2 minutes, and the increase in reflectivity was noted as a reliable sign of layer formation. After the wash cycles with dichloromethane and THF, the starting and final reflectivity level of THF were compared to determine if the layer was actually formed. Also, the shift in resonance angle was measured as the determination of the layer formation. The second layer was deposited with PS-COOH using the same cycle as for layer 1. Figure 34 presented below shows the five layer formation of amine and carboxylic acid star polymers. The results presented in this section gives evidence of the viability of using the SPR machine with a flow cell system and complementary kinetics mode of the LabView program to generate precise and accurate measurements. This accuracy of the software with the SPR machine plays an important role for further usage of the biosensor and potential binding studies.

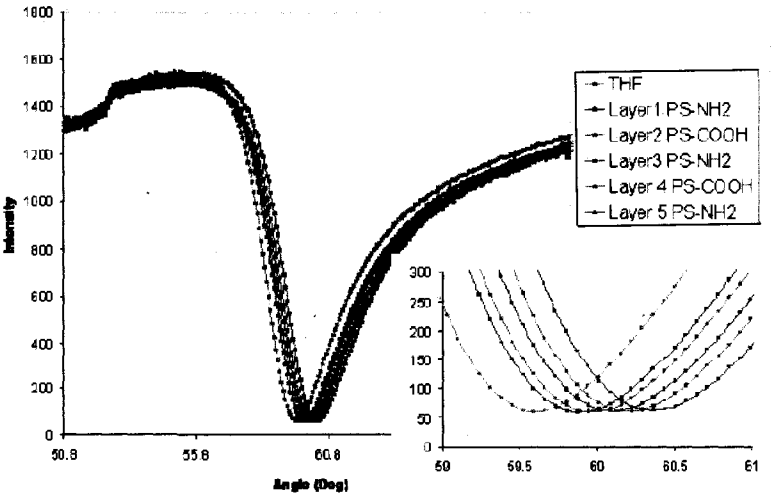

Figure 34. SPR of LBL formation of PS-NH_2 and PS-COOH (five layers).

5.2 Safety Concerns

The laser light is on throughout the experiment process. Users should be aware of positioning it in a way to avoid a direct eye contact with the laser light to avoid damage to the eyes. When the system has to be aligned, the light path should be checked in a way to minimize a direct eye contact with the laser light. The driving force of the SPR instrument is generated by voltage and highly dependent on electric power. Therefore, users have to be cautious about the proper usage of this instrument. The cable connected to the step motor and detector has to be taped to the breadboard and placed on a side to avoid any contact. In case of any power shortage, the source should be checked by professionals. The SPR machine is completely covered with an aluminum sheet to block the surrounding area from the laser shot.

However, in the case of running an experiment with the flow cell, the front shield needs to be removed to observe the behavior of the fluid transformation. In that case, users should monitor the process in a way to reduce eye contact to a minimum level. Also, some safety features were added to the LabView software to control the limit of movement of the rotator.

5.2 Nanostructuring Porous Biosensors

The current challenges associated with the design of SPR biosensors can be divided into two categories: "above" and "below" the sensor substrate. "Below" the substrate deals with increasing effectiveness of the SPR optical components. "Above" the substrate deals with increasing the effectiveness of substrate interactions with the target analyte as shown in Figure 35. This chapter describes "above substrate" research

aimed toward increasing the sensitivity of SPR sensors, for the nanoengineering of SPR substrates for the purpose of installing simultaneous capabilities of both size and chemo-selectivity onto the sensor surface.

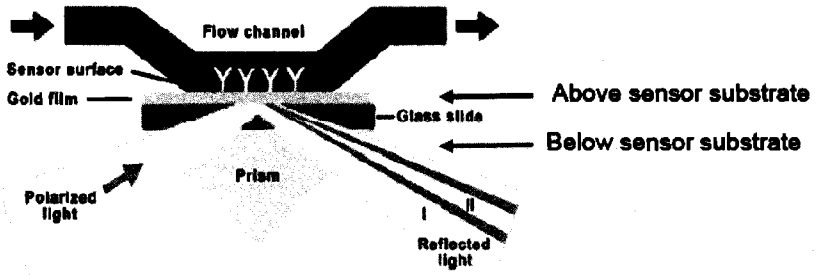

Figure 35. Existing challenges "above" and "below" challenges for current SPR biosensors.

5.2.1 Engineering Ultra Thin Organosilicate Films

The ability to make "thick" porous film from organosilicate (e.g.,, MSSQ) is known [52]. Porous organosilicate is an attractive alternative due to the mechanical stability of the process. What is not known is whether this process can be adopted to form films within the evanescent field of SPR biosensor (i.e.,<100 nm). For this purpose, a "dense film" was first prepared based on 21.5 wt % of MSSQ (LKD 2015) in PM Acetate to generate a thick film before being diluted further to produce solutions of different concentrations and thinner film thicknesses as a result. Preliminary experiments were performed on a silicon wafer. The solutions were then spun onto the substrate before being thermally cured. The films were then characterized using AFM. The AFM image can be used to reveal the morphology of the surface while the phase diagram shows the uniformity and homogeneity of the films. These two features together provide

valuable insight into the uniformity, coverage of both thin and thick dense films, as well as, porous thin films.

In dense films regardless of their thicknesses, a smooth uniform layer without pores on the surface was expected upon observation. The formation of a thick dense film with PM Acetate solvent on the silicon wafer was first investigated by AFM. The silicon wafer, with its native oxide layer, provides a smooth and flat background allowing easy distinction of the surface features after film formation, as shown at top image in Figure 36. A 2 μm image of 21.5 wt % dense thick film is shown in Figure 36

. It was observed from the AFM results that the dense film exhibited no significant surface features, and a complete and contiguous layer was formed on the silicon wafer.

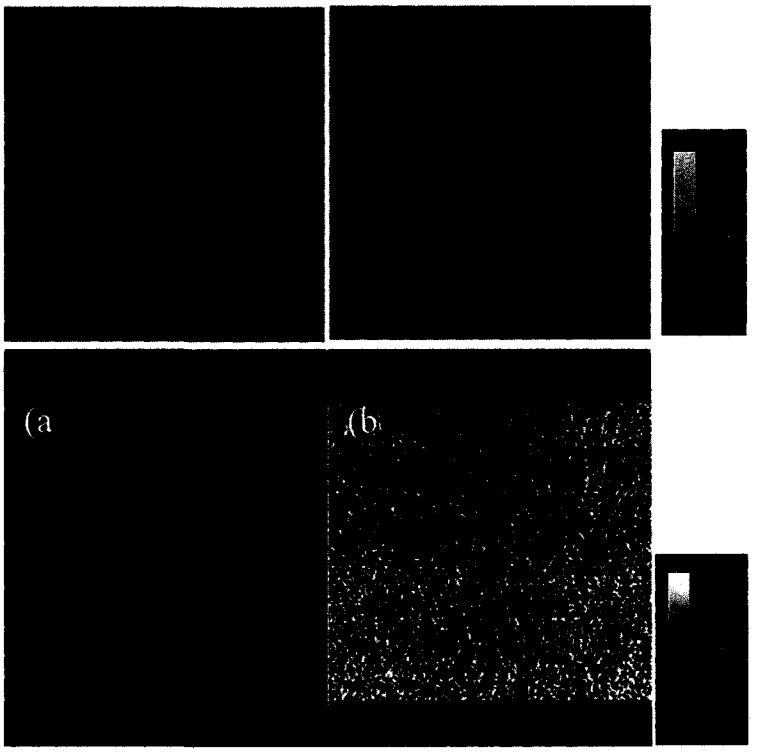

Figure 36. AFM image of a 21.5 wt % dense film (Thick film) on a silicon wafer, at 2 x 2 μm a) height image and b) phase image.

It is evident from the results of the thick film that a dense film could be created with a mixture of LKD 2015. Consequently, the process was carried out further to make a dense thin film applying similar techniques. The experiments were first established by making a 2.5 wt % thin film through the dilution of 21.5 wt % LKD 2015 with PM Acetate which was filtered with a 0.2 μm filter on a silicon wafer before the spin coating process. The dense thin film with a concentration of 2.5 wt % is shown in Figure 37.

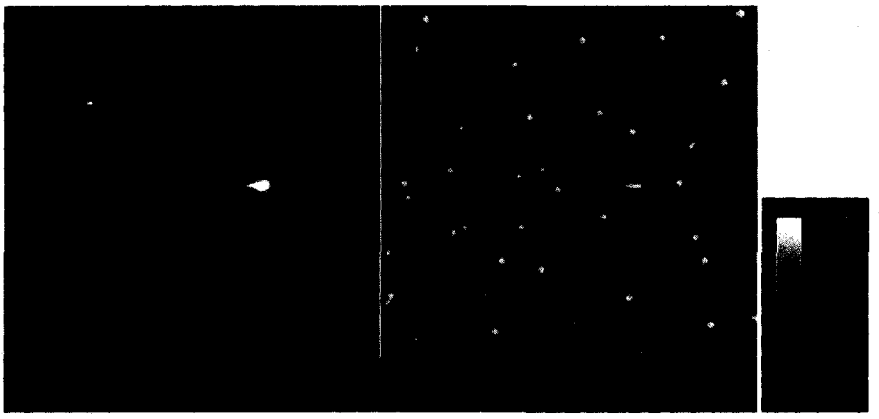

Figure 37. AFM image of a dense thin film of 2.5 wt % concentration of LKD 2015 at 5 x 5 μm Image.

The results in Figure 37 show the existence of some significant film features (e.g., uniform holes ~ 2 μm) previously were unobserved for the thick film. It was thought that the particles arise, from organic contamination either from the environment or handling of the sample, which generated holes during thermal curing steps. The investigation started by examining the use of different filters smaller than 0.2 μm to ensure no debris could penetrate through the filter and onto the surface. The strategy that was adopted was to use 0.1 μm, 0.02 μm, and the sequential filtering of the three filters.

Figure 38 and Figure 39 respectively show the results for 0.1 μm, and 0.02 μm filters with a comparison to the 0.2 μm image.

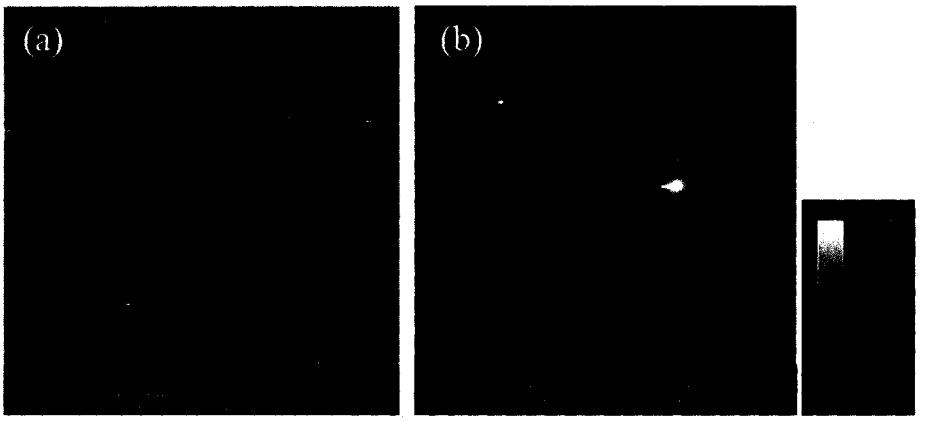

Figure 38. AFM image of a dense thin film of 2.5 wt% concentration of LKD2015 at 5 x 5 μm Image, a) 0.1 μm filter and b) 0.2 μm filter.

It can be observed in Figure 38 (a) that round particles from the 0.1 μm filter are larger than those shown in 27 (b) with the 0.2 μm filter. This size filter can not be an alternative solution for removing the particles. The AFM images for 0.02 μm are shown below in Figure 39.

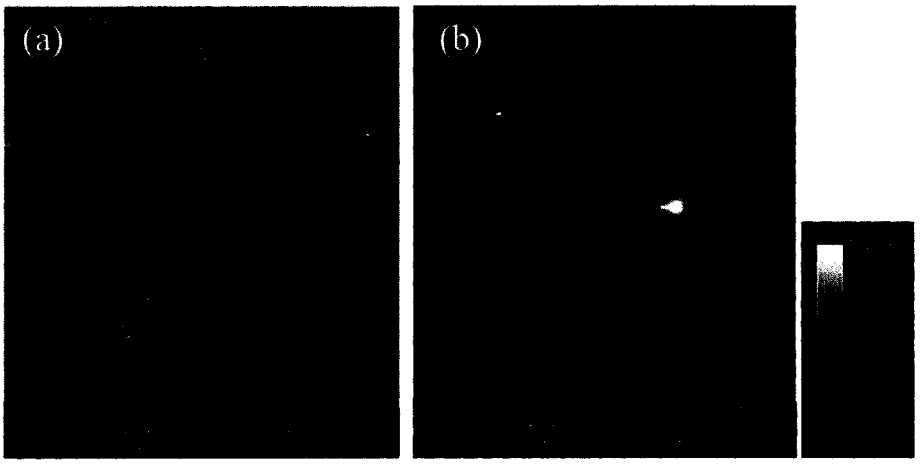

Figure 39. AFM image of a dense thin film of 2.5 wt % concentration of LKD2015 at 5x 5 μm Image, a) 0.2 μm filter and b) 0.02 μm filter.

There are a significant number of holes created using 0.02 μm filter in Figure 28 (b) compared to 0.2 μm filter in 28(a). Therefore, using the smaller filter size of 0.02 μm filter did not resolve the problem.

Figure 40 shows the filtration sequence from using a large size filter (0.2 μm) and moving down to smaller filters (0.1, 0.02 μm). In this process, the mixed solution was first filtered through a 0.2 μm filter, then filtered through a 0.1 μm filter, and lastly filtered through a 0.02 μm filter.

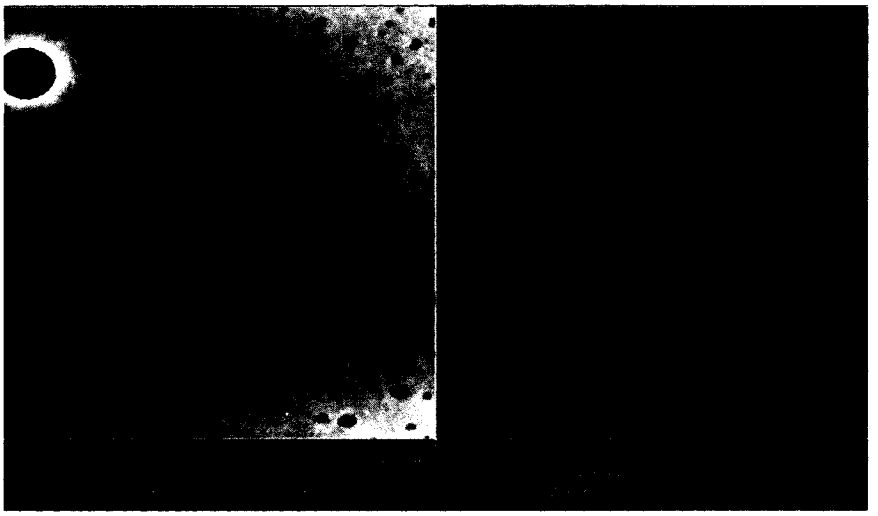

Figure 40. AFM image of a dense thin film of 2.5 wt% concentration of LKD 2015 at 2x 2 μm with sequential filtering: 0.2, 0.1, and 0.02 μm.

The results indicate that the subsequent filtering of the solution led to extra contamination on the surface due to the handling of the sample and exposing it to the open environment. As a result this was designated as the worst approach to obtain a featureless surface. In comparing a thick dense film in Figure 36 with a thin dense film, a question arose why the existence of such features only on a thin film, when the filter processes were completely the same. It was theorized that owing to the size of the

particles (relation to the film thickness), the features may buried within the thick film and only become exposed at a certain film thickness (i.e., thin films). This theory was explored by preparing a different thickness of a dense film and investigating the effect of the thickness on the appearance of the features on the surface. Thin films of approximately 29, 42, and 68 nm were prepared. It was expected with increasing the film thickness, the surface particles would decrease. However, the AFM images of these three films, as shown below in Figure 41, contradict with this theory.

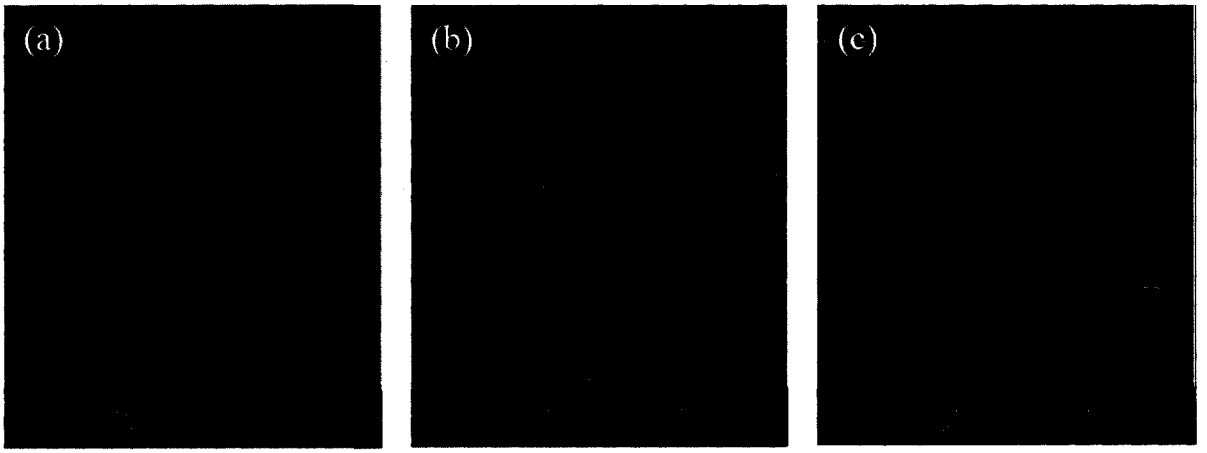

Figure 41. The effect of film thickness on the presence of particles on the surface at 5x 5 μm, a) 29nm, b) 49 nm, and c) 68 nm thin films.

It appears that the film thickness does not affect the particles by any rigid criteria. The pores are present with all the three films with no significant reduction in their presence. The solution used was then explored as a source for the particle contaminations.

The MSSQ solutions (LKD 2015) were originally supplied as a solution of Dowonal PnP; hence, this solvent could be used as one of the alternative solvents. Dilutions were made using PM Acetate owing to concerns about eventual porogen

solubility in Dowonal PnP. Dowonal PnP was then selected as an alternative solvent in conjunction with 0.2 μm filter size. It can be observed from Figure 42 shown below, that a significant number of features are removed from the surface, suggesting that the criteria adopted here could be optimal in creating smooth, uniform, and featureless dense films.

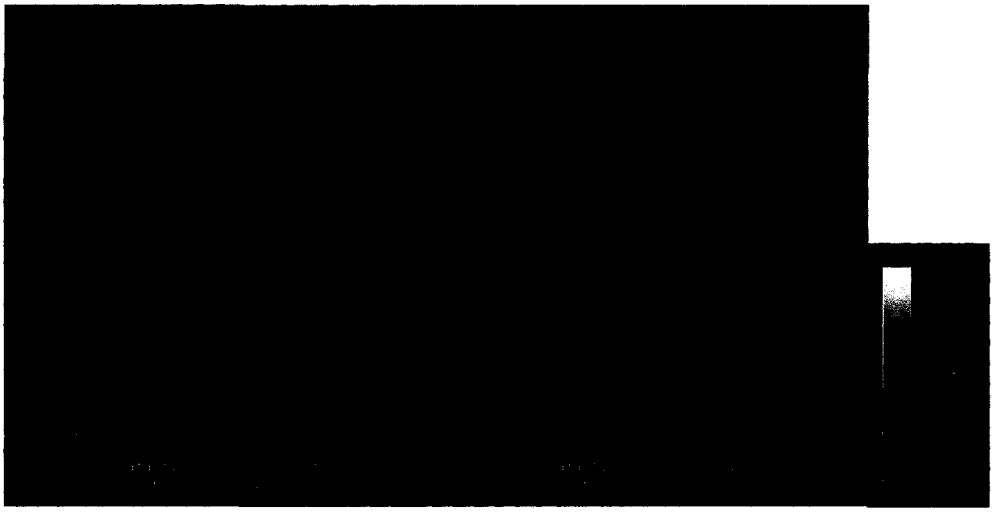

Figure 42. 2.5 wt % dense Film with Dowonal PnP, 0.2 μm filter.

This observation from Figure 42 together with all the earlier discussion led to the conclusion that the dense films, both thin and thick, could be structured using Dowonal PnP, with 0.02 μm filter and ozonolysis of the silicon wafer surface before spin coating the solution. As a result, the process of preparing dense films was then applied to an actual substrate which was the SPR substrate, as shown in Figure 43 for the thin film formation and Figure 44 for the thick film. It can be seen from the phase image provided in Figure 43 that the SPR substrate surface does not form as smooth a layer as on the silicon wafer. Because the SPR substrate surface does not accommodate a smooth uniform layer as a native structure for any further film deposition.

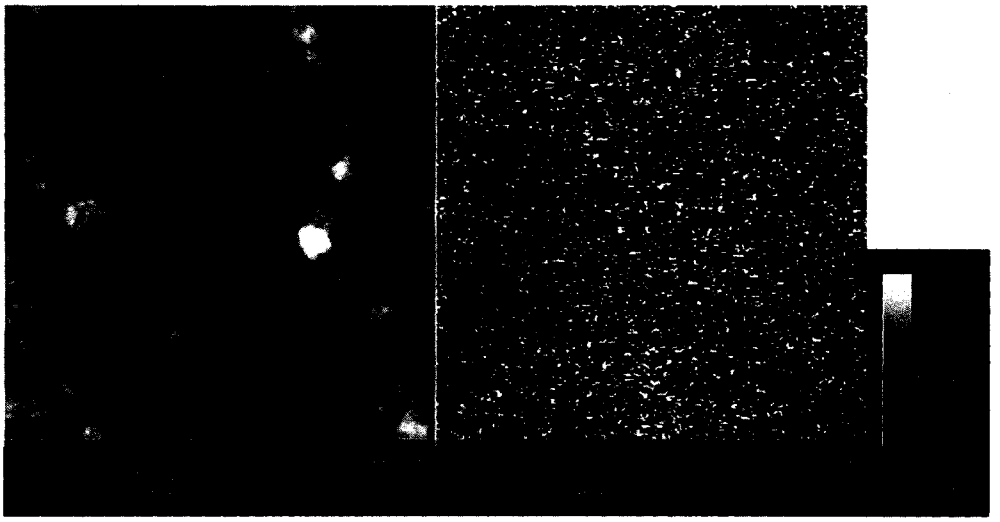

Figure 43. A dense thin film with the optimum condition on the SPR substrate at 2x 2 μm.

Figure 44. A dense thick film with the optimum condition on the SPR substrate at 2x 2 μm.

5.2.2 Determining the Optimum Thickness of Ultra Thin Organosilicate Films

After establishing the optimal condition for creating a dense film, the optimum thickness of the film had to be determined. For this reason, different concentrations of

LKD 2015 (1.0 - 3.5) wt % with incremental increase of 0.5 were evaluated for thin film formation.

In order to measure the thickness of each film based on different concentrations, ellipsometry was employed to measure the thickness and to investigate the uniformity of the film layer formed. Elliposometry requires a model which requires either the refractive index of the material to find the thickness, or the thickness to determine the refractive index. In this study, in order to use ellipsometry to evaluate the thickness, the refractive index of the films was first determined. Filmetrics allows for measurement of the refractive index and film thickness, greater than100 nm thickness over using reflectance measurements. The refractive index (n) of the dense thick film (21.5 wt % LKD 2015) was found to be 1.38 with a 723 nm thick layer. The refractive index value that was used in ellipsometry measured the thickness of the samples to provide information as to the uniformity of the thin film. Table 4 shows the different concentrations of LKD 2015, prepared on silicon wafers and related thicknesses determined from ellipsometry. The error reported by ellipsometry can be considered as an indication of the uniformity of the film. A film within an error of less than 5 angstrom was considered to be uniform for the process used in this work. Based on the results in Table 4, all the different thicknesses can be counted to be smooth uniform films.

Table 4. Control of the film thickness with variation of concentration of LKD 2015.

Sample	Concentration (%)	Thickness (nm)	Error
1	1.00	13.11	0.61
2	1.50	20.12	0.68
3	2.00	26.91	0.75
4	2.50	34.63	0.93
5	3.00	43.18	1.14

To further investigate the effect of varying the concentration of LKD on the film thickness, the values were plotted in Figure 45. These produced a linear relationship between thickness and concentration implying the ability for creating an ultra thin film with any desired thickness, which will be advantageous in further manipulation of the layers built on the SPR substrate.

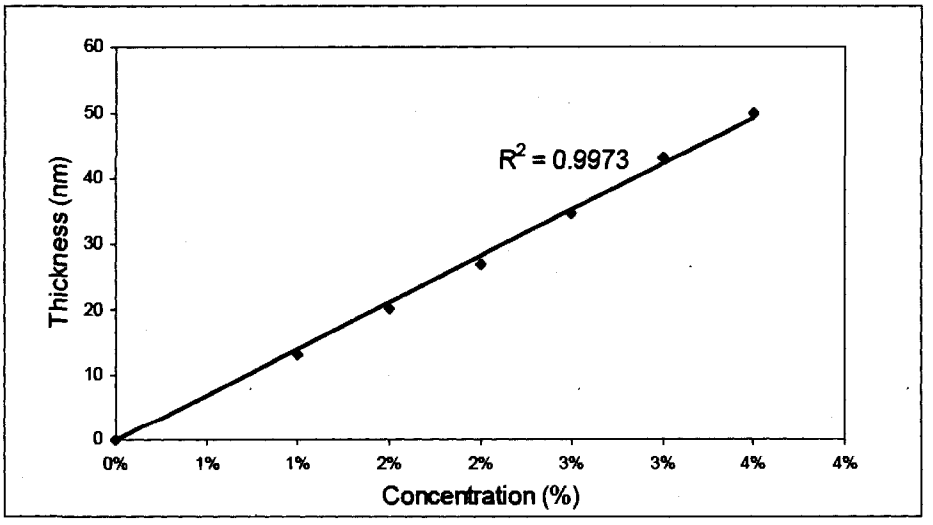

Figure 45. The ability to create any film thickness by varying the concentration of LKD 2015.

Consequently, the concentrations of 2.0-2.5 wt % with thicknesses of 26-34 nm were selected as the optimum concentrations from which to generate ultra thin films.

After the final concentration and thickness of the film were verified, this technique for the thin film formation was used on the SPR substrate, and surface plasmon resonance (SPR) experiments were conducted to study the behavior of the film thickness and the corresponding concentration. The substrate used was alkaline glass, SF11, with a chromimum adhesion layer and overlaying protective layer of sputtered silicon dioxide, as discussed in the Materials and Methods chapter. The substrates were then prepared with the different thicknesses similar to the thicknesses showed in Table 4. The angular scan mode was used to provide information about the shift in resonant angle (SPR angle) and to evaluate the behavior of different thicknesses relevant to the change in the SPR angle. Each individual sample at concentrations of 1.0-3.5 wt % was analyzed using the scan mode of the SPR machine, as shown in Figure 46. The first SPR curve on the left side of the graph includes the substrate without a film layer in order to analyze the effect of the film deposition with the SPR technique, a shift in the SPR angle from the original substrate to a substrate with 1.0 wt % concentration is observed. Similarly, the shifts in resonant angle can be observed for the other concentrations. The subsequent increase in the angle shift with the increase in the concentration, reveal the accuracy and sensitivity of SPR biosensors to detect such behavior. The increase in shift of angle relevant to the thickness of the film indicates thick layer formation of thin films which leaves more material on the surface, and, as a result, a larger shift on an angle can be observed.

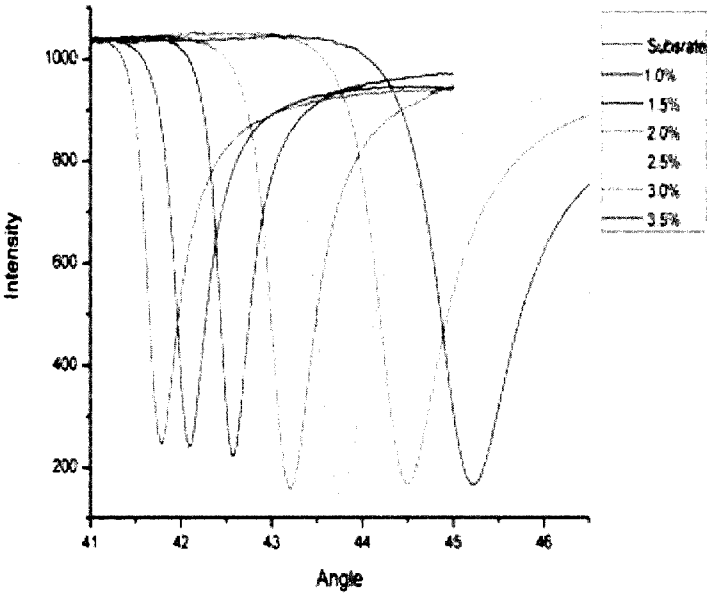

Figure 46. SPR responses of substrates prepared with different concentrations of LKD 2015.

The SPR results shown in Table 5 shows the relationship between the angles and the data collected from the ellipsometer. The SPR results confirm the complete control of the film thickness on the sensor surface, within the 100 nm criteria. It can also be observed from Figure 46 the dip of SPR curves is not the same. The reason for that is that the samples are performed separately and that each sample will take a different time to settle on the flow cell, both of which can result in the variation of the SPR angle.

Table 5. The effect of LKD concentration on the film thickness of the SPR substrate and the corresponded SPR angle.

Sample	Concentration (%)	Thickness (nm)	Angle (Deg)
1	1.00	12.23	42.08
2	1.5	18.68	42.57
3	2.00	26.51	43.21
4	2.50	33.31	43.77
5	3.00	39.61	44.49
6	3.50	42.14	45.20

5.2.3 Porous Film

The process of generating a dense film which involved complete control of the film thickness by varying the concentration of LKD, and the ability to understand the behavior of the process by monitoring the SPR angular response, led to a new concept, porous film, which is the vital area of this project. The main purpose of this study was to nanostructure the sensor surface to increase the sensitivity and selectivity of the detection technique. With the ability to generate organosilicate films in hand, the ability to introduce porosity into these films was explored using star polymer porogen. This was accomplished specifically by generating porous films which can increase the viability of the detection technique, as compared to the featureless surfaces (dense) used in other studies.

The porous film was generated by incorporating sacrificial star polymers into a silicate precursor solution (MSSQ) which was then spin coated onto the SPR substrates.

Upon thermal curing MSSQ produces an organoslilicate layer, and star polymer porogen burns out leaving random pores behind. For this approach, PM Acetate was chosen as a particular solvent as opposed to Dowonal PnP, since the porogen is not soluble in PnP. The porous film was prepared based on percent porogen loading, as explained in chapter four. This section will assess the formation of different porous films with relevant characterization techniques and study the versatility of size selective substrates.

5.2.3.1 Porosity Variation

The first step taken in the design of a porous film, was to explore the use of physical features and chemical ligation to increase sensitivity, followed by the exploration of a controlled porous sensor surface. In order to observe such phenomena, different porous films were prepared to determine the optimum porosity for the purpose of this study. The porosity of the films differed based on the percent of porogen loading. The porosity variation was assessed with porogen loading of 20%, 40%, and 60% (relative to MSSQ concentration) in order to provide insight into the behavior of nanostructered porous films. It was deduced based on the results of making ultra thin organosilicate films the proper concentration of LKD2015 to support a thin layer was 2.0 wt %, although the concentration could also have been increased to alternating concentration of 2.5 wt %.

In order to measure the thickness of each porosity, the corresponding thick film had to be prepared with the same percent loading as the thin film to ensure similar porosity. The thick film was then used to obtain a refractive index value for ellipsometry. The 40% porous thick film was prepared using 21.5 wt % LKD 2015 and PM Acetate on

a silicon wafer. The refractive index of the film was 1.21 with a film thickness of 710 nm.

Thin films were then prepared, as previously described, using 20%, 40%, and 60% porogen loading on a silicon wafer to validate the process. These porogen loading values were then used on the SPR substrate, and the behaviors of these films were then analyzed with the SPR biosensor. The results are provided in Figure 47.

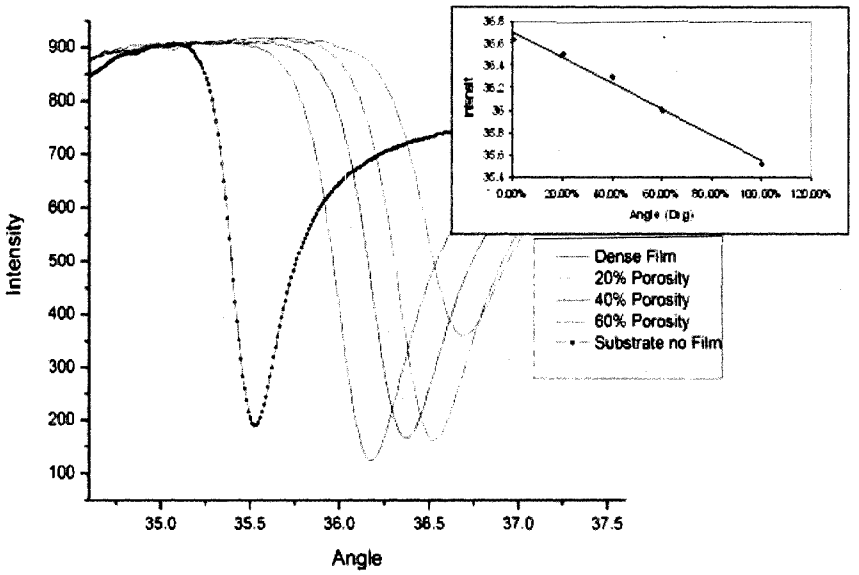

Figure 47. Successful installation of variable porosity on the thin silicate film surface.

The SPR responses verified the ability of making thin porous films. The curves shown in Figure 47 ranges from no porosity (substrate with no film) to 100% porosity (dense film). The changes in SPR angles provided in Table 6, show that with different porogen loading the refractive index in the medium changes, and, as a result, a different shift in SPR angle is observed.

Table 6. SPR angular response with porosity variation.

Porosity (%)	Angle (Deg)
20	36.50
40	36.37
60	36.17

At the higher porosity of 60%, the SPR signal approaches the substrate with no film. The decreasing trend of angular shift from 20% to 60% is shown in the inset of Figure 47. It can be seen from both Figure 49 and Table 6 as the porosity of the film increases, the SPR angle decreases. This is due to the fact that, basically, with higher porosity more pores are present on the surface than the silicate layer.

To ensure the accuracy of the measured sensor signals for each porosity, a theoretical calculation carried out by Dr. Risk at IBM in conjunction with this experimental work [51]. The theoretical model in Figure 48 was generated based on the thickness of the gold sensing layer and refractive indices of the thin film stack on the SPR substrate [51].

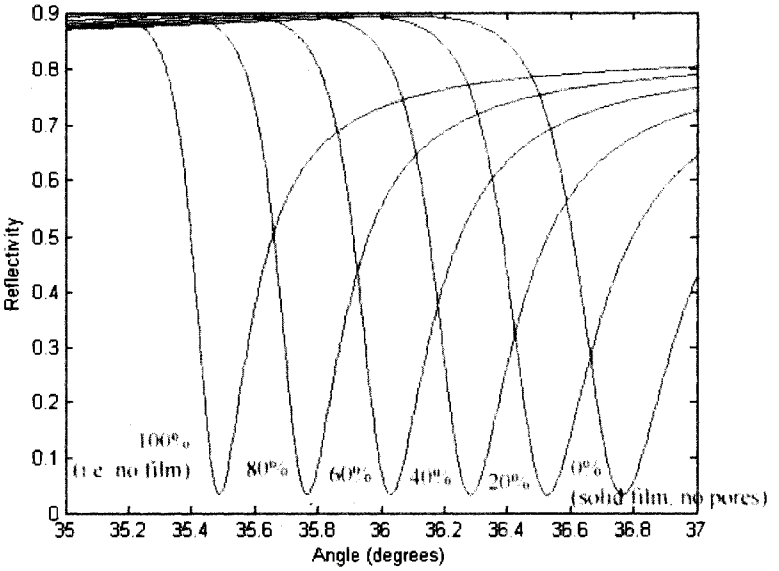

Figure 48. Theoretical calculation of thin film porosity variation [51] (reprinted with permission from B. Risk).

The values shown in Table 7 validate the assertion of the accuracy of measured data with the SPR biosensor.

Table 7.Theoretical and Experimental values of the SPR angle.

Porosity(%)	Theoretical	Experimental
20	36.52	36.50
40	36.28	36.37
60	36.04	36.7

The results highly confirm the effectiveness of the SPR in detecting ultra thin films. With regard to the valuable finding of the proper film thickness and star polymer porogen loading of 40%, four samples were prepared as the next step to examine the reproducibility of 40% porous thin films.

5.2.4 Preparation for Functionalization of Silicate Surface

With the ability to successfully generate ultra thin porous organosilciate films in hand, the exploration of chemical functionalization of these surfaces was conducted. A measure to provide a general chemical handle onto the surface would provide a convenient means of installing specific chemical functionality onto the physically nanostructured sensor surfaces. In order to accommodate such transformation on the surface, the silicate surface had to be prepared for functionalization. The organosilicate porous surface in general was hydrophobic after the curing process, indicating that there was only a small number of reactive silanols on the surface. To transform this inert (as it was) into a chemically active surface, the surface was exposed to a UV/ozone treatment which made it hydrophilic, indicating the restoration of the silanol group on the surface and thus making the surface more amenable to chemical functionalization. This transformation from a hydrophobic surface into a hydrophilic one was studied by taking contact angle measurements. Two factors were vital criteria for this process: the exposure to UV/ ozone, and the ability to preserve the native porous structure of the surface. The time of the exposure of the surface to UV/ozone treatment was critical: too short and the surface would not be fully activated, too long and the porous surface morphology could start to be eroded by the treatment.

As the first step, the exposure to UV/ ozone was monitored by conducting experiments at different exposure times. The initial exposure time was 5 minutes where the results were observed with the contact angle measurement to effectively see the transformation of the surface shown in Figure 49.

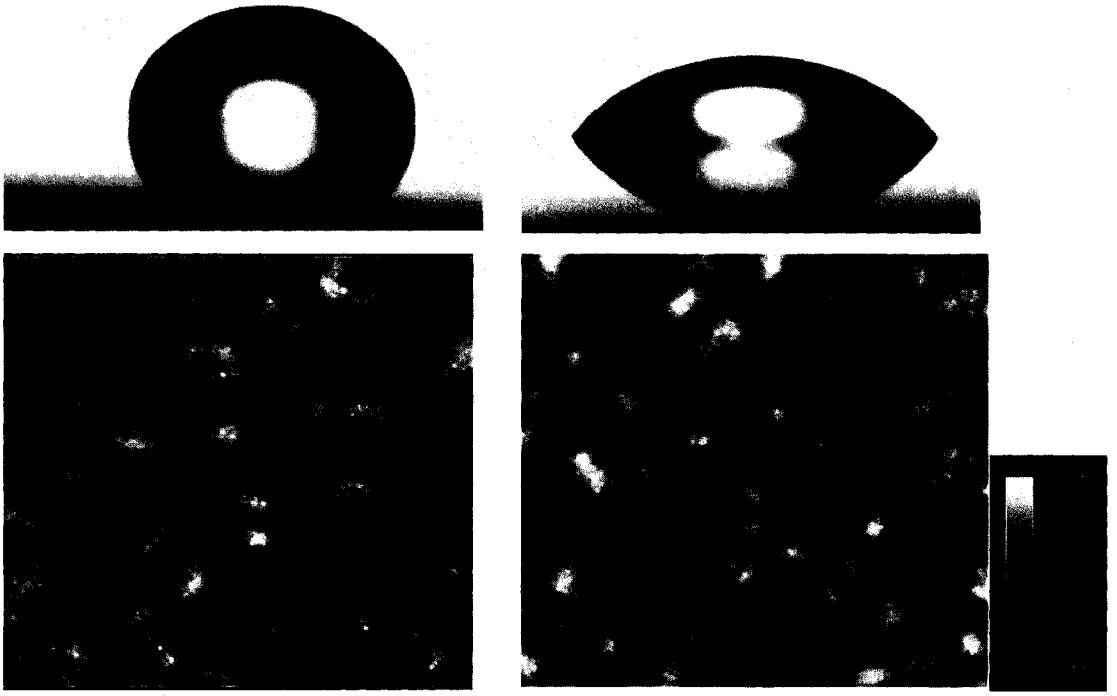

Figure 49. Exposure to UV/Ozone for 5 minutes, 40% porous film a) before UV/Ozone b) after UV/Ozone for 5 minutes.

For each exposure time, AFM results were also included to ensure the structure of the surface remained the same. As observed in Figure 49, the duration of 5 minutes was not sufficient enough to transform the surface into a more hydrophilic surface. Therefore, the UV/ Ozone exposure time was increased to 15 minutes.

It can be observed from Figure 50 that the contact angle decreased from 90^0 to 20^0, which can be considered as a complete hydrophilic surface. Despite the longer exposure time, the native structure of the ogranosilicate film was not affected. It was found that further ozolysis of the sample did not have an influence on the contact angle of the surface.

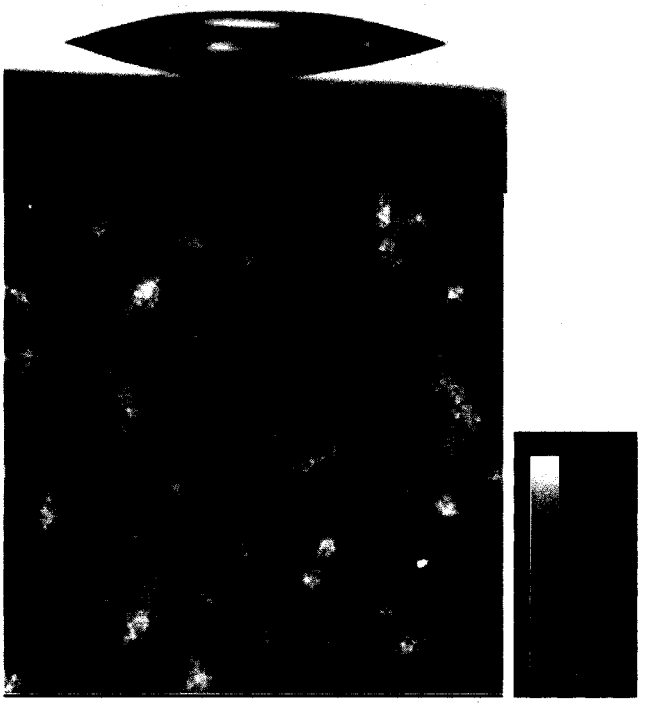

Figure 50. Optimum condition for further chemical functionalization: Exposure to UV/Ozone for 15 minutes.

5.2.5 Chemical Functionalization of the Surface with APTMS

The silanol functionalized surface described in the previous section was then chemically functionalized with gamma-aminopropyltrimethoxysilane (APTMS) to provide a versatile synthetic handle on the substrate. The amine functionalized surface thus formed could enable further specific detection and identification of biological analytes. The summary of transforming a hydrophobic surface into a hydrophilic surface along with chemical functionalization of the surface with APTMS is shown in Figure 51.

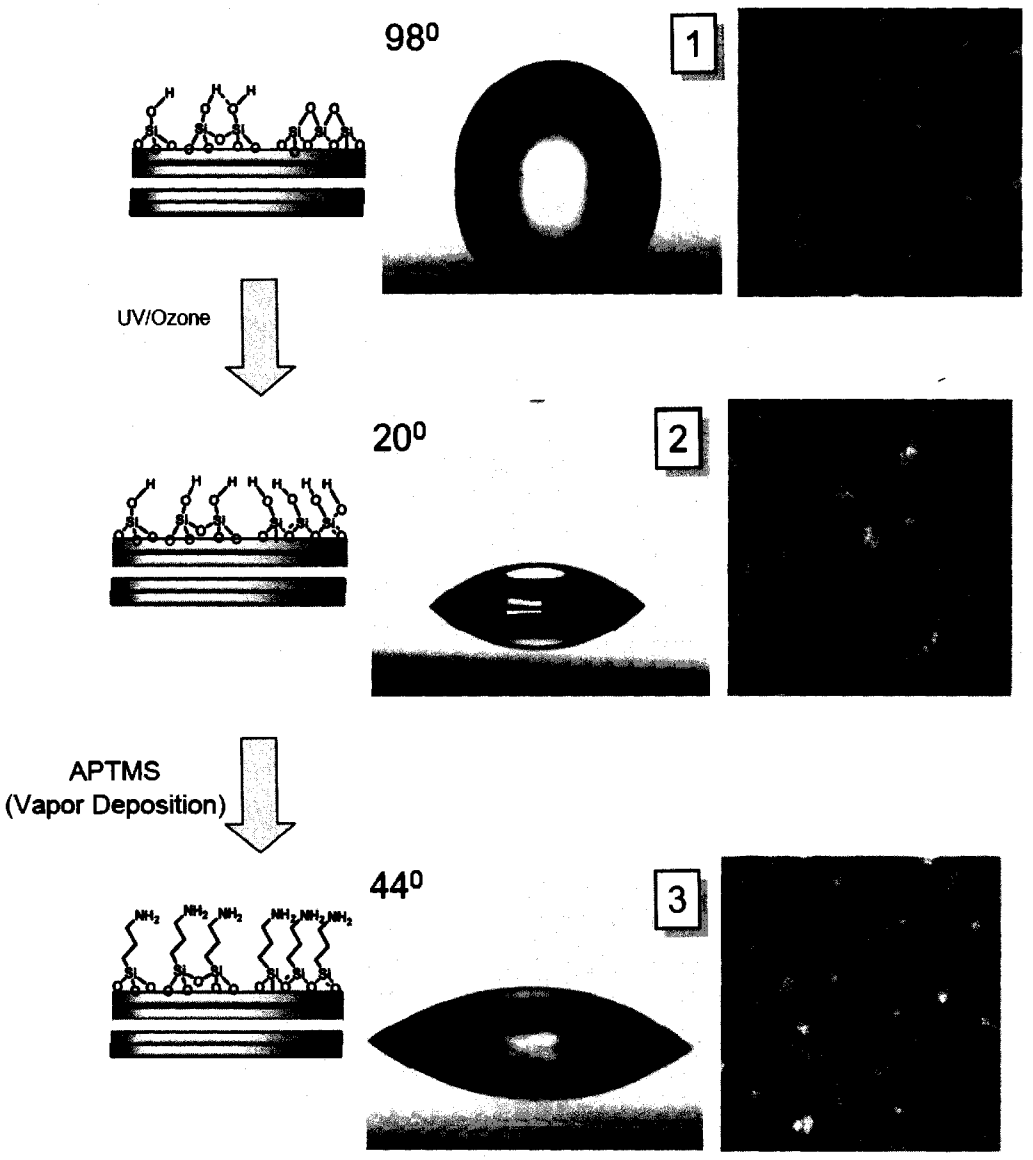

Figure 51. Surface preparation for chemical functionalization and installation of APTMS layer.

After the APTMS deposition, the surface was characterized by contact angle measurements and AFM. The results in Figure 52 indicate a contact angle of 44^0, which is a good indication of proper APTMS deposition having an increase in contact angle

measurements from 20^0 to 44^0. The AFM image in Figure 53 once again indicates the fact that the APTMS deposition did not change the surface.

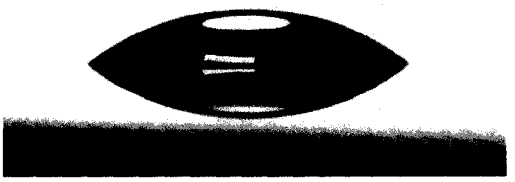

Figure 52. Contact angle measurement of a thin porous film with APTMS layer.

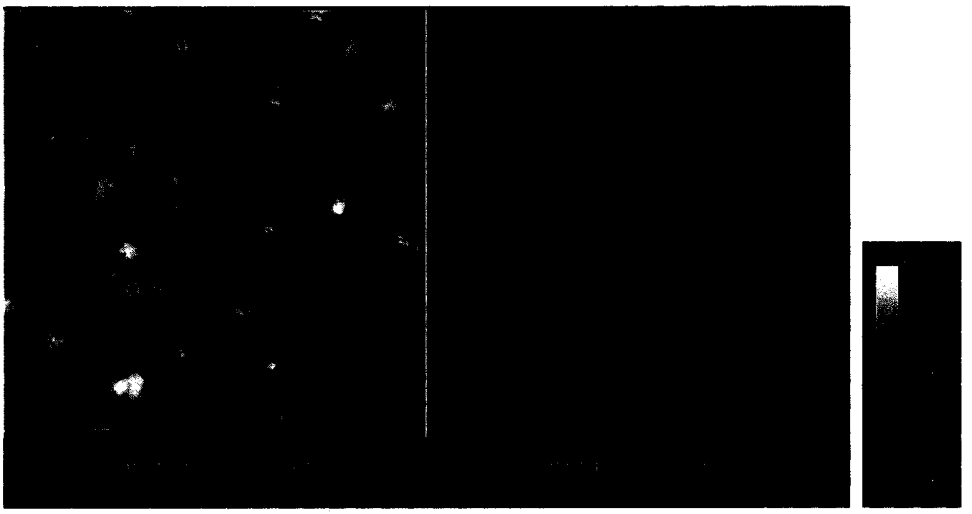

Figure 53. AFM result of 40% porous film with APTMS layer.

5.2.6 Stability Study of the Porous Film with APTMS Layer

Whilst the feasibility of generating an organosilicate porous film and chemically functionalizing the surface with APTMS was validated with combined SPR, AFM and contact angle measurements, the stability of the film under physiological conditions still remained a concern. Hence, the stability of the film was explored using a solution of an

approximate physiological pH (phosphate buffer, pH 7.45) and a more basic buffer solution (Tris buffer, pH 8.5). It was also decided to evaluate the stability of the organosilciate films with and without APTMS layer. Substrates were placed in the flow cell and 3 mL of buffer solution, at a rate of $1mL.hr^{-1}$ were introduced at 2 hrs interval, after which fresh solution was re-introduced. Figure 54 shows the results for both solutions with and without the APTMS surface treatment. For the non-APTMS surface in pH 7.45, as shown in Figure 54 (a), the angular shift changing only slightly during the first 2 hrs of measurements, and no further shift was observed for the period of observation (5 hrs). This can be interpreted as the surface porous initially filled in with water followed by no change in the surface. For the APTMS surface in pH 7.45 (Figure 54b), an angular shift of a constant 0.02 every 2 hrs was observed. The amount of shift in resonant angle, however, is small. It seems that over the course of five hours some part of the APTMS layer diminishes; however, as shown in Figure 61, the shift of film with no APTMS to APTMS layer is 0.13. Even though, after the course of five hours a shift of 0.06 can be observed, but in comparison to the actual shift of 0.13, the shift can be considered minimal. Further investigation of this event is in progress.

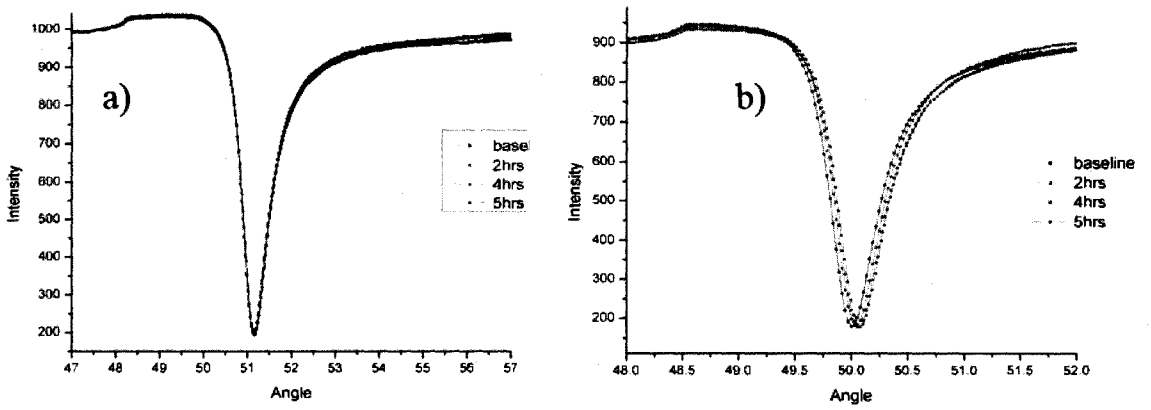

Figure 54. The stability study of 40% porous film, a) no APTMS layer and b) APTMS layer with phosphate buffer, pH 7.45 (physiological condition).

Films were also tested with Tris buffer, pH 8.5, to examine the stability of the films under a further increase in pH, as presented in Figure 55. As illustrated below, the thin porous film with the APTMS layer on top was stable even through an overnight period, with only an insignificant shift of 0.03.

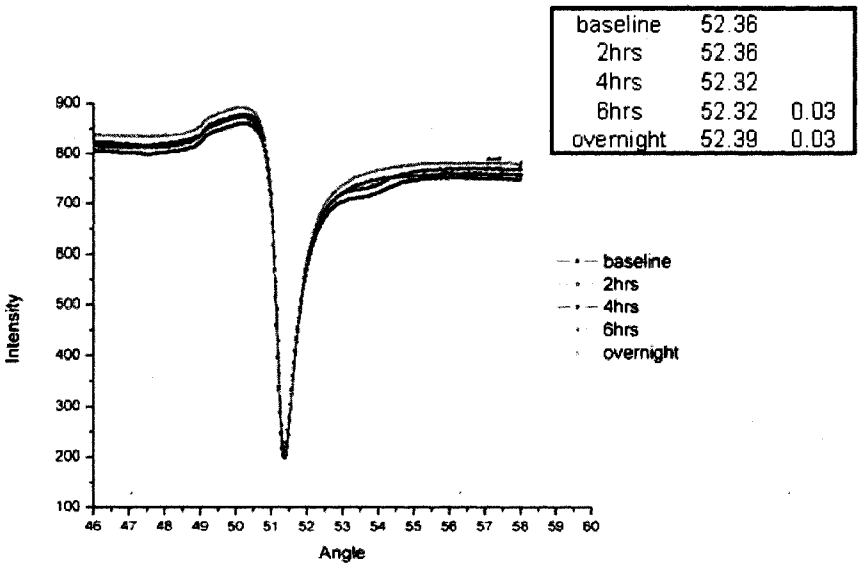

Figure 55. The stability study of 40% porous film, APTMS layer with Tris buffer, pH 8.5.

5.2.7 Surface Modification and Coupling Chemistry on Nanostructured Films

Based on the results of the SPR, contact angle, and AFM images, it was concluded that the installation of chemical functionalization onto the physically nano structured film were successfully accomplished. Hence, the methodology for tailoring both physical and chemical components of the sensor surface for specific applications was further investigated. Therefore, conditions were explored that would enable the transformation of the amino functionalized surface using chemistry generally used and compatible with biomolecules.

The surface modification and coupling chemistry selected for use involved standard amide forming reaction between a primary amine and an activated succinimidyl carboxylic acid ester.

The sensor surface with primary amines was reacted with *N*-Boc-protected succinimidyl ester of l-alanine in dichloromethane/triethylamine (19:1) for 18 hours, as shown in Figure 56. The substrate was then washed with dichloromethane and air dried to produce the *N*-Boc-alanine functionalized surfaces.

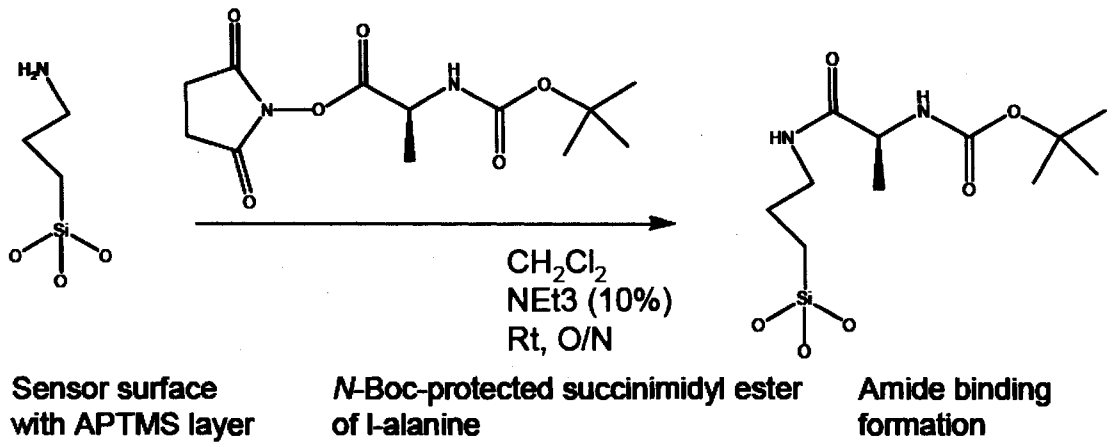

Figure 56. Coupling chemistry on the sensor surface with succinimidyl ester.

The success of this coupling chemistry onto the sensor surface was verified using contact angle measurements and AFM. The change in contact angle, as illustrated in Figure 57, indicated the successful surface chemical transformation of the organosilicate porous thin films. As observed below in Figure 57, the contact angle changes from 44^0 (sensor surface with APTMS) to 70^0 after the chemistry formation on the surface. This completely agrees with the theory that the increase in contact angle was expected since the Boc-protected group introduced during the surface functionalization makes it more hydrophobic, thus the primary amine surface formed.

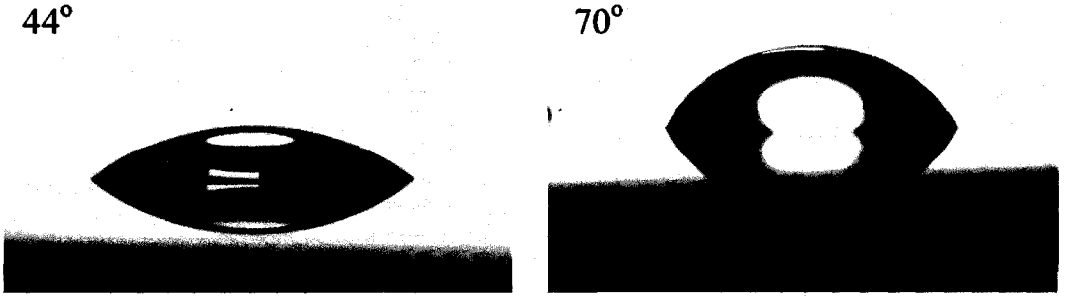

Figure 57. Contact Angle measurement of surface transformation with succinimidyl ester.

Figure 58 (a) demonstrates the sensor surface did not appear as a smooth and uniform layer with the evaluation of a mean square surface (RMS) roughness of 1.819 nm. The reason behind the surface roughness was attributed to excess starting material remaining on the surface. After the surface was immersed in dichloromethane for a day, a smoother surface was obtained, as shown in Figure 58 (b). The RMS values in Figure 58(b) reduced to 1.615 nm.

(a)

(b)

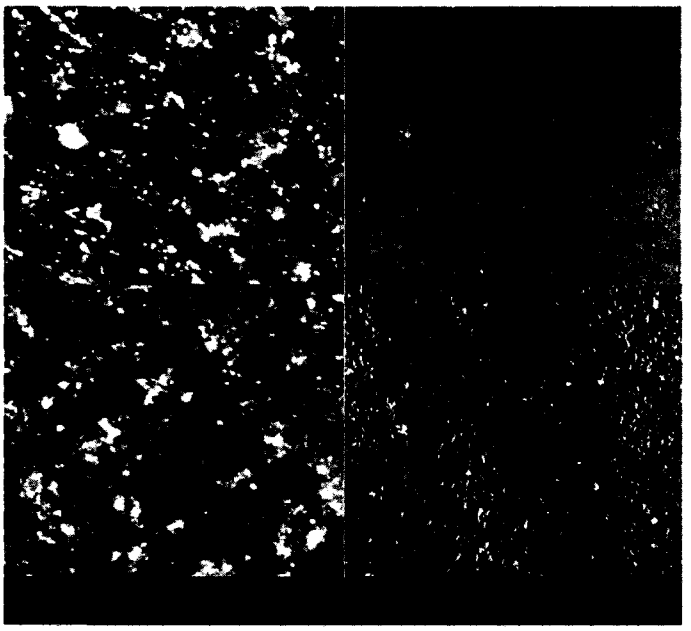

Figure 58. The effects of 24 hours wash with chloroform ($CHCl_3$) a) 1.819 and b) 1.615.

In order to evaluate the ability to conduct a chemical transformation onto the substrate surface, the Boc-protected surface was then subjected to two further reaction steps. The first step involved deprotecting the Boc group using trifluoroacetic acid (TFA). The substrate was immersed in a solution of dichloromethane/ TFA (19:1) for 18 hrs at room temperature before being wash with dichloromethane. This was evaluated using contact angle measurements, as shown in Figure 59. Due to the removal of the Boc protected group from the surface, the angle of the surface decreased from 70^0 to 53^0, as

could be expected, as the hydrophobic Boc-protected group is transformed into a more hydrophilic amine group.

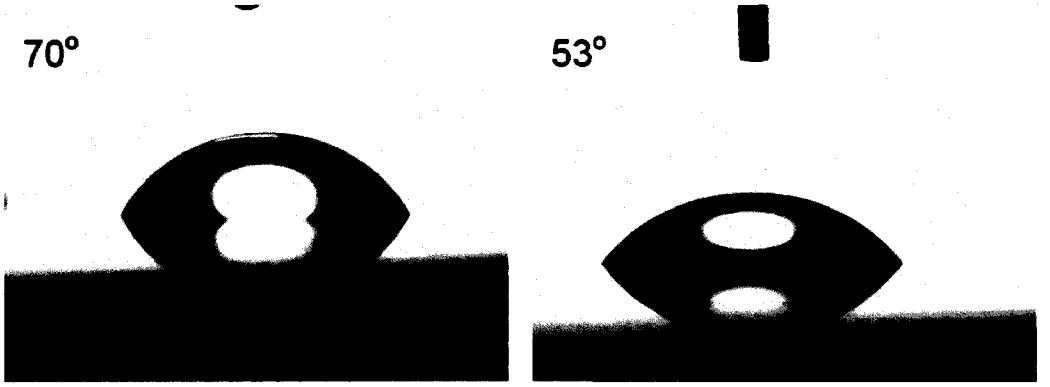

Figure 59. Surface transformation with detachment of Boc protected group.

The second step in the sequential coupling chemistry was completed by introducing a dye molecule as the last step. A fluorescent dye, 7-diethylaminocoumarin-3-carboxylic acid succinimidyl ester was used for this purpose, using the same chemistry as applied to the transformation of the amine surface. The Fluorescence microscope imaging was used to evaluate the effect of the surface reaction with the fluorescent dye molecule. Prior to exposure of the surface to the dye molecule, the image of the sensor surface was first captured, as shown in Figure 60 with the sensor surface generating a dark blue background. After the dye reacted with the sensor surface, a light blue fluorescent color was detected; that was indicative that a significant amount of the surface was successfully functionalized. This behavior, together with the other two surface chemistries, strongly indicates that various surface chemistry can be successfully applied to the surface of organisilicate porous film.

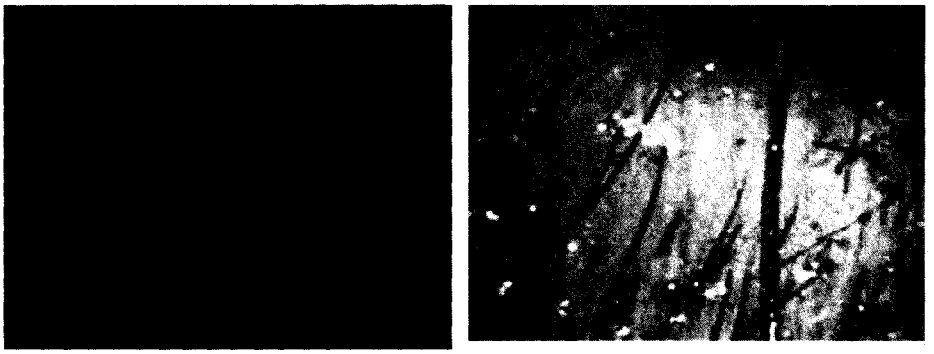

Figure 60. Reaction of the sensor surface with fluorescence dye molecule.

The summary of the three reactions: formation of amide binding, detachment of the Boc protected group, and reaction of the dye molecule are shown in Figure 61.

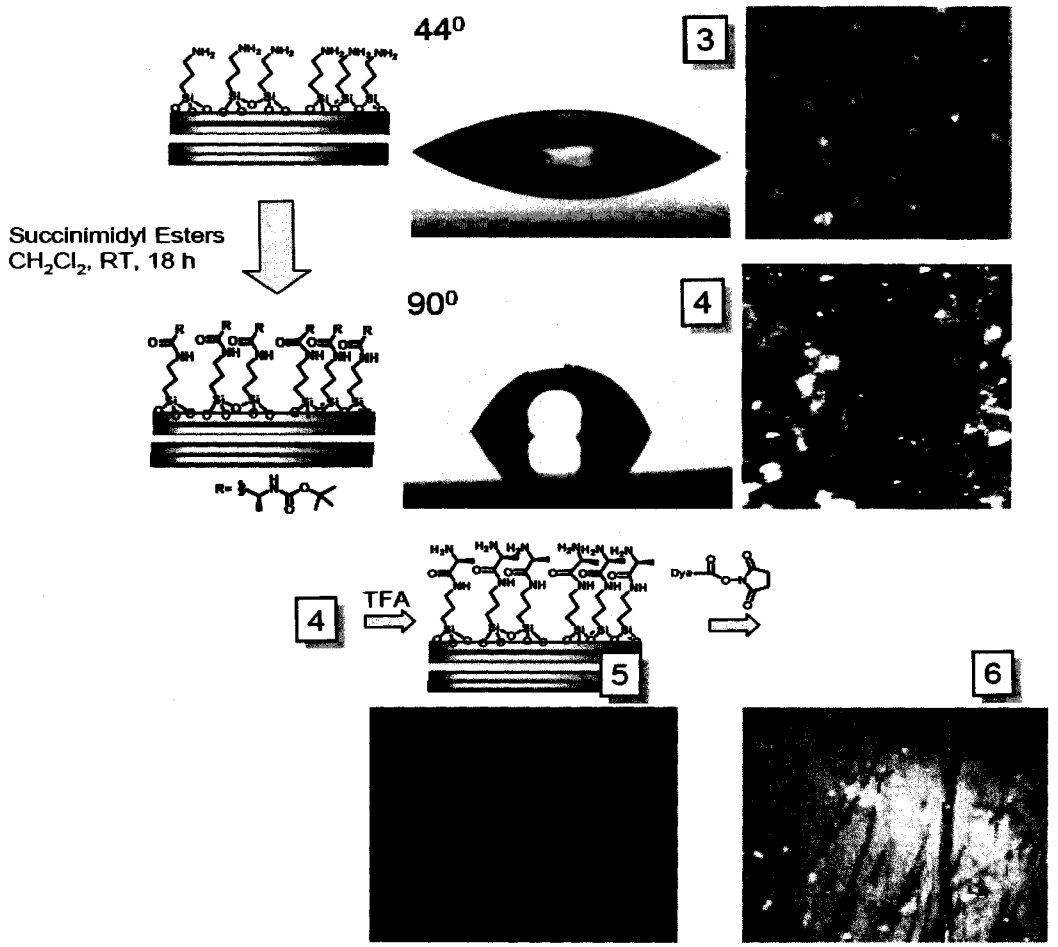

Figure 61. Complete surface chemistry on the organisilicate porous film with APTMS.

One interesting fact about the sequential coupling chemistry was the conversion rate of each reaction which was evaluated to be 90%, resulting in an overall conversion rate of 70% for three reaction steps. The success of the last step in a series of sequential transformation indicates a capacity for transferring, retaining, and converting surface functionality with high efficiency. The efficiency of the reactions, as presented in Figure 51 and Figure 61, was also evaluated using SPR. The ability to detect potential changes in small molecules attached to the substrate surface may be considered to be an extreme

test for the sensitivity of the SPR machine. For this purpose, the scanning SPR was taken after each step described previously for the sequential chemistry transformation. It should be noted that the resonant angle with associated numbers in Figure 62 represents each chemistry reactions, as discussed in Figure 51 and Figure 62.

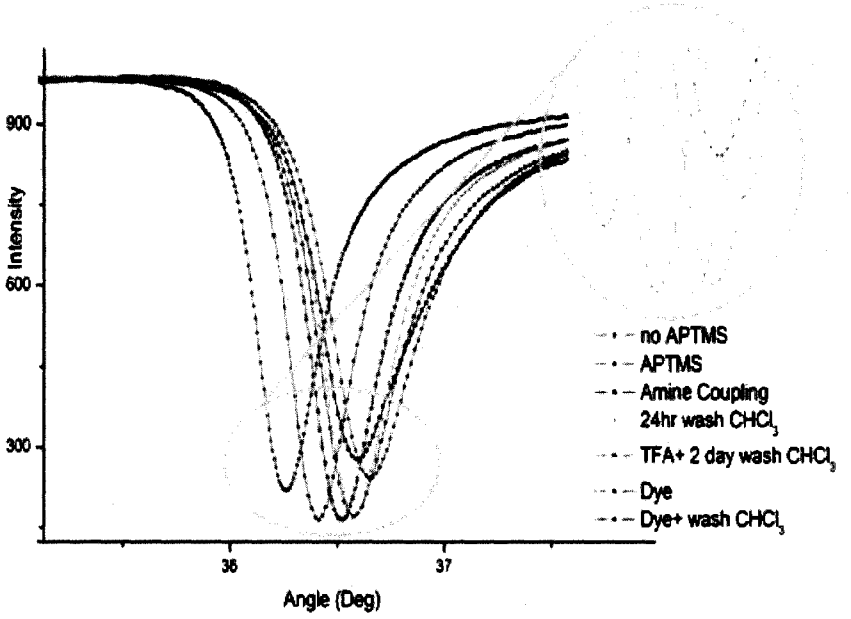

Figure 62. The SPR analysis of coupling chemistry on the sensor surface.

Shifts in resonant angle for each step of the chemical transformation sequence were detectable both in direction and relative shift that were expected for each process. The SPR angle of the curves in Figure 62 is shown in Table 8.

Table 8. The SPR angle values for sequential coupling chemistry

Sample	SPR angle (Deg)
No APTMS	32.26
APTMS	36.40
Amine Coupling	36.59
24hr wash $CHCl_3$	36.57
TFA + 2 days wash $CHCl_3$	36.51
Dye	36.66
Dye + wash $CHCl_3$	36.60

For example, after the APTMS deposition on the surface, the shift in resonant angle, 0.14, was observed due to the addition of an extra layer to the surface, or with the amine coupling on the APTMS layer, a greater shift of angular response of 0.19 was observed. After a day wash of the film with $CHCl_3$ the SPR angle decreased from 36.59 to 36.57, which confirms the process of washing the extra material from the surface. Also, with deprotecting the Boc group, the SPR angle shifted to 36.51 which sits at a lower angle than amine coupling. With the dye reaction, the SPR angle shows a significant shift of 0.15 from the previous step. However, after 2 days wash of the substrate with $CHCl_3$, the angle shifted backward toward the amine coupling, indicating that the excessive amount of dye was removed from the surface and the shift is closer to the amine coupling, where the succinimidyl ester was involved.

These results from the SPR analysis shown in Figure 62 are also consistent with the results from the contact angle measurements, AFM, and Fluorescence microscope

imaging. This confirms that the intended surface chemical transformation were successful. But more importantly, the SPR biosensor is sensitive enough to detect sub-molecular changes.

CHAPTER SIX
CONCLUSIONS

A highly sensitive surface plasmon resonance (SPR) biosensor was successfully designed to detect and characterize biomolecular interactions. A complementary software programming, LabView, was included to facilitate data measurements, kinetics analysis and system calibration. The custom-made flow cell was incorporated in the design to provide greater versatility for different measurements. The performance of SPR was evaluated by studying two main fundamentals of the SPR concept. The measured TIR, in comparison to the model, predicted from theory and confirmed the accurate alignment of the optical path for occurrence of SPR phenomenon. The SPR angle was measured for air and was compared to the theoretical model. This also confirmed the well behavior of the designed SPR biosensor. The functionality of the flow cell was studied by evaluating the effect of different solvents on the system. The kinetics feature of the LabView program was verified by studying the layer by layer process of star polymers and tracking the formation of five layers.

The second part of this work included the investigation of increasing the SPR sensitivity by nanostructuring SPR sensor surfaces. This was achieved by making nanoporous organo silicate thin films on a sensor surface. Random pores were created within these silicate films by star polymers. Chemical functionalization of the sensor surface was then achieved using UV/ozone and gamma-aminopropyltriethoxysilane treatment. This provided a convenient means for installing chemical functionality onto

physically nanostructured sensor surfaces. The binding capability of the sensor surfaces was verified with surface modifications and coupling chemistry.

The physically nanostructured surfaces are capable of bindings and interactions with different molecules. This strongly enhances the possibility of binding biological mixtures to sensor surface.

CHAPTER SEVEN
FUTURE WORK

In medicine, as with cancer treatment or other types of drug delivery mechanisms, the absorption of proteins on materials surfaces has been a focus of many studies over several decades. Due to the importance of these types of protein applications to drug delivery, biomaterials, and diagnostics, such systems continue to receive a large amount of attention. Therefore, it is useful for students to expand their knowledge in these areas by using SPR detection specifically for measuring biomolecular interactions such as protein bindings. Among all of the protein bindings, the streptavidin and biotin bindings is a stable well-studied system that will allow users to investigate the structure and binding characteristics of the proteins. Current work on increasing the sensitivity of the SPR biosensor by nanostructuring the sensor surface suggests further investigating the strategies for introducing non-specific adsorption of poly ethylene glycol (PEG) molecule along with chemical ligation motifs onto the sensor surface.

REFERENCES

1. Homola, J., S.S. Yee, and G. Gauglitz, *"Surface plasmon resonance sensors: Review,"* Sens. Actuators, **54,** 3-15, (1999).

2. Shankaran, D.R. and K.V. Gobi, *"Recent advancements in surface plasmon resonance immunosensors for detection of small molecules of biomedical, food and environmental interest,"* Sens.Actuators, **121,** 158-177, (2006).

3. W.Knoll., *"Interfaces and thin film as seen by bound electromagnetic waves,"* Annu. Phys. Chem, **49,** 569-638, (1998).

4. D.Hallidat, R.Resnick, Fundamentals of Physics, (John Wiley & Sons, LtD.,1970).

5. Leidberg, B., C. Nylander, and I. Lundstrom, *"Biosensing with surface plasmon resonance-how it all started,"* Biosen. Bioelectronics, **10,** (1995).

6. K.Kurihara, K.Nakamura, and K.Suzuki, *"Asymmetric SPR sensor response curve-fitting equation for the accurate determination of SPR resonance angle,"* Sens. Actuators, 86, 49-57 (2002).

7. P.B.Johnson and R.W.Christy, *"Optical constants of the noble metals,"* Phys. Rev., **6**, 4370-4379 (1969).

8. Wang, S., S. Boussad, and N.J. Tao, *"Surface plasmon resonance enhanced optical absorption spectroscopy for studying molecular adsorbants,"* Rev. Sci, Instrum, 72, 3055-3060 (2001).

9. Biacore, *"An introduction to Biacore's SPR technology,"* [online], available at http://www.biacore.com (accessed 22 August 2008).

10. X.Liu, D.Song, Q.Zhang, Y.Tian, L.Ding, and H.Zhang, *" Wavelength-modulation surface plasmon resonance sensor,"* Trends in Analytical Chemistry, 24, 887-893 (2005).

11 E.M.Yeatman, *"Resolution and sensitivity in surface plasmon microscopy and sensing,"* Biosens. Bioelectronics,11, 635-649 (1996).

12. F.C. Chien and S.J. Chen, *"A sensitivity comparison of optical biosensors based on four different surface plasmon resonance modes,"* Biosen. Bioelectronics, **20,** 633-642 (2004).

13. R.Geordiadis, K.P.Peterlinz, and A.W.Peterson, *"Quantitative measurements and modeling of kinetics in nucleic acid monolayer films using SPR spectroscopy,"* J.A. Chem. Soc., 3166-3173 (2000).

14. K.A. Peterlinz and R. Georgiadis, *"In situ kinetics of self-assembly by surface plasmon resonance spectroscopy,"* langmuir, **12,** 4731-4740 (1996).

15. Melles Griot Inc., " Optics guide 5," Catalogue, 1990.

16. " *Lenses*", [online]. Available at http://learnquebec.ca/learn/content (accessed 20 September 2007).

17. J. Homola, *" Surface plasmon resonance sensors for detection of chemical and biological species,"* Chem.Rev., **108**, 462-493 (2008).

18. S.M. Borisov and O.S.Wolfbeis, " *Optical biosensors*," Chem.Rev., **108**, 423-461 (2008).

19. P.I. Nikitin, A.A. Belglazov, V.E. Kochergin, M.V. Valeiko, and T.I. Ksenevich, *"Surface plasmon resonance interferometry for biological and chemical sensing,"* Sens. Actuators, **54,** 43-50 (1999).

20. N. Scholler, B. Garvik, T. Quarls, S. Jiang, and N. Urban, *" Method for generation of in vivo biotinylated recombinant antibodies by yeast mating,"* Immunol. Methods, **317,** 132-143 (2006).

21. K. Alfthan, *"Surface plasmon resonance biosensors as a tool in antibody engineering,"* Biosen. Bioelectronics, **13,** 653-663 (1998).

22. M.N. Win, J.S. Klein, and C.D. Smolke, *" Codein-binding RNA aptamers and rapid determination of their binding constants using a direct coupling surface plasmon resonance assay,"* Nucleic Acids Res, 34, 5670-5682 (2006).

23. Z. Wang, T. Wilkop, D. Xu, Y. Dong, G. Ma, and Q. Cheng, *" Surface plasmon resonance imaging for affinity analysis of aptamer-protein interactions with PDMS microfluidic chips,"* Anal.Bioanal.Chem, 389, 819-825 (2007).

24. S. Lofas, B. Johnsson, A. Edstrom, A. Hansson, G. Lindquist, R.M.M. Hillgren, and L.Stigh, *"Methods for site controlled coupling for carboxymethyldextran surfaces in surface plasmon resonance sensors,"* Biosen. Bioelectronics, **10,** 813-822 (1995).

25. M. Mrksich, G.B. Sigal, and G.M. Whitesides, " *Surface Plasmon Resonance Permits in Situi Measurement of Protein Adsorption on Self-Assembled Monolayers of Alkanethiolates on Gold,"* Langmuir, **11**, 4383-4385 (1995).

26. L. Deng, M. Mrksich, and G.M. Whitesides, *"Self-assembled monolayers of alkanethiolates presenting tri(propylene sulfoxide) groups resist the adsorption of proteins,"* J.Am. Chem. Soc, **118**, 5136-5137 (1996).

27. E.A. Perikins, and A.S. Squirell, *"Development of instrumentation to allow the detection of microorganisms using light scattering in combination with surface plasmon resonance,"* Biosen. Bioelectronics, **14,** (2000).

28. P. Englebienne, A.V. Hoonacker, and M. Verhas, *"Surface plasmon resonance: principles,methods and application in biomedical sciences,"*Spectroscopy, **17,** 255-273 (2003).

29 I. Pockrand, J. D. Swalen, J. G. Gordon, II and M. R. Philpott, *"Surface plasmon spectroscopy of organic monolayer assemblies,"*Surface Sci, **74,** 234-244, (1978).

30. A.K Ray and A.V Nabok, "*Composite polyelectrolyte self-assembled films for sensor applications*," in Handbook of Polyelectrolytes and their Applications: Volume 3:Applications of Polyelectrolyte and Theoretical Models, edited by S.K. Tripathy and J. Kumar (American Scientific Publishers, Stevenson Ranch, CA, 293-297 (2000).

31. C.S.Bonifacio, *"Self-assembled layer-by-layer star polymers by electrostatic interactions,"* Graduate Thesis (2008).

32. L.R. Rich and D.G. Myszka, *"Review,Survey of the year 2004 commercial optical biosensor literature,"* J. Molecular Recognition, **21** (2004).

33. L.R. Rich and D.G. Myszka, *"Survey of 2001 commercial optical biosensor literature,"* J. Molecular Recognition, **15,** 352-376 (2002).

34. L.R. Rich and D.G. Myszka, *"Review,Survey of the year 2005 commercial optical biosensor literature,"* J.Molecular Recognition, **19,** 478-534 (2005).

35. R.W. Wood, *"On a remarkable case of uneven distribution of light in a diffraction grating spectrum,"* Phil Magm, **4** (1902).

36. J.G. Gordon II and S. Ernest, *"Surface plasmons as a probe of the electrochemical interface,"* Surface Sci, **101,** 499-506 (1980).

37. Lynder, C., B. Liedberg, and T. Lind, *"Gas detection by means of surface plasmon resonance,"* Sens. Actuators, **3,** 77-79, (1982).

38. H. Arwin, S. Lundstorm, *"Reflectance method for immunoassay on solid surfaces,"* Nonisotropic Immunoassay, 313-330 (1982).

39. *" Texas instrument"*, [Online], available at http://www.ti.com (accessed Nov 1 2007).

40. J. Homola, *"On the sensitivity of surface plasmon resonance sensors with spectral interrogation,"* Sens. Actuators, **B41,** 207-211 (1997).

41. R.C. Jorgnnson and S.S. Yee, *"A fiber-optic chemical sensor based on surface plasmon,"* Sens. Actuators, **B12,** 213-220 (1993).

42. Myszka, D.G., *"Improving Biosensor Analysis,"* J. Molecular Recognition, **12,** 279-284 (1999).

43. H. Kim, C.R. Kreller, K. A. Tran, V. Sisodiya, S. Angelos, G. Wallraff, S. Swanson, and R. D. Miller, *" Nanoporous thin films with hydrophilicity-contrasted patterns,"* Chem. Mater, **22**, 4267-4272 (2004).

44. M.A. Cooper, *"Label-free screening of biomolecular interactions,"* Anal Bioanal Chem, **377**, 834-842 (2003).

45. P.B. Deacon, J.K. Deacons, D.G. Pedly, *" Surface plasmon resonance applied to immunosensing,"* Sens. Actuators, **15**, 11-18 (1988).

46. Morgan, H., D.M. Tayolor, and C.D. Silva, *"Surface plasmon resonance studies of chemisorbed biotin-stretavidin multilayers,"* Thin Solid Films, **209,** 122-126 (1992).

47. S. Lofa ,and B. Johnsson, *"A novel hydrogel matrix on gold surfaces is surface plasmon resonance sensors for fast and efficient covalent immobilization of ligands,"* J. Chem. Soc. Chem. Commun, **21,** 1526-1528 (1990).

48. G.Boisset (2007). Thin Film and Bulk Index of Refraction and Photonics Calculations [online]. Available at www.luxpop.com (accessed 22 July 2008).

49. V.Y. Lee and R.D. Miller, IBM Corporation, private communication (2007).

50. M. Commandre, P. Roche, J. -P. Borgogno, and G. Albrand, *"Absorption mapping for characterization of glass surfaces,"* Appl. Opt., **34,** 2372 (1995).

51. W.P. Risk, IBM Almaden Research Center, private communication (October 2007).